THESIS

UNDERSTANDING THE ROLE OF OCEAN DYNAMICS IN CLIMATE VARIABILITY

Submitted by

Casey R. Patrizio

Department of Atmospheric Sciences

In partial fulfillment of the requirements

For the Degree of Master of Science

Colorado State University

Fort Collins, Colorado

Summer 2021

Master's Committee:

Advisor: David Thompson
Co-Advisor: David Randall

Maria Rugenstein
Jeremy Rugenstein
Justin Small

ABSTRACT

UNDERSTANDING THE ROLE OF OCEAN DYNAMICS IN CLIMATE VARIABILITY

The ocean plays a key role in regulating Earth's *mean* climate, both because of its massive heat capacity, but also its heat transport by slow-moving circulations and other dynamics. In principle, fluctuations in such ocean heat transport can influence the *variability* in the climate, by impacting the sea-surface temperature (SST) variability and in turn the atmospheric variability through surface heat exchange, but this is incompletely understood, particularly in the extratropics. The goal of this dissertation is to clarify the role of ocean dynamics in climate variability, first focussing on the role of ocean dynamics in SST variability across the global oceans (Chapter 2 and Chapter 3), and then on the impact of midlatitude ocean-driven SST anomalies on the atmospheric circulation (Chapter 4).

In Chapter 2, the contributions of ocean dynamics to ocean-mixed layer temperature variance are quantified on monthly to multiannual timescales across the globe. To do so, two methods are used: 1) a method in which monthly ocean heat transport anomalies are estimated directly from a state-of-the-art ocean state estimate spanning 1992-2015; and 2) a method in which they are estimated indirectly using the energy budget of the mixed layer with monthly observations of SSTs and air-sea heat fluxes between 1980-2017. Consistent with previous studies, both methods indicate that ocean dynamics contribute notably to mixed layer temperature variance in western boundary current regions and tropical regions on monthly to interannual timescales. However, in contrast to previous studies, the results also suggest that ocean dynamics *reduce* the variance of Northern Hemisphere mixed layer temperatures on timescales longer than a few years.

In Chapter 3, the role of ocean dynamics in midlatitude SST variability is further understood using Hasselmann's model of climate variability, wherein midlatitude SST anomalies

are driven entirely by atmospheric processes. Motivated by the results of Chapter 2, here Hasselmann's climate model is extended to include the forcing and damping of SST variability by ocean processes, which are estimated indirectly from monthly observations. It is found that the classical Hasselmann model driven only by observed surface heat fluxes generally produces midlatitude SST power spectra that are too *red* compared to observations. Including ocean processes in the model reduces this discrepancy by decreasing the low-frequency SST variance and increasing the high-frequency SST variance, leading to a *whitening* of the midlatitude SST spectra. This happens because ocean forcing increases the midlatitude SST variance across many timescales but is outweighed by ocean damping at timescales > 2 years, particularly away from the western boundary currents. It is also shown that the whitening of midlatitude SST variability by ocean dynamical processes operates in NCAR's Community Earth System Model (CESM).

In the final chapter, the atmospheric circulation response to midlatitude ocean-forced SST anomalies is explored. In particular, the extended Hasselmann model is used to isolate the oceanic and atmospheric-forced components of the observed SST variability in the Kuroshio-Oyashio Extension (KOE) region. The associated atmospheric circulation anomalies are diagnosed by lagged-regression of monthly sea-level pressure (SLP) anomalies onto the KOE-averaged SST anomalies, and their oceanic and atmospheric-forced components. Consistent with previous studies, a large-scale SLP pattern is found to lag the KOE SST anomalies by one month. Here it is shown that this pattern is linked to the oceanic-forced component of the SST variability, but *not* the atmospheric-forced component. The results hence suggest that the midlatitude ocean dynamical processes in the North Pacific influence the variability of the large-scale atmospheric circulation.

ACKNOWLEDGEMENTS

I am so grateful for all of the wonderful people in my life who have supported me in many different ways throughout my PhD process.

I would like to thank my two advisors, Dave Thompson and Dave Randall, first, for seeing potential in me, and second, for your mentorship. I am extremely grateful to have had the opportunity to work with such exceptional scientists and also caring advisors. I would not have made it to this stage without your continual support and active contributions to my research amidst many other responsibilities. I also greatly appreciate the encouragement and flexibility you offered to me during challenging times, especially during the transition to my PhD from my MS as well as during the current pandemic.

I would like to acknowledge my committee members: Justin Small, for valuable conversations about my research and including me in many useful group meetings, and Maria and Jeremy Rugenstein, for your insights on climate dynamics and for joining the committee on relatively short notice. I would also like to give thanks to my former committee member, Sue van den Heever, for teaching me cloud dynamics, which I will hopefully put to good use in future research.

Next, the students, faculty and staff in the Atmospheric Sciences Department at CSU: I am a better researcher, and more importantly, person, because of the relationships and experiences I have had with you all. A special thanks to Sarah Tisdale for extremely prompt help with graduate school matters, Kelley Branson for computing support over the many years, and to Jim Hurrell for words of wisdom and for introducing to me to many wonderful scientists and staff at NCAR. I would also like to thank Christine Chiu for encouraging me to step outside of my comfort zone, and Peter Jan van Leeuwen for teaching me the basics of physical oceanography, half in-person and half remotely.

I would like to acknowledge all of the students and faculty that participated in the Dynamics group meetings over the years. I have not always been the most active participant

in the meetings, but I have always appreciated the effort that you have put forth to keep the meetings active and the connection to community that the meetings provide. Thank you to both the Thompson and Randall groups, including Shim, Luke, Jingyuan, Drea and Alex, for useful conversations and for your general support over the course of my time here at CSU. I would also like to thank Lantao Sun for very useful help with CESM, which I hope to put into practice in future experiments.

I am so thankful for my amazing friends, particularly during the last year of my PhD when social isolation was reality. If the global pandemic has taught me one thing, it is that you are all essential to my well-being. I am so grateful to have each and every one of you in my life and hope that we can stay connected in the next chapter.

Thank you to my mom, Michelle Patrizio, for being undoubtedly the biggest supporter of my scientific pursuits. You have followed me every step of the way, from Langara College to UBC to CSU, and I have been able to count on you for unwavering interest and encouragement the whole time.

Thank you to my dad, Robert Patrizio, for supporting my education from the beginning. And to my brothers, Alec and Remi, for being great sources of distraction from the stressors of school.

I am thankful for my grandparents, Luciana and Richard Pinto, for providing a loving atmosphere that has shaped and inspired me in so many ways.

I am so thankful for my wife, Rachel Eby, for helping me maintain balance in my life. Thank you for making me laugh when I have felt stuck, and for reminding me that I am deserving of great things in life when I have felt discouraged. Words cannot fully express how much I appreciate the support you have offered to me from the very beginning.

Finally, I would like to acknowledge myself for having pursued growth in the face of difficulty and acceptance that I am doing the best that I can. I also acknowledge the privileges I have as a white man, which have made my life and experiences in academia easier than women, non-white people, and other marginalized groups. It is my responsibility

to learn more about systemic biases that favor white men, relinquish my privilege, and strive to empower others in my future career.

TABLE OF CONTENTS

LIST OF TABLES

LIST OF FIGURES

Chapter 1

Introduction

1.1 Climate variability

Earth's climate is gradually warming (climate *change*), but the climate also exhibits variability across the globe and across many timescales (climate *variability*). Climate variability is typically measured as the deviation of climatic statistics (e.g. mean air temperature) over a given period of time (e.g. a month, season or year) when compared to long-term statistics for the same time period. Such variability is important for reasons that are similar to that for individual weather events. Like the weather, climate variability is associated with anomalies in atmospheric variables like air temperature and precipitation, that can have significant societal impacts. For example, an anomalously warm season impacting arid or semi-arid regions (e.g. in Colorado) may promote drought. Unlike the day-to-day weather, however, climate variability is associated with anomalies in the long-term climate statistics and thus may have profound, longstanding impacts. Hence the mechanisms of climate variability must be understood as a key step toward its prediction and toward the benefit of societies across the globe.

Climate variability arises from dynamics that are intrinsic to the atmosphere, as well as from the interaction between the atmosphere and the other components of Earth's climate system: the ocean (and other water bodies), the cryosphere (ice), lithosphere (land) and biosphere (living organisms). The variability that arises from processes within the climate system is referred to as internal climate variability, but when the system is perturbed from the outside the resulting variability is referred to as external climate variability. For example, the Antarctic "ozone hole" caused by anthropogenic emission of ozone-depleting substances is considered external climate variability, whereas the variability associated with the El Niño–Southern Oscillation is considered internal climate variability.

This dissertation is focussed on understanding the role of the ocean in climate variability.

1.2 The ocean and climate

The ocean is one of the most important components of Earth's climate system. With a massive heat capacity that is about 1000 times greater than that of the atmosphere, the ocean plays a critical role as a source and sink of energy to the atmosphere across most of the globe. Such energy exchanges are enabled by the ocean mixed layer, which is a vertically-mixed turbulent layer of the upper-ocean in direct contact with the atmosphere. As a result of the large heat capacity of water, small fluctuations in the ocean-mixed layer temperature and likewise sea-surface temperature (SST) are often associated with large heat exchanges with the overlying atmosphere. Understanding such ocean-mixed layer variability is thus critical to understanding the role of the ocean in climate variability.

In addition to storing and releasing heat, the ocean also moves heat around. The ocean plays an essential role in governing the long-term *mean* climate through its relatively slow moving circulations that are set in motion by the atmosphere. For example, wind-driven western boundary currents and meridional overturning circulations transport heat poleward to high latitudes where heat is released to the atmosphere (e.g. Dijkstra, 2008; Hartmann, 2015). The surface cooling at high latitudes promotes deep convection and mixing that links the upper-ocean gyres to the deep-ocean circulations on millennial timescales (e.g. Dijkstra, 2008; Pedlosky, 2013). Overall, the ocean circulations account for nearly a third of the long-term mean meridional heat transport in the combined atmosphere-ocean system (Trenberth and Caron, 2001).

The role of the ocean in climate *variability* is less well-understood. First, it is instructive to consider the role of the ocean in climate variability in the absence of ocean heat transport. In this "passive ocean" case (Fig. 0.1a), the ocean is driven predominantly by surface heat fluxes via atmospheric variability. Examples of passive ocean models will be discussed in more detail in Chapter 2 and Chapter 3, but in general, in such cases the fast atmospheric

fluctuations are suppressed because of the large heat capacity of the ocean, yielding relatively slow variability in SSTs. On the other hand, in the "dynamic ocean" case (Fig. 0.1b), heat transport by ocean dynamical processes can drive variability in SSTs, and in turn the atmosphere through surface heat exchange. Throughout this dissertation, an ocean dynamical process refers to any process that transports heat in the ocean, such as the advection of heat by wind-driven currents, ocean eddies, vertical mixing at the bottom of the ocean mixed layer, among other processes.

Ocean dynamical processes are known to play a key role in one of the most prominent modes of climate *variability* known as the El Niño-Southern Oscillation (ENSO). ENSO is associated with year-to-year (interannual) variability in SSTs in the Tropical Pacific, as well as large-scale changes in atmospheric convection and the atmospheric circulation, which influence the climate variability in remote regions, such as precipitation in North America

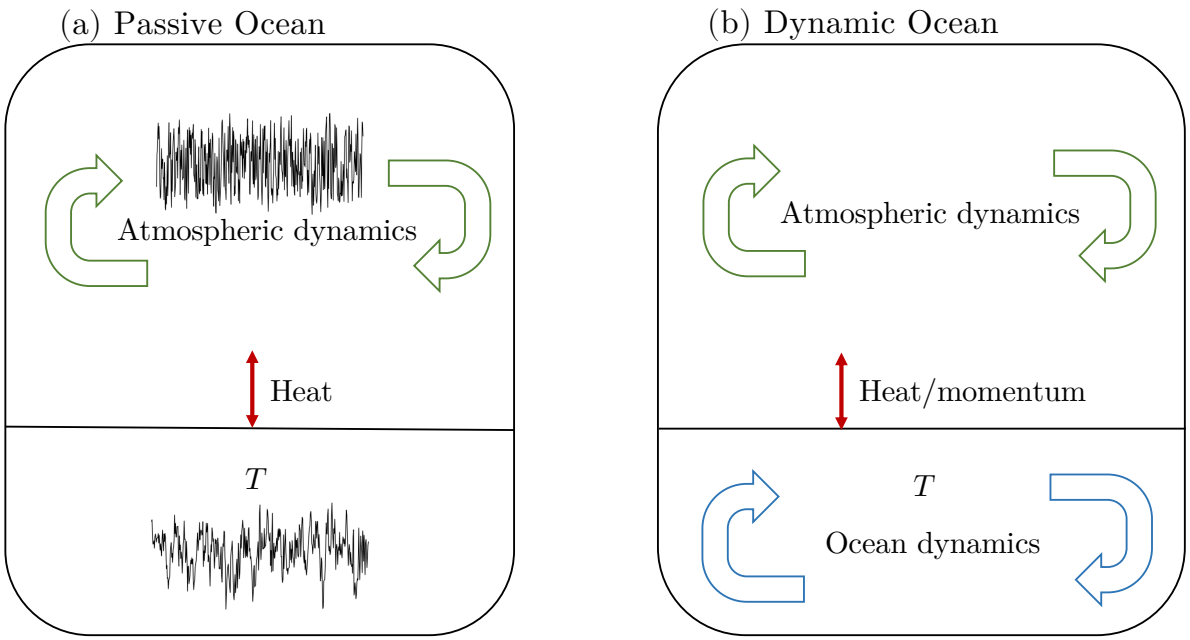

Figure 0.1: Conceptualizations of the role of the ocean in climate variability. In the passive ocean case (left), the ocean simply acts to suppress fast atmospheric variability, yielding relatively slow SST (T) variability as a result of the large heat capacity of the ocean. In the dynamic ocean case (right), heat transport by ocean dynamical processes drives variability in SSTs, and in turn the atmosphere through surface heat flux exchange.

(e.g., Philander, 1983; Jin, 1997; McPhaden et al., 2006). The dynamics of ENSO are complex, but one of its essential mechanisms involves a positive feedback loop between atmospheric processes and oceanic processes, particularly vertical upwelling (e.g. Wang and Picaut, 2004; Dijkstra, 2006).

Apart from ENSO, however, the role of the ocean in climate variability is not well-understood. Part of the problem lies in our still-evolving understanding of the role of ocean dynamical processes in driving ocean mixed-layer and thus SST anomalies across the globe in the first place. Consider, for example, a large-scale pattern of decadal SST variability in the North Atlantic known as the Atlantic Multidecadal Oscillation (AMO; Folland et al., 1986; Schlesinger and Ramankutty, 1994) or Atlantic Multidecadal Variability (AMV). There is ongoing debate regarding the relative roles of atmospheric and oceanic processes in driving AMV. On the one hand, some studies have argued that AMV is mainly driven by atmospheric processes. For example, Clement et al. (2015) showed that the spatial and temporal characteristics of AMV are not significantly different in climate simulations run on general circulation models (GCMs) with ocean dynamics (so-called fully-coupled models) compared to simulations run on GCMs without ocean dynamics (so-called slab-ocean models). On the other hand, studies have also argued that ocean circulation plays an important role in AMV (e.g, O'Reilly et al., 2016), particularly the Atlantic meridional overturning circulation (AMOC). In general, the role of ocean dynamics in driving SST variability in extratropical regions remains incompletely understood, particularly at lower-frequencies. This topic is the focus of Chapter 2 and Chapter 3.

Another part of the problem in understanding the role of ocean dynamics in climate variability outside of ENSO lies in the relatively subtle response of the atmosphere to extratropical sea-surface temperature (SST) anomalies (e.g. Kushnir et al., 2002). Consider, for example, the SST variability that occurs in the western boundary region of the Pacific basin. In this region, a strong northward ocean current known as the Kuroshio current arises from wind-stress exerted on the ocean surface by the atmospheric circulation. There is increasing

evidence that ocean dynamical processes play a key role in interannual variability of SSTs in this region. For example, year-to-year variability in currents and ocean eddies can be seen in satellite snapshots of SSTs during a strong meandering of the Kuroshio current (Fig. 0.2). Note that ocean eddy variability as exemplified by Fig. 0.2 generally occurs at mesoscales (10–100km) in contrast to variability in atmospheric eddies, which generally occurs at synoptic spatial scales ($\sim$ 1000 km). This is because the Rossby radius of deformation (i.e. a length scale at which planetary rotational effects become dynamically important) is about an order of magnitude smaller in the ocean relative to the atmosphere. In general, substantial progress has been made in understanding the role of ocean dynamics in SST variability in the Kuroshio region and other western boundary current regions, however the role that such extratropical ocean-driven SST variability plays in driving variability in the atmosphere and hence climate is not well-understood. This topic is the focus of Chapter 4.

1.3 Outline of dissertation

Overall, it is unclear whether the ocean primarily behaves passively (Fig. 0.1a), or whether ocean dynamics have an important role in driving climate variability observed in nature

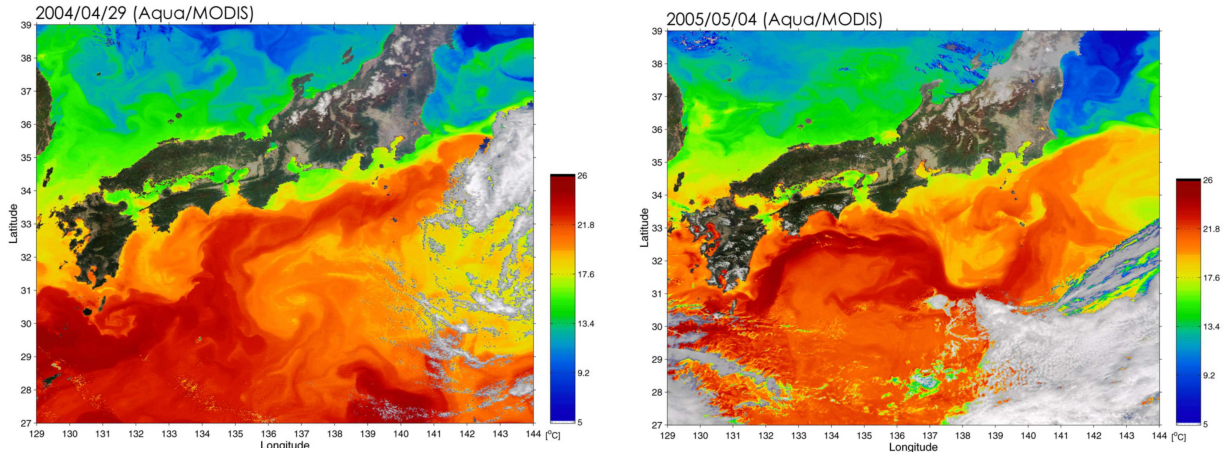

Figure 0.2: Satellite snapshots of SSTs in the Kuroshio current region observed by Aqua/MODIS during 2004/04/29 (left) and 2005/05/04 (right). These plots have been sourced from https://www.eorc.jaxa.jp/en/earthview/2005/tp050620.html

(Fig. 0.1b). In order to address this outstanding issue, this dissertation is focussed on addressing the two following general questions:

1. What is the role of ocean dynamics in SST variability? For example, to what extent do ocean dynamics increase/decrease SST variance, and what is the regional/timescale dependency? (Chapter 2 and Chapter 3)

2. What are the impacts of midlatitude ocean-driven SST variability on the atmosphere? (Chapter 4)

In Chapter 2, the role of ocean dynamics in ocean mixed-layer temperature variance is quantified across the global oceans using a variety of methods and observationally-based products. Chapter 3 and Chapter 4 focus on the role of midlatitude ocean dynamics in climate variability, where there are large gaps in knowledge. In Chapter 3, a simple climate model is used to better understand the role of ocean dynamics in midlatitude SST variability, and in Chapter 4, a novel method is applied to study the impacts of midlatitude ocean-driven SST anomalies on the atmospheric circulation.

Chapter 2

Quantifying the Role of Ocean Dynamics in Ocean Mixed-Layer Temperature Variability

2.1 Introduction

As highlighted in the introduction of this dissertation, the role of ocean dynamics in ocean-mixed layer and hence sea-surface temperature (SST) variability is not well-understood. It is clear that ocean dynamical processes are fundamental to the El Niño-Southern Oscillation (ENSO) (e.g. Philander, 1983; Jin, 1997; McPhaden et al., 2006), but it is less clear whether they play a similarly important role in SST variability outside of the Tropical Pacific. If the SST variability over a particularly region is driven predominantly by the surface heat fluxes associated with atmospheric processes, then the ocean plays a relatively passive role in climate variability. But if the SST variability is also driven by ocean dynamical processes, then the ocean can play a much more active role in the climate system.

In Chapter 2, this issue is addressed by quantifying the role of ocean dynamics in ocean mixed-layer temperature variability across the global oceans. Note that this work has been published in Journal of Climate (Patrizio and Thompson, 2021a). First, some of the most basic theories of SST variability are reviewed before summarizing key studies on the role of ocean dynamics in SST variability.

The basic role of the ocean in SST variability can be conceptualized from the simple models shown in Fig. 2.1. In both models, variations in SSTs are assumed to be linearly proportional to variations in mixed-layer temperatures. In the simplest model (Fig. 2.1a), atmospheric temperatures (T_a) are driven by atmospheric heat transport by weather (F_a), and ocean mixed-layer temperatures (T_o) are, in turn, driven by the resulting turbulent and radiative fluxes of heat at the sea-surface ($Q_s\,(F_a)$). Mixed-layer temperatures are

damped by the linear term ($-\lambda_o T_o$), which parametrizes the damping due to the surface heat fluxes. The atmospheric forcing term (F_a) is a representation of weather, and so it is often assumed to be a stochastic (i.e. random) process. This means that its variance is uniformly distributed across all timescales and hence has a *white* power spectrum. In this model, the high-frequency component of the atmospheric forcing variability is suppressed by the large heat capacity of the mixed-layer (C_o), yielding a *reddened* SST response. Note that, in contrast to a white power spectrum, a red power spectrum has more low-frequency variance than high-frequency variance. The reddening process of the ocean mixed-layer thus yields SST variability with more memory (i.e. autocorrelation) than the atmospheric forcing variability, where the reddening is a function of the heat capacity thus the depth of the mixed-layer.

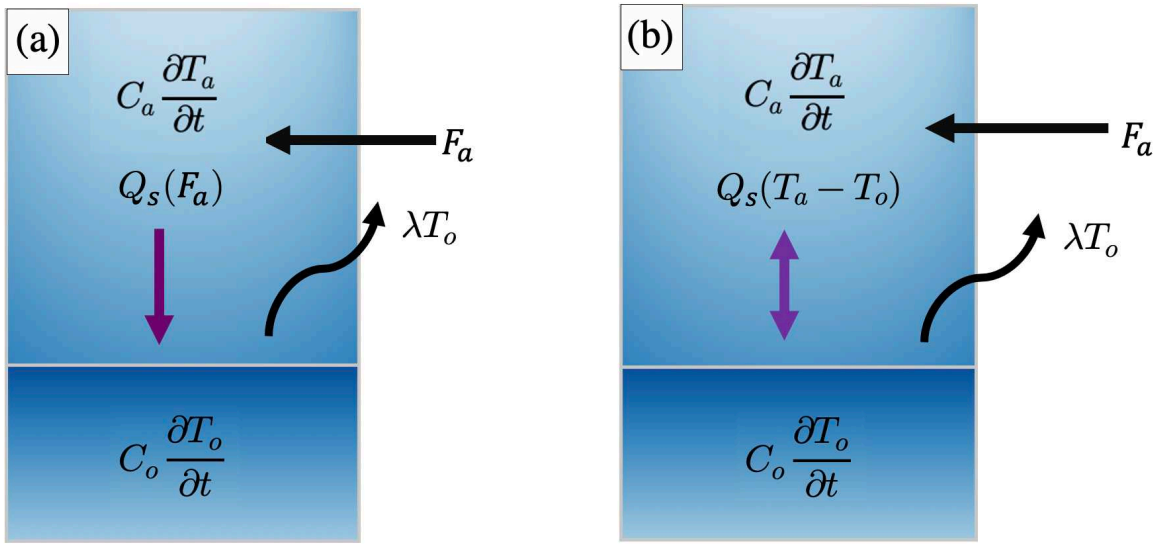

Figure 2.1: Passive ocean mixed layer models. (a) atmospheric-noise forced ocean mixed layer (e.g. Frankignoul and Hasselmann, 1977) and (b) thermally-coupled ocean mixed layer (e.g. Barsugli and Battisti, 1998). F_a is the atmospheric heat transport Q_s is the surface heat flux (latent, sensible and radiative), Q_o is the ocean heat transport, C_a and C_o are the heat capacities of the mixed layer and ocean, respectively. T_a and T_o are mixed layer and atmospheric temperatures, respectively, and λ is the mixed layer damping parameter. The models are discussed in more detail in the text.

A more realistic model of the mixed-layer can be formed by allowing temperatures in the atmosphere and ocean to respond to each other (Fig. 2.1b; Barsugli and Battisti, 1998). In this case, the surface fluxes between the atmosphere and ocean respond to the temperature difference between both media ($Q_s\,(T_a - T_o)$). This thermodynamic coupling between atmosphere and ocean surface temperatures results in reduced thermal damping, which acts to redden the variance of not only SSTs but also atmospheric temperatures.

Whether coupled (Barsugli and Battisti, 1998) or uncoupled (Hasselmann, 1976), these simple models of SST variability can be considered to be passive ocean models in that they do not include ocean dynamical processes. Despite their simplicity, such models are able to capture some aspects of climate variability, such as the observed power spectrum of midlatitude SSTs (e.g. Frankignoul and Hasselmann, 1977; Frankignoul, 1985; Barsugli and Battisti, 1998) and the covariability between the surface heat fluxes and SSTs (e.g. Cayan, 1992a,b). As such, these passive ocean models are often used as a starting point for understanding atmosphere-ocean interaction, especially in the extratropics where atmospheric weather drives large variations in the surface heat fluxes (e.g. Hasselmann, 1976; Frankignoul and Hasselmann, 1977).

However, there is increasing evidence that ocean dynamical processes play an important role in SST variability even in the extratropics. For example, Deser et al. (2003) and De Coëtlogon and Frankignoul (2003) demonstrated that the memory of midlatitude SST anomalies is enhanced from one winter to the next via the "reemergence" mechanism, whereby winter SST anomalies are sequestered at depth through the summer and then entrained into the mixed layer during the following winter. Roberts et al. (2017) estimated the ocean heat transport as a residual in the mixed layer energy budget, and argued that ocean dynamics play an important role in driving interannual variability of upper-ocean temperatures in the western boundary currents and the Antarctic circumpolar current. Bishop et al. (2017) and O'Reilly and Zanna (2018) estimated the role of ocean heat transport from the lead-lag correlations between observed surface heat fluxes and SSTs across the global oceans, and

reached broadly similar conclusions. Buckley et al. (2014, 2015) estimated ocean heat transport directly from an observation-assimilating ocean model and found that ocean dynamics play a dominant role in driving interannual variability in upper-ocean temperatures in the Gulf Stream and North Atlantic subpolar gyre. Numerous studies have also shown that mesoscale ocean dynamics play an important role in driving midlatitude atmosphere-ocean interactions in both observations (e.g. Small et al., 2008; Frenger et al., 2013; Ma et al., 2015) and global climate models (e.g. Kirtman et al., 2012; Ma et al., 2016; Siqueira and Kirtman, 2016; Putrasahan et al., 2017; Saravanan and Chang, 2019; Small et al., 2019b,a; Bellucci et al., 2020).

Despite rapid improvements in our understanding of the role of ocean dynamics in SST variability, key aspects remain unclear. In large part, this is due to the difficulties inherent in observing and simulating ocean variability. Consider, for example, the cases of decadal SST variability in the North Pacific and North Atlantic oceans. The most important pattern of decadal variability in the North Pacific sector is known as the Pacific Decadal Oscillation (PDO; Mantua et al., 1997). Both atmospheric and ocean dynamical processes seemingly contribute to the PDO, but their relative roles remain uncertain. Some studies have argued that the PDO is driven primarily by internal atmospheric dynamics and the extratropical atmospheric response to ENSO (e.g. Alexander et al., 2002; Newman et al., 2003; Deser et al., 2004). But others have argued that the PDO is also driven by ocean dynamical processes such as dynamic adjustment of the North Pacific gyre and Kuroshio Extension (e.g. Latif and Barnett, 1994; Schneider et al., 2002; Qiu et al., 2007; Kwon and Deser, 2007; Alexander et al., 2010; Newman et al., 2016; Wills et al., 2019b) and the seasonal reemergence of North Pacific SSTs (Alexander and Deser, 1995; Deser et al., 2003; Alexander et al., 2010; Newman et al., 2016)

The picture is even less clear in the case of Atlantic Multidecadal Variability (AMV). Several studies have argued that the spatial structure and time variability of AMV are due primarily to atmospheric processes. As evidence they note that 1) the structure of the

AMV can be recovered in numerical simulations run on slab-ocean models (Clement et al., 2015), 2) the lag-relationships between the surface heat fluxes and SSTs associated with the AMV can be recovered in idealized models of the mixed-layer that are primarily forced by stochastic atmospheric dynamics as shown in Fig. 2.1a (Cane et al., 2017) and 3) AMV is consistent with the surface temperature response to the radiative effects of anthropogenic aerosol emissions (Booth et al., 2012; Murphy et al., 2017; Bellomo et al., 2018). However, other studies have argued that the AMV is fundamentally dependent on ocean dynamical processes. As evidence they argue that 1) in observations, the surface-heat fluxes act to damp rather than drive the SST anomalies associated with the AMV (e.g. Gulev et al., 2013; O'Reilly et al., 2016; Zhang et al., 2016; Zhang, 2017) and 2) in numerical models, the ocean meridional overturning circulation contributes to variations in the simulated AMV (e.g. Zhang and Wang, 2013; Buckley and Marshall, 2016; Delworth et al., 2017; Zhang, 2017; Kim et al., 2018; Yan et al., 2018; Wills et al., 2019a; Zhang et al., 2019). Whether ocean dynamical processes contribute to SST anomalies associated with the PDO and AMV has important implications for understanding and predicting the role of both phenomena in the climate system.

The goal of this chapter is to provide a comprehensive survey of the role of ocean dynamics in driving ocean-mixed layer temperature variability across the globe and across a range of timescales. To do so, two different but complementary methods are used: 1) A method in which ocean heat transport is calculated *directly* from a state-of-the-art ocean state estimate, as in (Buckley et al., 2014, 2015) and 2) A method in which the ocean heat transport is calculated *indirectly* from observations and the energy equation for the ocean mixed layer, as in (Roberts et al., 2017). The work extends previous studies in several important ways:

- Previous work based on ocean state estimates has generally focused on select regions (e.g. Buckley et al., 2014, 2015)

- Previous work has not explicitly compared the role of ocean dynamics as inferred from observations with that derived from state estimates (e.g. Roberts et al., 2017; Small et al., 2019b)

- Previous studies have frequently relied on the use of lead/lag correlations to infer causal relationships between the surface heat fluxes and SSTs (e.g. Gulev et al., 2013; O'Reilly et al., 2016; Bishop et al., 2017; O'Reilly and Zanna, 2018). Here we use a diagnostic equation for the temperature variance to infer causal relationships, and highlight shortcomings of results based on lead/lag correlations.

- Previous studies have not explored the role of ocean dynamics in SST variability as a function of time scale using both observations and ocean state estimates across the global ocean. Here we exploit such analyses to reveal novel and important aspects of the role of ocean dynamics in SST variability at increasingly low frequency timescales.

This chapter is divided into four subsequent sections. The Data and Methods are reviewed in Section 2.2. Results are presented in Section 2.3. Key results and findings are discussed in Section 2.4. Section 2.5 provides concluding remarks.

2.2 Methods & Data

This section includes two parts. In Section 2.2.1 we derive the equation that we use to diagnose the drivers of mixed layer temperature variance across the globe. In Section 2.2.2 we describe how the equation is used to estimate ocean heat transport using two different methods: A method where ocean heat transport is estimated directly from an ocean state estimate, and a method where ocean heat transport is estimated indirectly from observed sea surface temperatures/surface heat fluxes and the energy budget of the mixed layer. Note that we do not use lead-lag correlations between the surface heat fluxes and mixed layer temperature variability to infer the role of ocean dynamics in temperature variability, as done by Gulev et al. (2013), O'Reilly et al. (2016), Bishop et al. (2017), and O'Reilly

and Zanna (2018). As discussed in Section 2.4, the use of lead-lag correlations does not unambiguously identify the role of ocean dynamics in mixed layer temperature variability.

2.2.1 The diagnostic equation for mixed layer temperature variance

The details of the following are provided in Appendix A. Here the most salient aspects of the derivation are summarized.

The first law of thermodynamics for month-to-month temperature variability in the ocean mixed layer can be expressed as:

$$\overline{C}_o \frac{\partial T'}{\partial t} = Q'_s + Q'_o \tag{2.1}$$

where primes denote monthly-mean anomalies; the overbar denotes the climatological-mean; C_o is the heat capacity of the mixed layer; T is the monthly-mean mixed layer temperature; Q_s is the net surface heat flux (i.e., the sum of the latent, sensible, net shortwave and longwave fluxes at the surface); and Q_o is the heat flux convergence due to all ocean dynamics, including both advective processes (e.g. wind-driven Ekman flow and geostrophic currents) and diffusive processes. The climatological mean heat capacity of the mixed layer is estimated as $\overline{C}_o = \rho c_p \overline{h}$, where $\overline{h}$ is the climatological-mean mixed layer depth averaged over all months. The mean mixed layer depth is estimated from the ECCO ocean state estimate, as described in the next subsection, and is shown in Fig. 2.2. Note that in the above we have neglected variations in the heat capacity. This is consistent with Roberts et al. (2017) and Buckley et al. (2014), who both used a time-invariant mixed layer depth, except that they use the maximum – rather than mean – mixed layer depth drawn from the 12-month climatology. We found that use of the maximum mixed layer depth leads to a systematic overestimate of ocean mixed heat storage when estimating the heat storage

tendency in observations. It would be interesting to investigate the role of the seasonal cycle in mixed layer depths on the results in future work.

The diagnostic equation for the ocean mixed layer temperature variance is formed by squaring both sides of Eq. (2.1), time averaging, and taking the centered finite difference of the temperature tendency term so that:

$$\sigma_T^2 \approx \frac{2\Delta t^2}{[\overline{C_o}^2\,(1-r_2)]}\left(\overline{Q_s'^2} + \overline{Q_o'^2} + 2\overline{Q_s' Q_o'}\right) \tag{2.2}$$

where σ_T^2 is the mixed layer temperature variance, r_2 is the mixed layer temperature lag-2 autocorrelation and Δt is the sampling time-period (one month). Using Eq. (2.1) to

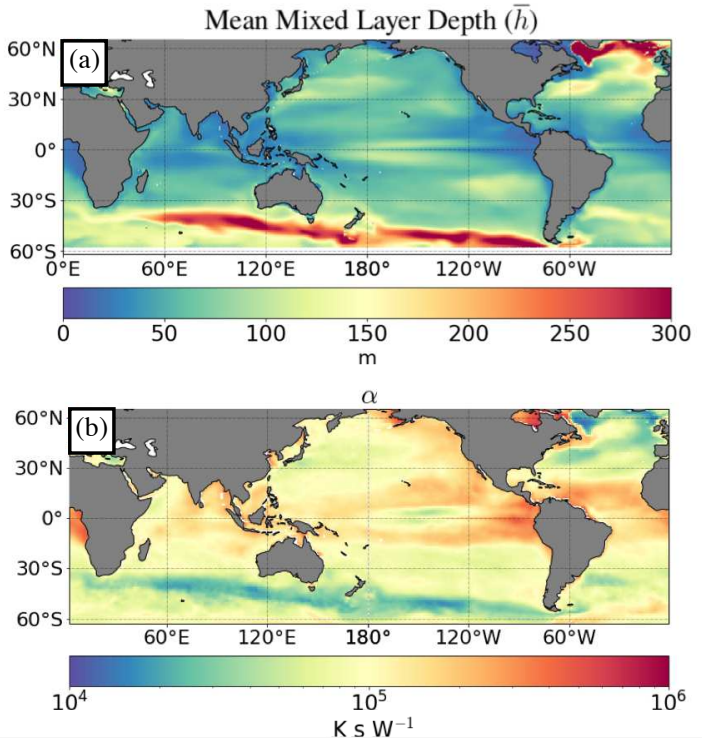

Figure 2.2: (a) Climatological mean mixed layer depth, $\overline{h}$ (m), from ECCO. (b) The α coefficient (K s W-1) from Eq. (2.3) as computed from ECCO mixed layer temperatures and mixed layer depths. As discussed in Section 2.2.1, α corresponds to the ability of surface heat fluxes and ocean heat transport to generate mixed layer temperature variance.

substitute for one $Q'_s + Q'_o$ term in Eq. (2.2) and defining

$$\alpha = \frac{2\Delta t^2}{[\overline{C}_o\,(1 - r_2)]} \tag{2.3}$$

yields the simple diagnostic relationship:

$$\sigma_T^2 \approx \widetilde{Q}_s + \widetilde{Q}_o \tag{2.4}$$

where

$$\widetilde{Q}_s = \alpha\overline{\frac{\partial T'}{\partial t}Q'_s} \tag{2.4a}$$

is defined as the contribution of the surface heat fluxes to the temperature variance and

$$\widetilde{Q}_o = \alpha\overline{\frac{\partial T'}{\partial t}Q'_o} \tag{2.4b}$$

is defined as the contribution of the ocean heat transport to the temperature variance.

Note that from Eq. (2.2), the surface heat flux and ocean dynamical contributions can also be expressed as:

$$\widetilde{Q}_s = \frac{\alpha}{\overline{C}_o}\left(\overline{Q'^2_s} + \overline{Q'_s Q'_o}\right) \tag{2.4c}$$

and

$$\widetilde{Q}_o = \frac{\alpha}{\overline{C}_o}\left(\overline{Q'^2_o} + \overline{Q'_s Q'_o}\right) \tag{2.4d}$$

From Eq. (2.4)a-d, it is clear that the surface heat flux and ocean heat transport contributions to temperature variance can be found as either 1) the product of the temperature (Eq. 2.4a and Eq. 2.4b) or 2) the sum of the variances of the surface heat fluxes/ocean heat

transport and their covariance (Eq. 2.4c and Eq. 2.4d). Here, the contribution of ocean dynamics (or surface heat fluxes) to the monthly-mean mixed layer temperature variance at any given location is found using Eq. (2.4)a and Eq. (2.4)b, that is by calculating the covariance between the ocean heat transport (or surface heat fluxes) and the time tendency of mixed layer temperatures, and scaling the results by α. These equations state that ocean dynamics (or surface heat fluxes) contribute to mixed layer temperature variance in regions where the temperature tendency and ocean heat transport (or surface heat fluxes) are positively correlated. For example: If the heat transport and temperature tendency are both positive, then the diagnostic equation indicates that ocean heat transport is contributing to the temperature variance. The α coefficient, in turn, quantifies the ability of the fluxes or transport to generate temperature variance. As is evident from Fig. 2.2a and Fig. 2.2b, α is dominated by the term $\overline{C}_o^{-1}$ and thus closely resembles the spatial pattern of $\overline{h}^{-1}$. Thus covariability between the fluxes or transport and the temperature tendency are most effective in generating mixed layer temperature variability in regions such as the subtropics and tropics where $\overline{h}$ and thus the heat capacity is small.

As summarized in Appendix A, similar approaches to that outlined above were used by Yu and Boer (2006), Buckley et al. (2014) and Roberts et al. (2017) to understand the drivers of upper-ocean temperature variability.

2.2.2 "Direct" and "indirect" methods for estimating ocean heat transport

The contributions of the surface heat fluxes and ocean heat transport to mixed layer temperature variance (i.e. $\widetilde{Q}_s$ and $\widetilde{Q}_o$, respectively) are quantified from Eq. (2.4)a,b using two methods: 1) a method in which the ocean heat transport Q'_o is estimated directly from the ECCO ocean state estimate and 2) a method in which the ocean heat transport Q'_o is estimated indirectly from observations and the energy budget of the ocean mixed layer. In all analyses, the seasonal-cycle is removed from the data by subtracting the long-term,

climatological-means for each calendar month. All time series are detrended to minimize the effects of climate change on the results. A Butterworth filter is applied in cases where results are calculated as a function of frequency band. In this case, the temperature and flux data are filtered before calculating all covariances.

In the case where the ocean heat transport is calculated directly, the surface heat fluxes (Q'_s), ocean heat transport (Q'_o), mixed layer temperatures (T') are all derived from v4r3 of the ECCO ocean state estimate (Forget et al., 2015; Fukumori et al., 2017). ECCO provides estimates of ocean heat transport, temperature and the surface fluxes for 1992-2015 at 1° horizontal resolution throughout the global ocean. In brief, the ECCO output is produced as follows (see Forget et al., 2015 and Fukumori et al., 2017 for more details). First, a vast quantity of ocean observations are fit in a least-squares sense to a state-of-the-art ocean GCM (the MITgcm). The best fit to the observations is accomplished by iteratively adjusting the model initial conditions, mixing coefficients, and surface forcings. Note that the ECCO surface fluxes are included in the adjustment. The adjusted input are then integrated forward in a free-running configuration of the MITgcm to produce the ocean state estimate. The key aspects of the ECCO output are that 1) the fitting procedure ensures that the output is consistent with the observations within their estimated uncertainties and 2) running the model in a free-running configuration ensures that the output is consistent with the laws of physics and thermodynamics, as they are represented in the numerical model. The temperature profiles used to constrain the model are sourced from gridded products (e.g. Reynolds et al., 2007), as well as a variety of in-situ measurements, including from Argo floats (Argo, 2000), expendable bathythermographs (XBT), and conductivity-temperature-depth (CTD) sensors.

In the case where the ocean heat transport is estimated indirectly, the surface heat fluxes and sea surface temperatures are estimated from observations, and the ocean heat transport is found as a residual in the energy budget of the ocean mixed layer (i.e., Eq. 2.1). The primary data sources are the objectively-analyzed surface turbulent heat fluxes (i.e., the sum

of the latent and sensible heat fluxes) and SSTs from OAFlux (Yu et al., 2008), and surface radiative heat fluxes and wind stress from MERRA-2 reanalysis (Gelaro et al., 2017). Note that the OAFlux SSTs are from the NOAA Optimum Interpolation (OI) 0.25° SST analysis produced by Reynolds et al. (2007) that has been averaged onto a 1° degree grid. We use the OAFlux product since it provides global coverage of the air-sea heat fluxes across multiple decades and is derived using state-of-the-art bulk flux parameterizations (Yu et al., 2008). All data are applied over the period 1980-2017 and at 1° resolution. For brevity we refer to the combined OAFlux/MERRA-2 data as the "OAFlux" dataset throughout the rest of the paper, although it should be understood that radiative fluxes are from MERRA-2. We also tested the robustness of select OAFlux results to the use of different atmospheric reanalyses, including MERRA-2, ERA5 (Hersbach and Dee, 2016), and NOAA-CIRES-DOE Twentieth Century Reanalysis, V3, (Slivinski et al., 2019).

Note that indirect estimates of ocean heat transport are inevitably influenced by biases in the SST and surface heat flux data (e.g. Hall and Bryden, 1982; Talley, 1984; Bryden and Imawaki, 2001). The uncertainties in the OAFlux air-sea heat fluxes due to biases in the various input data are provided in the OAFlux product. The contributions of observational error to uncertainties in the mixed layer temperature variance (i.e. uncertainty in Eq. 2.4a and Eq. 2.4b) is reviewed in Appendix A.

The equations used to estimate ocean heat transport and temperature variance (Eqs. 2.1-2.4) are based on mixed layer temperatures, but we use observations of sea surface temperatures since mixed layer temperatures are not as widely available. Sea surface and mixed layer temperatures are linearly related to each other but have different amplitudes. For example, Fig. 2.3a shows the SST variances (σ^2_{SST}) from the OAFlux product and Fig. 2.3b the mixed layer temperature variances (σ^2_T) from ECCO. The patterns of the variances are nearly identical, with maxima in the western boundary currents and the equatorial Pacific. However, as shown in Fig. 2.3d, the amplitudes are very different, with larger SST variances found at subtropical and extratropical latitudes but larger mixed layer temperature variances found

in the deep tropics. Note that a very similar pattern of variance ratios arises between mixed layer and sea surface temperatures derived from ECCO (Fig. 2.3e), which reveals that the differences in Fig. 2.3d are not solely a result of differences between the ECCO SST and OAFlux SST.

From Fig. 2.3d, it is clear that using SSTs rather than mixed layer temperatures in Eq. (2.1) would systematically overestimate the importance of ocean heat transport in the extratropics but underestimate it in the tropics. To avoid this bias, we linearly scale the observed SST tendencies by the square root of the ratio of the 1) ECCO mixed layer temperature variance to 2) the ECCO SST variance. That is, we estimate the observed mixed

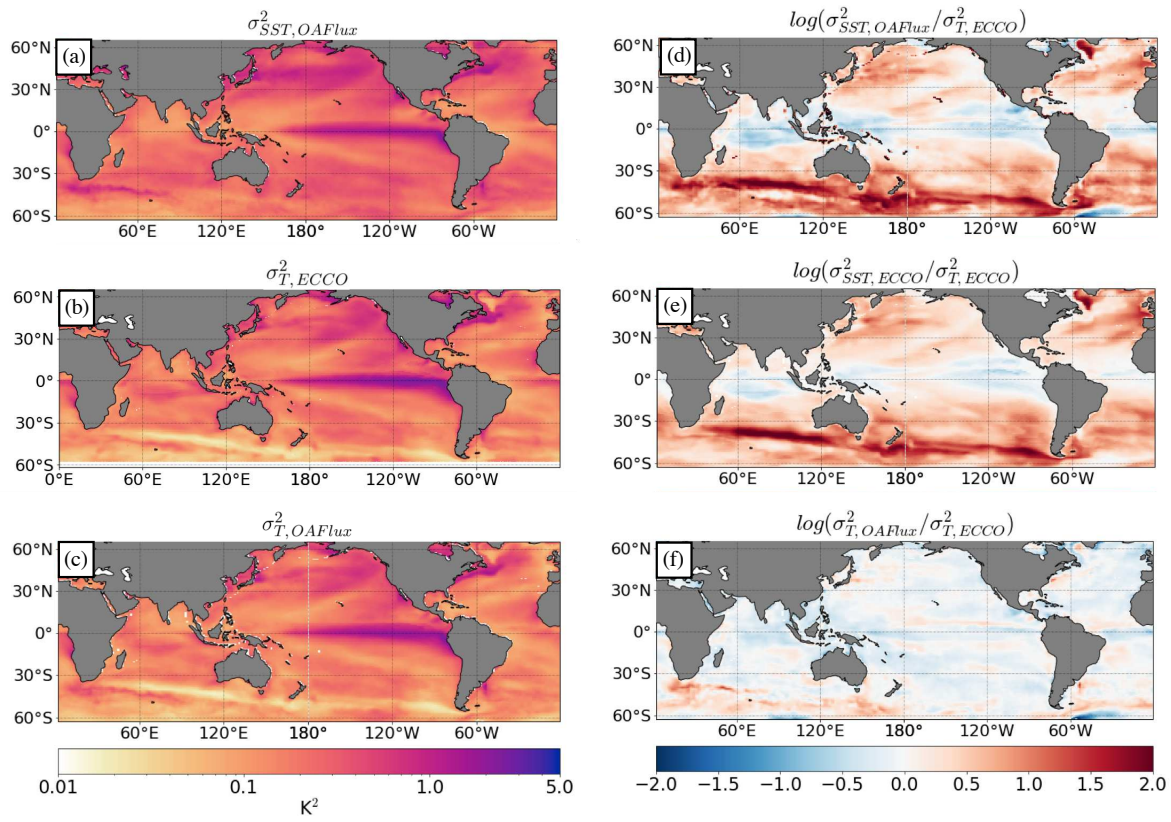

Figure 2.3: (a) Monthly SST variance (K^2) from OAFlux. (b) Monthly mixed layer temperature variance (K^2) from ECCO. (c) OAFlux estimate of monthly mixed layer temperature variance (K^2) from equation (Eq. 2.5). (d) Log-ratio of the OAFlux monthly SST variance to the ECCO monthly mixed layer temperature variance. (e) Log-ratio of the ECCO monthly SST variance to the ECCO monthly mixed layer temperature variance (K^2). (f) Log-ratio of the OAFlux estimate of monthly mixed layer temperature variance to the ECCO monthly mixed layer temperature variance (K^2).

layer temperature tendencies for Eq. (2.1) as:

$$\frac{\partial T}{\partial t} = \sqrt{\frac{\sigma^2_{T,\,\mathrm{ECCO}}}{\sigma^2_{SST,\,\mathrm{ECCO}}}}\frac{\partial SST}{\partial t} \tag{2.5}$$

where T denotes mixed layer temperatures. The above scaling provides an estimate of the "observed" mixed layer temperature tendencies that a) are perfectly correlated with the observed SST tendencies and b) preserve the ratio of SST variances to mixed layer temperature variances found in ECCO. Figure 2.3c shows the resulting "observed" mixed layer temperature variances and Fig. 2.3f shows the corresponding (log) ratio of the observed to ECCO mixed layer temperature variances. The differences between the OAFlux estimate of σ^2_T and the ECCO σ^2_T are generally small.

Select results are reproduced using mixed layer temperatures derived from version 4.1.1 of the Met Office Hadley Centre gridded analyses of in-situ ocean temperature profiles (EN4; Good et al., 2013). The main sources for EN4 analyzed temperature profiles are the World Ocean Database (WOD09; Boyer et al., 2009), the Global Temperature and Salinity Profile Program (GTSPP) (U.S. National Oceanographic Data Center, 2006), and Argo floats. The EN4 temperature profiles provide an additional residual estimate of ocean heat transport based on observed mixed layer rather than sea surface temperatures.

2.3 Results

2.3.1 Diagnosis of monthly-mean mixed layer temperature variability

Figure 2.4a,b shows the variances of ocean mixed layer temperatures from the observations (left) and ECCO output (right). Recall that the observed mixed layer temperature variances are derived from observed SSTs using Eq. (2.5). Figure 2.4c-f shows the associated contributions of ocean dynamics and the surface heat fluxes to the temperature variances ($\widetilde{Q}_o$ and $\widetilde{Q}_s$). As a check on the analyses, we confirmed that the sums of $\widetilde{Q}_s$ and $\widetilde{Q}_o$ are equal

to the total variances in the top row. Figure 2.5a-d shows the same results as Fig. 2.4c-f, but here the ocean dynamical and surface heat flux contributions are shown as a fraction of the total temperature variances. Recall that 1) the ocean dynamical contributions include heat transport by both advection and diffusion and 2) the surface fluxes are a combination of the radiative fluxes and the turbulent fluxes of latent and sensible heat. The decomposition of the ocean dynamical contributions into its various components is discussed further below.

The ocean dynamical contributions to mixed layer temperature variance provided by the observations and ECCO exhibit similar patterns but different amplitudes (Fig. 2.4c and Fig. 2.4d). Both methods indicate that ocean dynamics contribute most to mixed layer temperature variance in the vicinity of the Kuroshio current region and its downstream extension; the Gulf Stream current and its extension; the Agulhas return current (i.e., a segment of the major western boundary current in the South Indian Ocean); the Malvinas current (i.e., a segment of the major western boundary currents in the South Atlantic Ocean); and in various regions throughout the tropics, including the eastern tropical Pacific and the equatorial Atlantic. The most pronounced differences between the methods are found in the extratropics, where the observational estimates of the ocean dynamical contributions are nearly twice as large as the ECCO-based estimates. The differences are even more clear when the ocean dynamical contributions are shown as a fraction of the total variances in mixed layer temperatures (Fig. 2.5a,b).

The surface heat flux contributions provided by the observations and ECCO likewise exhibit similar spatial patterns but different amplitudes (Fig. 2.4e,f). Both methods indicate that the surface fluxes act to drive SST variability (i.e., they are positive) everywhere except in the equatorial cold tongue regions, where they act to damp SST variability. Both observations and ECCO also indicate maxima in $\widetilde{Q}_s$ in the subtropics, which are most clear when $\widetilde{Q}_s$ is scaled by the total temperature variances (Fig. 2.5c,d). The subtropical maxima are consistent with large variability in the latent heat fluxes at subtropical latitudes (e.g. Chiang and Vimont, 2004; Xie and Carton, 2004; Amaya et al., 2017). As anticipated, the

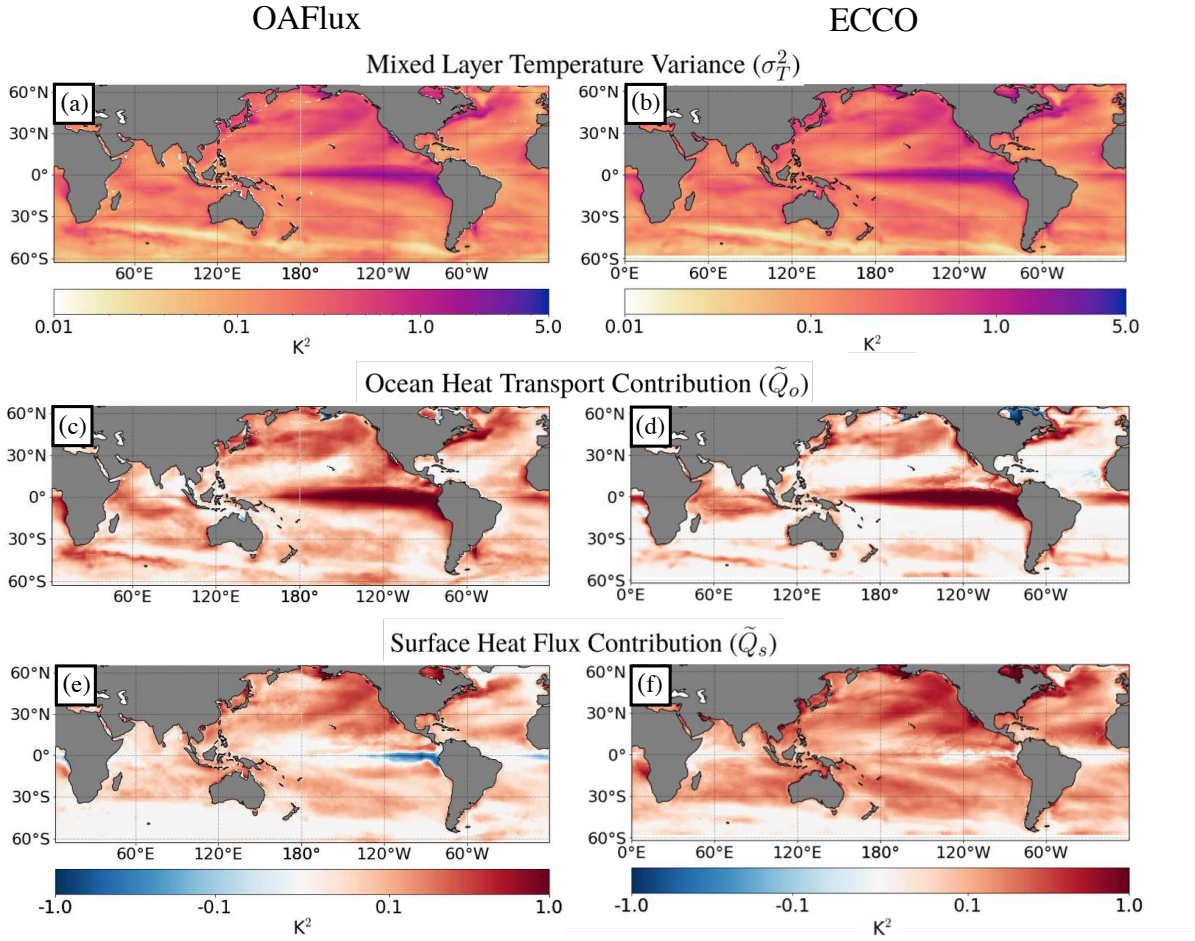

Figure 2.4: (a), (b) Monthly mixed-layer temperature variance (σ_T^2; K^2) from OAFlux and ECCO, respectively. As discussed in Section 2.2.2, the OAFlux mixed-layer temperature variance is estimated from Eq. (2.5). (c), (d) Ocean heat transport contribution to mixed-layer temperature variance ($\widetilde{Q}_o$; K^2) derived from the indirect method using OAFlux and the direct method using ECCO. (e), (f) Surface heat flux contribution to mixed-layer temperature variance ($\widetilde{Q}_s$; K^2) for OAFlux and ECCO.

most pronounced differences between the observational and ECCO-based results are again found in the extratropics, where the ECCO-based estimates of $\widetilde{Q}_s$ are roughly twice as large as the observational-based estimates (Fig. 2.5c,d). Note that in general, the surface flux results in Fig. 2.5 are dominated by the turbulent fluxes of latent and sensible heat, and that the radiative fluxes play a relatively small role.

The relative importance of the surface heat fluxes and ocean heat transport for mixed layer temperature variability is summarized in Fig. 2.5e-f, which show the differences in the fractional contributions from the top panels. Warm colors indicate regions where the surface heat fluxes account for a larger fraction of the mixed layer temperature variance than ocean dynamics, and vice versa. Both the observational and ECCO-based results indicate that ocean heat transport dominates mixed layer temperature variability in the tropical oceans (blue shading in Fig. 2.5e and Fig. 2.5f). But as noted above, the two methods differ widely in the extratropics. The observations suggest that ocean dynamics account for a slightly larger fraction of the temperature variance than the surface heat fluxes over most of the extratropics (Fig. 2.5e). In contrast, the ECCO-based results suggest that the surface heat fluxes account for the predominance of the temperature variance at extratropical latitudes (Fig. 2.5f), with notable exceptions found in major current regions such as the Kuroshio, Gulf Stream, Aghulas, Malvinas and the Antarctic circumpolar currents.

Figures 2.6 and 2.7 explore the decomposition of the total ocean heat transport contributions into various physical processes. The top row in Fig. 2.6 shows the total ocean dynamical contributions reproduced from Fig. 2.4c,d. Subsequent rows show the contributions from the horizontal Ekman heat transport computed using the surface wind stresses from MERRA-2 (Fig. 2.6c) and ECCO (Fig. 2.6d), and the residuals due to all other ocean dynamical processes, found as the differences between the top and middle panels (Fig. 2.6e,f). Figure 2.7 shows a different decomposition of the ocean dynamical contributions based on the ECCO estimates of diffusive and advective heat transport. Here the top panel shows the total ocean dynamical contributions from ECCO (reproduced from Fig. 2.4d and Fig. 2.6b).

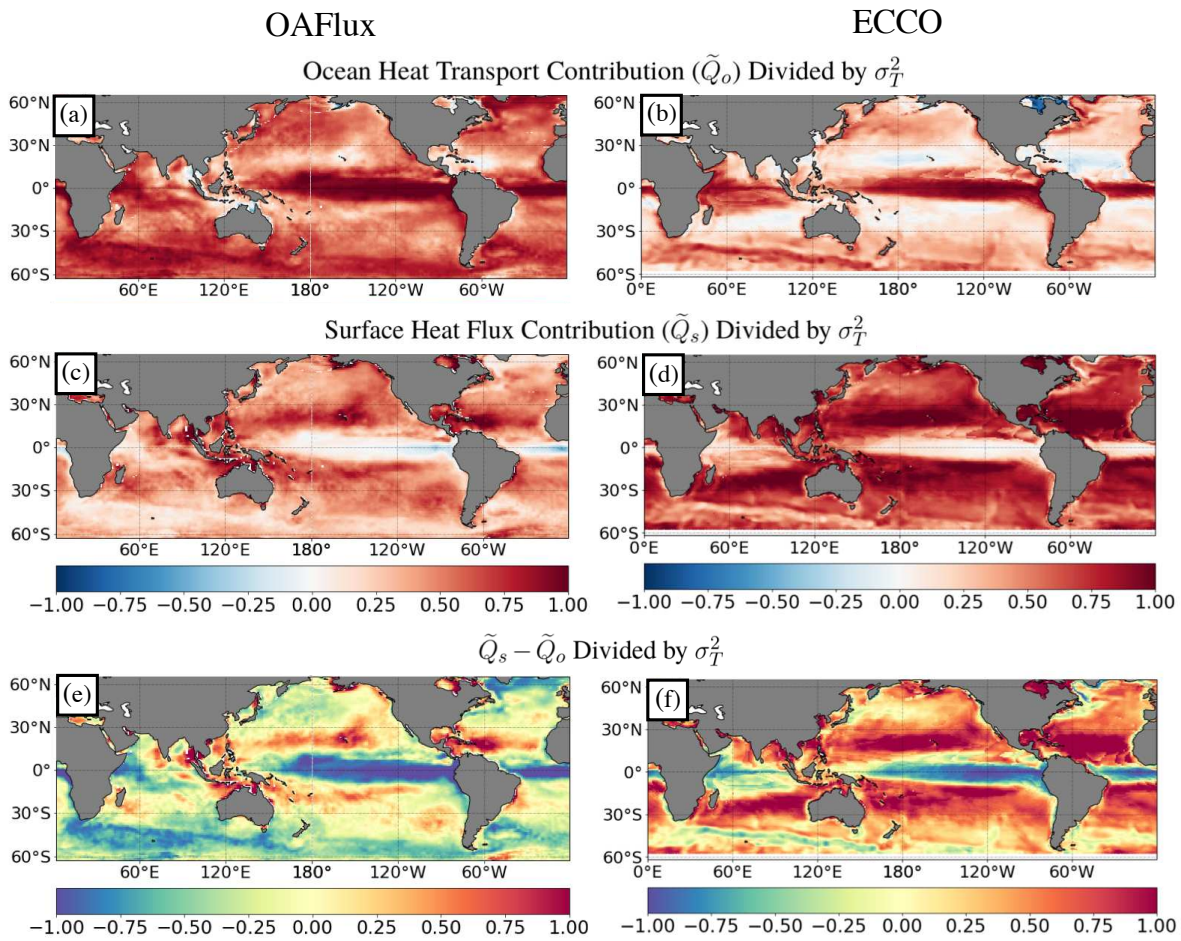

Figure 2.5: (a)-(d) As in Fig. 2.4c-e, except results are divided by the mixed-layer temperature variance (σ_T^2). (e), (f) The difference between the surface heat flux contribution and the ocean heat transport contribution ($\widetilde{Q}_s$ - $\widetilde{Q}_o$) divided by the mixed-layer temperature variance using the indirect method (OAFlux) and the direct method (ECCO). Warm colors: surface heat flux contribution is dominant, cool colors: ocean heat transport contribution is dominant.

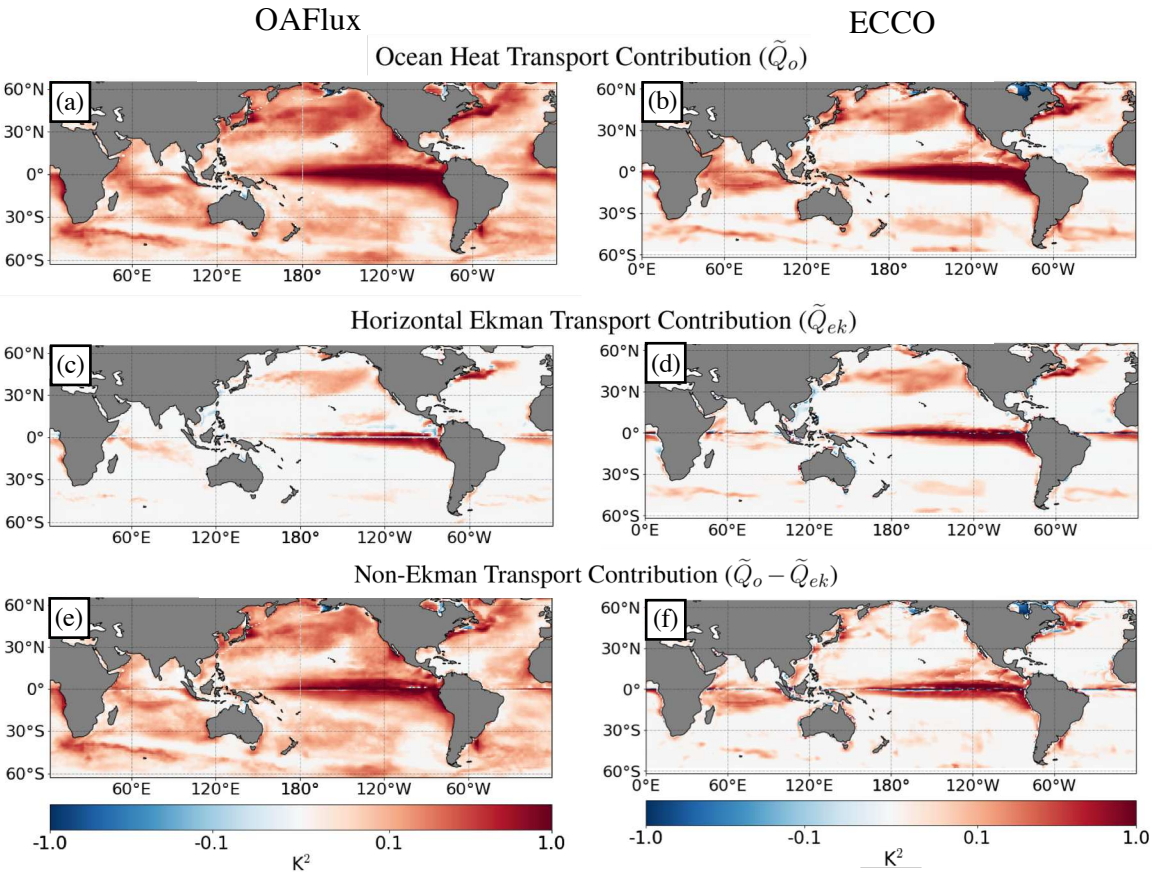

Figure 2.6: (a), (b) Ocean heat transport contribution to mixed-layer temperature variance ($\widetilde{Q}_o$; K^2) derived from the indirect method using OAFlux and the direct method using ECCO, respectively. (c), (d) Horizontal Ekman transport contribution to mixed-layer temperature variance ($\widetilde{Q}_{ek}$; K^2), calculated using surface wind stress from MERRA-2 reanalysis in (c) and surface wind stress from ECCO in (d). (e), (f) Non-Ekman transport contribution to mixed-layer temperature variance ($\widetilde{Q}_o - \widetilde{Q}_{ek}$; K^2), calculated as the difference between the top and middle panels for OAFlux and ECCO, respectively.

But now the middle panel shows the components due to diffusive mixing (Fig. 2.7b) and the bottom panel the components due to advective heat transport (Fig. 2.7c). Note that Fig. 2.7b includes mixing due to convective processes and parameterized isopycnal diffusion (Redi, 1982; Gaspar et al., 1990), whereas Fig. 2.7c includes advective heat transport due to explicitly resolved large-scale currents and eddy-induced transport as parameterized by the Gent and McWilliams (1990) scheme.

The observational and ECCO-based estimates of horizontal Ekman heat transport are nearly identical (Fig. 2.6c,d). Hence, the resulting residual contributions from all other ocean dynamical processes differ greatly between the two methods (Fig. 2.6e,f). As such, the horizontal Ekman heat transport accounts for roughly half of the total ocean dynamical contributions to mixed layer temperature variability in the ECCO product, but a much smaller fraction of the total ocean dynamical contributions in the observations. Additionally, the differences in the total ocean dynamical contributions to SST variability shown in Fig. 2.6a,b arise almost entirely from non-Ekman processes. As evidenced in Fig. 2.7, diffusive processes account for a very small fraction of the temperature variance on monthly-mean timescales. However, as shown in the next section, diffusive processes play a more important role on lower frequency timescales.

The results in Figs. 2.4 to 2.7 provide novel and comprehensive estimates of the ocean dynamical contributions to mixed layer temperature variability. They are broadly consistent with results shown in recent studies (e.g. Bishop et al., 2017; Roberts et al., 2017; Small et al., 2019b), and indicate that ocean dynamics play an important role in monthly-mean mixed layer temperature variability in equatorial regions and in the vicinity of the major extratropical boundary currents. However, the results also reveal important inconsistencies in the ocean dynamical contributions estimated from observations and the ECCO product. In general, the observations suggest a much larger role for ocean dynamical processes in SST variability than the ECCO output does. The inconsistencies have potentially important implications for our understanding of the role of the ocean in extratropical climate variability.

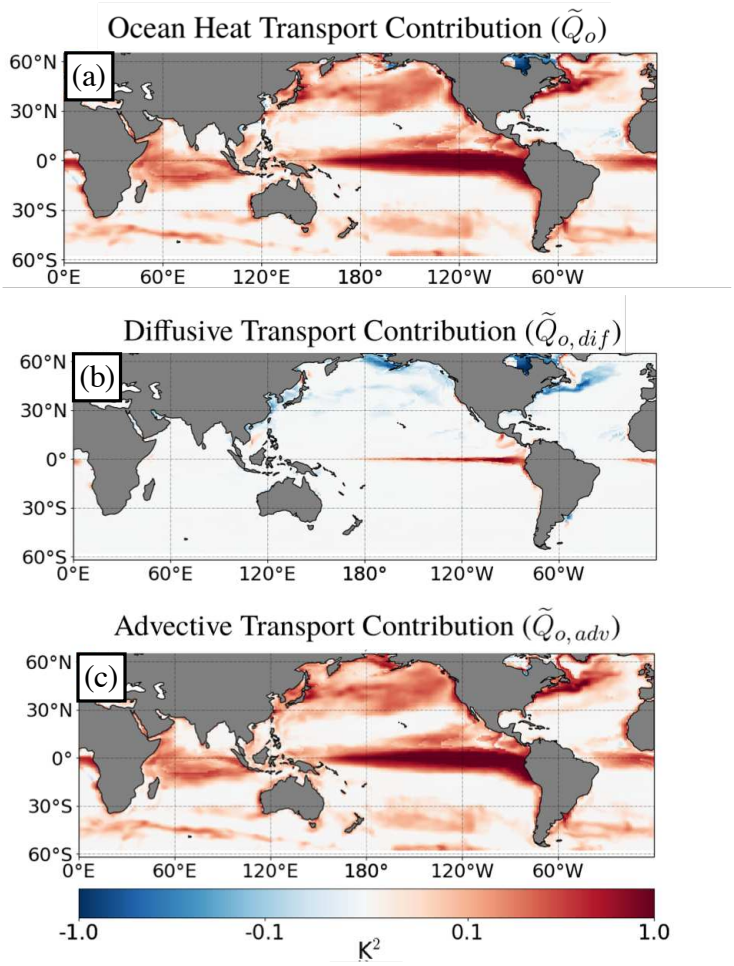

Figure 2.7: (a) Ocean heat transport contribution to mixed-layer temperature variance from ECCO (repeated from Fig. 2.6b). (b), (c) The components of the contribution due to diffusive heat transport ($\widetilde{Q}_{o,dif}$; K^2) and advective heat transport ($Q_{o,adv}$; K^2).

It is unclear why the observations suggest a larger role for ocean dynamical processes. One possible explanation is that the 1° ECCO product used here underestimates the role of mesoscale ocean dynamics in driving mixed layer temperature variability. Mesoscale ocean processes play an important role in facilitating atmosphere-ocean interactions (Ma et al., 2016; Siqueira and Kirtman, 2016; Saravanan and Chang, 2019; Small et al., 2019b,a) and substantial differences in vertical and horizontal ocean heat transports arise in simulations with fine ($\sim 0.1°$) ocean resolution relative to more coarse ($\sim 1°$) resolution (Griffies et al., 2015). It would be interesting to assess higher-resolution ocean state estimates using the methods described in this study in future work.

2.3.2 Timescale dependence

Here we explore the contributions of ocean dynamics to mixed layer temperature variance in data that have been low pass filtered with a Butterworth recursive filter. Note that the temperature and flux data are filtered before calculating the covariances in Eq. (2.4). We first explore the spatial patterns of four-year low-pass filtered variability. We then explore the sensitivity of the results to different filter cut-offs. As done above for unfiltered data, it has been confirmed that the sums of $\widetilde{Q}_s$ and $\widetilde{Q}_o$ are equal to the total variances in all low-pass filtered results.

Fig. 2.8a,b show the 4-year low-pass filtered mixed layer temperature variances from the observations and ECCO products. In general, the low-pass filtered variances are very similar to their unfiltered counterparts, albeit with small amplitudes (compare Fig. 2.4a,b and Fig. 2.8a,b). Both exhibit centers of action in the eastern tropical Pacific, the extra-tropical North Pacific and the vicinity of the Gulf Stream and its extension. In contrast, the contributions of ocean dynamics to the temperature variances (Fig. 2.8c,d) are dramatically different between the low-pass filtered and unfiltered data, particularly in the Northern Hemisphere. Ocean dynamics act to enhance mixed layer temperature variability throughout the NH when all timescales are included in the analysis (Fig. 2.4c,d). In contrast, they

appear to oppose mixed layer temperature variance in regions throughout the North Pacific and in the Gulf Stream extension region of the North Atlantic on timescales longer than 4 years (Fig. 2.8c,d). The result is reproducible in both the observations and ECCO output. Thus the discrepancies between the observed and ECCO-derived estimates of $\widetilde{Q}_o$ highlighted in Fig. 2.4 are primarily due to ocean dynamics on timescales between one-month and four years.

The apparent suppression of multiannual mixed layer temperature variance by ocean dynamics in the North Pacific and North Atlantic is surprising. Ocean dynamics are generally believed to play an increasingly important role in SST variability on low-frequency

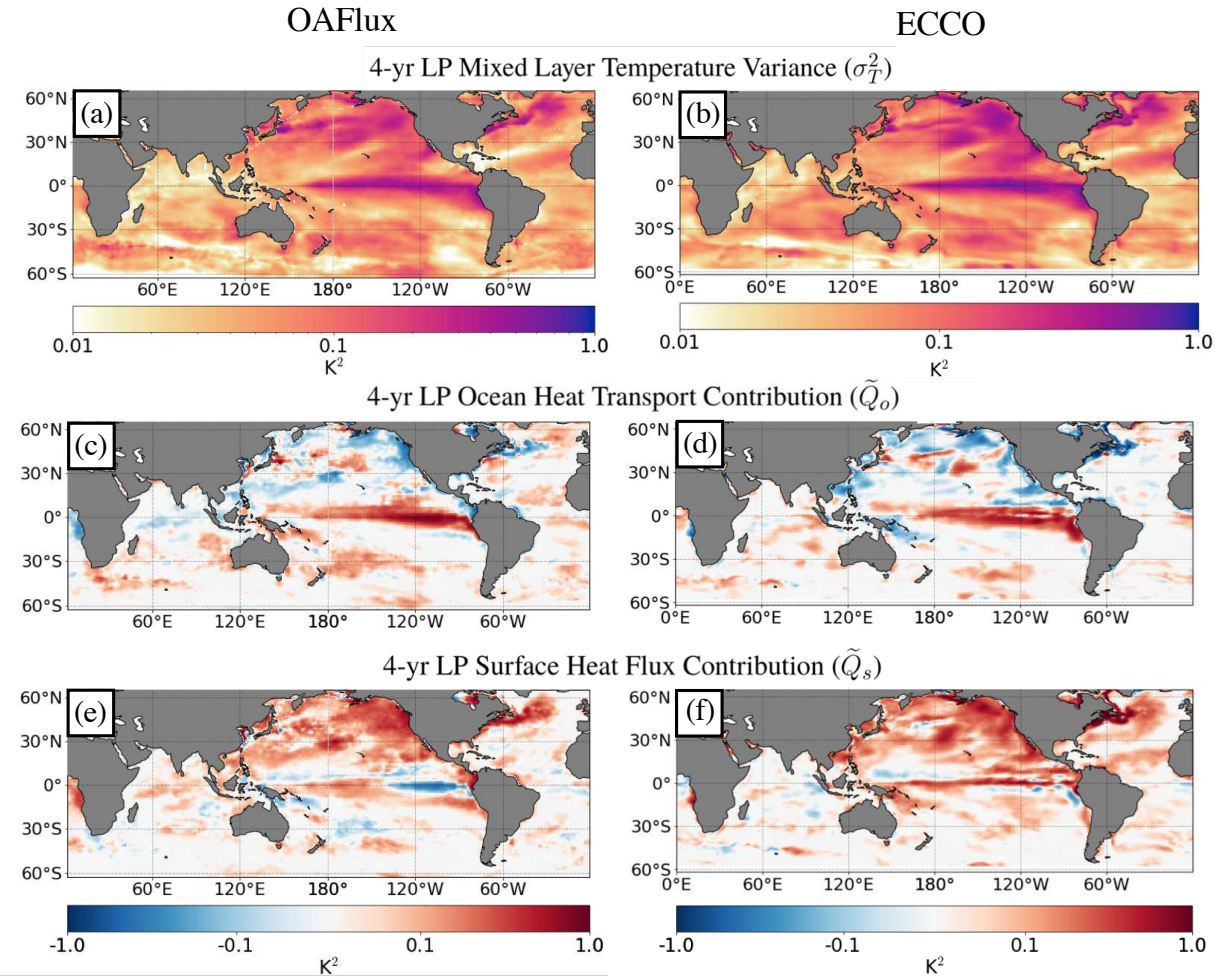

Figure 2.8: As in Fig. 2.4, except for 4-year low-pass (LP) filtered data.

timescales (e.g Bjerknes, 1964; Gulev et al., 2013; Buckley et al., 2014; O'Reilly et al., 2016). Decadal SST variability in the North Pacific has been frequently linked to dynamic adjustments of the North Pacific gyre and Kuroshio Extension that occur via oceanic Rossby-wave propagation (e.g. Latif and Barnett, 1994; Kwon and Deser, 2007; Wills et al., 2019b). And previous studies have linked multidecadal SST variability in the North Atlantic to variations in the Atlantic meridional overturning circulation (e.g. Buckley and Marshall, 2016; Kim et al., 2018; Yan et al., 2018; Zhang et al., 2019). It is possible that ocean dynamics play an important role on timescales longer than those that can be resolved in the relatively short records afforded by the ECCO and OAFlux products (1992-2015 and 1980-2017, respectively). However, the results in Fig. 2.8 suggest that—on the timescales resolvable in the analysis—multiannual mixed layer temperature variability in both the North Pacific and North Atlantic is generally damped by ocean dynamics.

Why do ocean dynamics suppress mixed layer temperature variance on multiannual timescales? As discussed above, the ocean dynamical contributions to mixed layer temperature variability arise advective heat transport and diffusion by convective and parameterized isopycnal mixing at the base of the mixed layer. Figure 2.9 shows the advective and diffusive contributions for four-year low pass filtered data. The key result in Fig. 2.9 is that while convective and parameterized isopycnal mixing play a very small role in the unfiltered data (Fig. 2.7b), they play a prominent role on low-frequency timescales (Fig. 2.9b). Hence the results suggest that the role of diffusive mixing overwhelms the role of advection in mixed layer temperature variability on timescales longer than a few years in the extratropical Northern oceans.

To more clearly illustrate the timescale dependency of the results, Fig. 2.10 explores the contributions of the surface heat fluxes and ocean heat transport to SST variability as a function of low-pass filter length. Results are shown for variances averaged over the globe, the extratropical NH and SH, and the tropics (note that the results show the spatial averages of the variances, not the variances of the spatial averages). The top half of the plot

(marked OAFlux) indicates results derived from the observations over the period 1980-2017: the first row shows the total area-averaged mixed layer temperature variance (black), the contributions to temperature variance due to ocean dynamics (blue), and the contributions to temperature variance due to surface fluxes (green); the second row shows the fractional rather than total contributions due to ocean dynamics (blue shading) and surface fluxes (green shading). The uncertainties in the variance estimates due to uncertainties in the observations are indicated by the transparent colored shadings in the top row (see Appendix A for details of the uncertainty analysis). The bottom half of the plot (marked ECCO) shows the same results, but calculated for ECCO over the ECCO period of record 1992-2015. The figure highlights three key results:

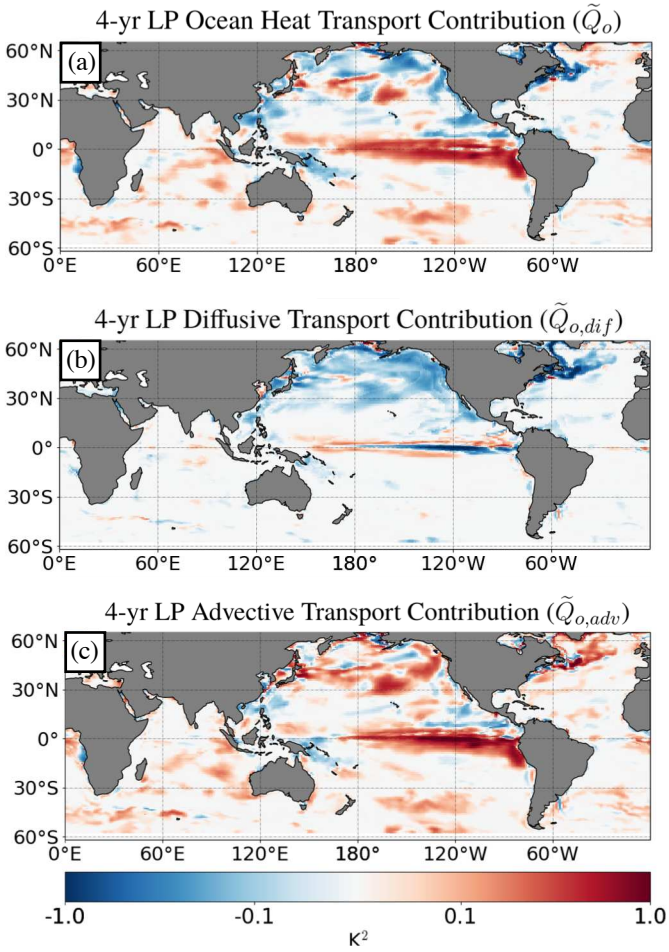

Figure 2.9: (a)-(c) As in Fig. 2.7a-c, except for 4-year low-pass (LP) filtered data.

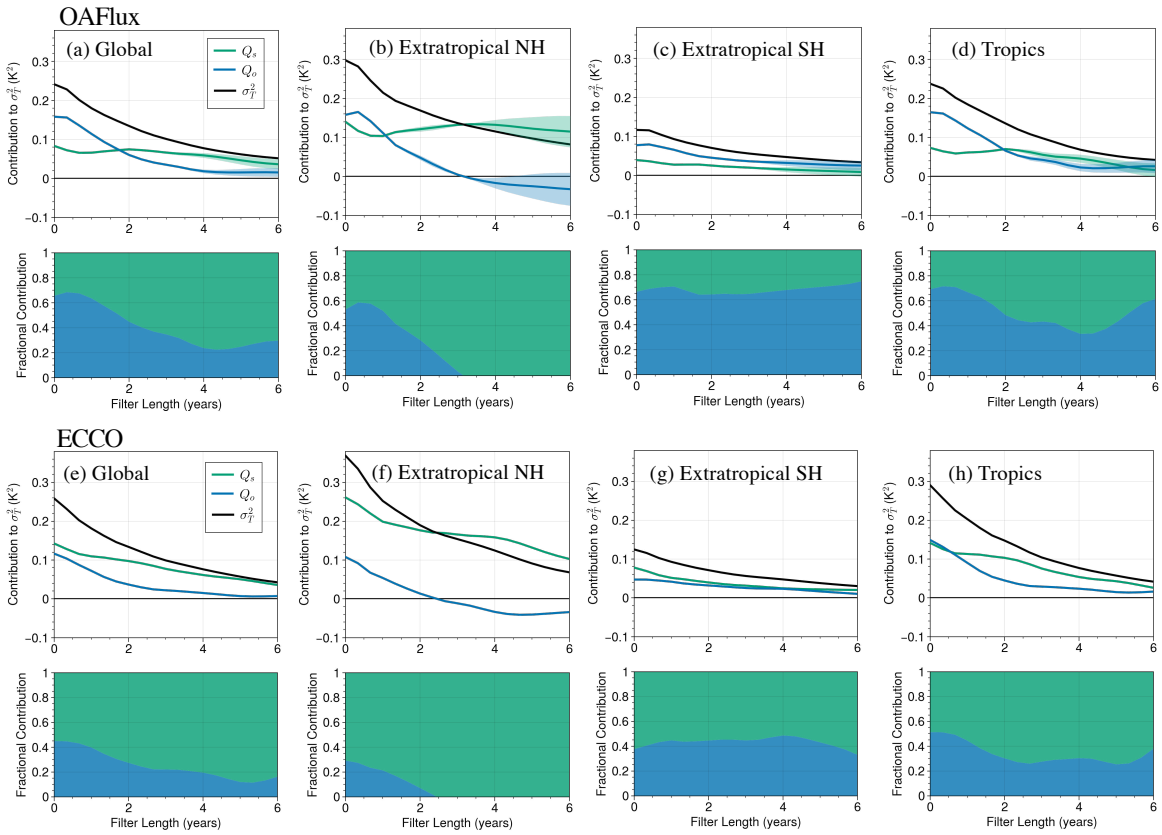

Figure 2.10: Spatially-averaged contributions of ocean dynamics (blue) and surface heat fluxes (green) to mixed-layer temperature variance (black). Results are shown as a function of low-pass filter length, as indicated on the horizontal axis. (a)-(d) show results for the observations based on OAFlux. (e)-(h) show results based on ECCO. The domains are: the global oceans (60°S-60°N), extratropical Northern hemisphere (NH; 30°N-60°N), extratropical Southern hemisphere (SH; 30°S-60°S), and the tropics (30°S-30°N) The line plots indicate the total contributions in K^2. The shading indicates the fractional contributions.

1. As expected, temperature variances - and thus the ocean dynamical and heat flux contributions to temperature variances - decrease as the filter length is increased.

2. The contributions of ocean dynamics to the mixed layer temperature variances are roughly twice as large in observations as they are in ECCO output at all timescales. In the case of unfiltered data (i.e., filter length 0), the observations suggest that ocean dynamics account for ∼55% of unfiltered mixed layer temperature variability averaged over the extratropical Northern Hemisphere, ∼65% averaged over the extratropical Southern Hemisphere, and ∼65% averaged over the globe. In contrast, in the ECCO output, ocean dynamics account for only ∼30%, ∼35%, and ∼45% averaged over the same respective domains. The differences between the unfiltered OAFlux and ECCO results are not explained by uncertainties in the OAFlux estimates (transparent shading in the top row). They are also reproducible when the OAFlux results are computed for the ECCO period of record (not shown).

3. Both the observations and ECCO indicate that the fractional contribution of ocean dynamics to NH mixed layer temperature variability decreases at increasingly low frequencies (blue shading in Fig. 2.10b,f). In fact, the contribution of ocean dynamics to NH temperature variance is negative at filter lengths longer than ∼3 years (blue lines in Fig. 2.10b,f). The striking differences between the contributions of the surface fluxes and ocean dynamics far exceed the uncertainties in the OAFlux estimates (green and blue transparent shading in Fig. 2.10b). We repeated the analysis shown in Fig. 2.10 for the extratropical North Pacific and North Atlantic basins separately (Fig. B1a,f and Fig. B2a,f). Both datasets indicate that ocean dynamics play a vanishingly small role in driving SST variability in both basins on timescales longer than ∼4 years and that the results are robust to the uncertainty estimates provided in the OAFlux product. Both datasets also indicate that the ocean dynamical contributions are weakly negative - i.e., that they suppress SST variance - at frequencies longer than a few years in the North Pacific (Fig. B1a,f). Only ECCO indicates that the ocean

dynamical contributions are negative in the North Atlantic (Fig. B2a,f). The signature of increasingly small fractional contributions of ocean dynamics at increasingly low frequencies is less pronounced in the tropics and nonexistent in the Southern Hemisphere (Fig. 2.10c,d,g,h), but is apparent in the global mean (Fig. 2.10a,e).

Clearly, the vanishingly small contribution of ocean dynamics to multiannual mixed layer temperature variability in the Northern Hemisphere has important implications for under-

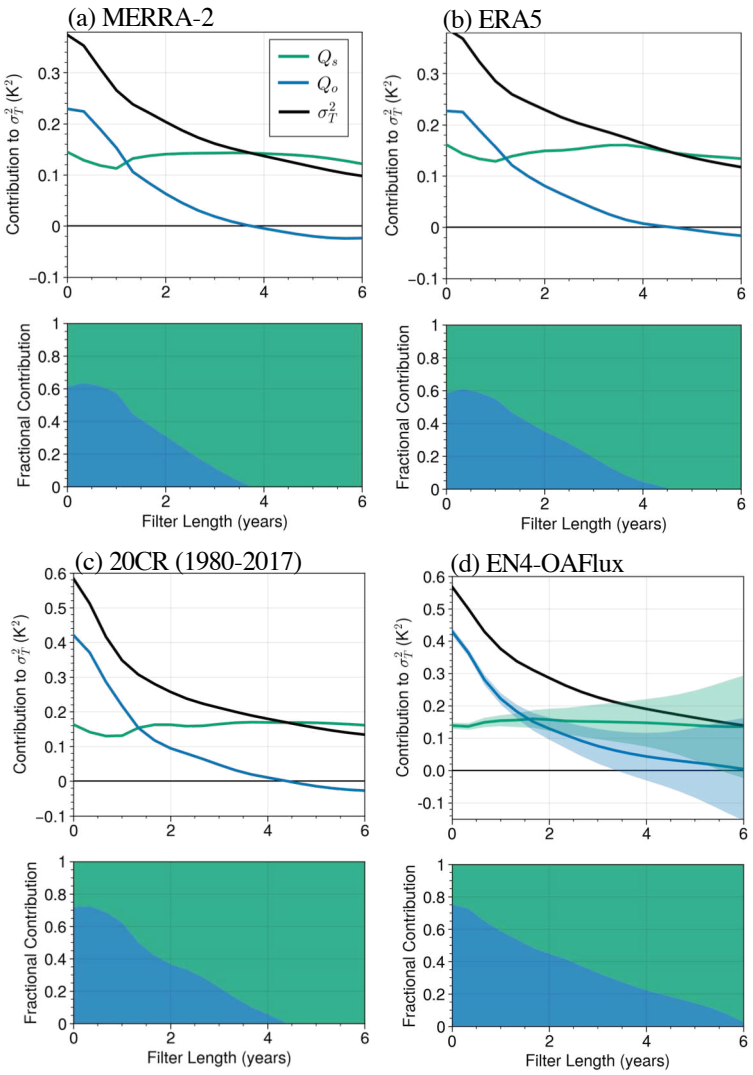

Figure 2.11: As in Fig. 2.10b, f, but for output from (a) MERRA-2, (b) ERA5, (c) NOAA-CIRES-DOE 20th Century Reanalysis (20CR), and (d) the combined EN4-OAFlux dataset. All results are based on the 1980-2017 period.

standing the drivers of North Pacific and North Atlantic climate variability. Figure 2.11 tests the reproducibility of this key result in four other data sources: Output from the MERRA-2 and ERA5 Reanalyses products (Fig. 2.11a,b), output from the NOAA-CIRES-DOE 20th Century Reanalysis (20CR; Fig. 2.11c); and a combination of the OAFlux fluxes with mixed layer temperature tendencies from EN4 (Fig. 2.11d). All results are based on the 1980-2017 period to facilitate comparison with the observational (OAFlux) results shown in Fig. 2.10. Figure 2.11 shows results integrated over the Northern Hemisphere; Fig. B1b-d and Fig. B2b-d show results integrated over the North Atlantic and Pacific basins, separately. Note that the analysis of the combined EN4-OAFlux data allows us to better understand how the observational results depend on the scaling used to convert SST to mixed layer temperature variances (Eq. 2.5).

As evidenced in Fig. 2.11, the increasingly small fractional contributions of ocean dynamics to low-frequency Northern Hemisphere mixed layer temperature variability is reproducible in all datasets considered in the figure. The contributions are negative, indicating that ocean dynamics are suppressing low-frequency temperature variance, in all data sources except for mixed layer temperatures derived from EN4. But even in this case, the fractional contribution of ocean dynamics to the temperature variance is considerably less than that associated with the surface heat fluxes, albeit the uncertainties in the EN4 estimates calculated using the formulation in Appendix A are large on timescales longer than a few years. Note that output from all the observational data sources indicates a larger role for ocean dynamics in unfiltered data than output from ECCO (roughly 60% for observations vs. 30% for ECCO). Thus, the differences in $\widetilde{Q}_o$ between the indirect method and direct method are not due to the SST-tendency-scaling given in Eq. (2.5).

The observational results in Figs. 2.10 and 2.11 are based on the period of record following 1980. That is because remotely-sensed data are widely available from the late 1970s, and thus major reanalyses such as ERA5 and MERRA2 are only available after 1979. However, the 20CR product is available extending back to 1836. The results in Fig. 2.11c have been

reproduced using the 20CR product over periods of record extending from 1950-2017, 1900-2017 and 1836-2017 (Fig. 2.12b,c,d). As in Fig. 2.11c, the ocean dynamical contributions to mixed layer temperature variability decrease more rapidly than the surface heat flux contributions at increasingly low frequencies. Unlike Fig. 2.11c, the ocean dynamical contributions do not become negative at low frequencies. However, the SST and flux measurement data are relatively sparse and exhibit more notable biases during the early and middle 20th century (e.g. Kent et al., 2017, Davis et al., 2019 and references therein). Thus, estimates of ocean dynamics for the early and middle 20th century are much more uncertain than estimates for the last few decades.

2.4 Discussion

The results in the previous section highlight two surprising results: 1) The fractional contribution of ocean dynamics to NH-mean and global-mean mixed layer temperature variability deceases as the timescale increases; and 2) Over certain areas of the extratropical North Atlantic and North Pacific, ocean dynamics act to *reduce* rather than increase the temperature variance on multiannual timescales. The results emerge from analyses of the temperature variance budget, as summarized in Section 2.2. And they are reproducible in

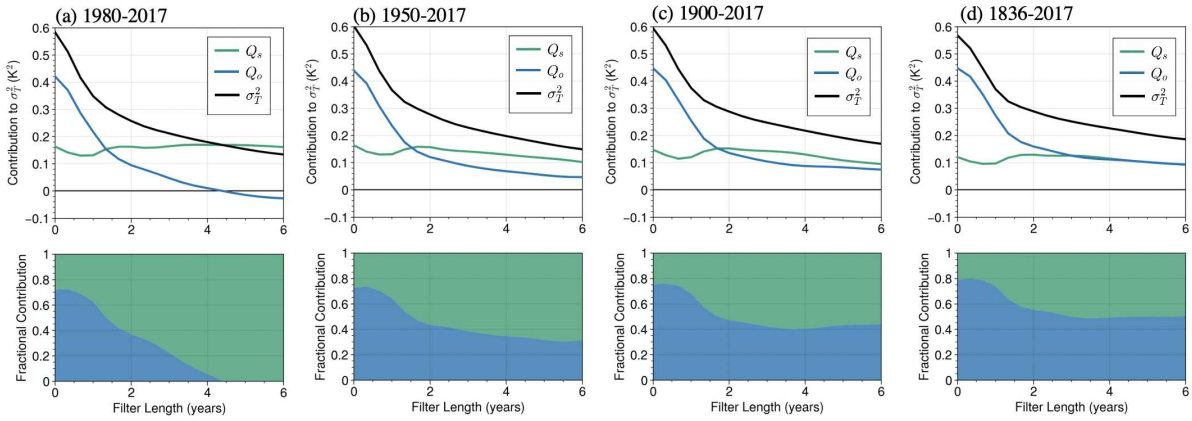

Figure 2.12: As in Fig. 2.11c, but for results calculated for the 20CR reanalysis period of record between (a) 1980-2017 (repeated for reference), (b) 1950-2017, (c) 1900-2017 and (d) 1836-2017.

estimates of ocean heat transport derived both indirectly from observations of surface heat fluxes and SSTs, and directly using the ECCO ocean state estimate. However, they also contradict previous findings in which the role of ocean dynamics in SST variability is inferred from lag-correlations between the surface heat fluxes and SSTs. Here, the differences and similarities between the methods used here and in previous analyses are discussed.

Numerous studies have used lag-correlations between SSTs and the surface heat fluxes to infer the role of ocean dynamics in SST variability (e.g. Gulev et al., 2013; O'Reilly et al., 2016; Bishop et al., 2017; Zhang, 2017; O'Reilly and Zanna, 2018). The reasoning is as follows: If the surface heat fluxes Q_s (defined positive down) are positively correlated with SSTs when leading the SST field, then the surface heat fluxes enhance temperature anomalies. Conversely, if the fluxes Q_s are negatively correlated with SSTs when leading the SST field, then the surface heat fluxes damp SST anomalies and and thus the temperature anomalies must be driven by ocean heat transport. On the basis of this logic, previous studies have interpreted positive correlations between Q_s and increasing SSTs on monthly and annual timescales as evidence that the surface heat fluxes are driving high-frequency SST variability. Likewise, they have interpreted negative correlations between Q_s and increasing SSTs on multiannual to multidecadal timescales evidence that ocean dynamics are driving low-frequency SST variability (e.g. Gulev et al., 2013; O'Reilly et al., 2016; Bishop et al., 2017; Zhang, 2017; O'Reilly and Zanna, 2018).

However, as also emphasized in Cane et al. (2017), the sign of the lag-correlation between SSTs and the surface heat fluxes does not unequivocally identify the role of ocean dynamics. Consider the North Atlantic as an example. The results suggest that ocean dynamics play a fractionally smaller role in driving SST variability as the timescale of the variability increases, with ocean dynamics suppressing SST variability over the Gulf Stream region on timescales longer than $\sim$4 years (Fig. 2.8c,d). In contrast, Gulev et al. (2013), O'Reilly et al. (2016) and others have used lead-lag correlations between SSTs and the surface heat fluxes to argue

that ocean dynamics must play a key role in driving North Atlantic SST variability at low-frequencies.

Figures 2.13 and 2.14 make clear how results of the current study relate to those in previous studies, and highlight the shortcomings of using lag-correlations between the surface heat fluxes and the SSTs to infer the role of ocean dynamics. The left column in Fig. 2.13 is derived from the left column of Fig. 2.4 but is focused on the North Atlantic. The top panel shows the total variance in mixed layer temperatures, the middle the contributions of ocean dynamics, and the bottom the contributions of the surface heat fluxes. All results are derived from the indirect method with OAFlux data. The right column is similar to the left column of Fig. 2.8, and shows the respective results for 5-year low-pass filtered data. As discussed earlier in the text, ocean heat transport contributes substantially to temperature variance in the Gulf Stream extension region in the unfiltered data (Fig. 2.13b), but acts to decrease temperature variance in the Gulf Stream region at lower-frequencies (Fig. 2.13e).

Figure 2.14 shows the lead/lag correlations between SSTs and (top) the surface heat fluxes and (bottom) ocean heat transport averaged over the Gulf Stream extension region (as indicated by the dashed boxes in Fig. 2.13). Negative lags denote the fluxes/transport lead the SST field. The sign of the heat fluxes and ocean heat transport is positive into the local ocean mixed layer. To facilitate comparison between the lag-correlation method and the method outlined in Section 2.2.2, the contributions of the surface heat fluxes and ocean dynamics to the temperature variance (i.e., $\widetilde{Q}_s$ and $\widetilde{Q}_o$, respectively) averaged over this region are indicated in the bottom left of each panel.

Starting with the unfiltered results (left column): The correlations between Q_s and the SSTs are positive when the fluxes lead SSTs and negative when the fluxes lag SSTs (Fig. 2.14a; recall that Q_s is positive down). According to the logic discussed previously, this suggests that Q_s enhances SST anomalies and hence contributes to SST variability. In this case, inferences based on lag-correlations are consistent with the results derived from Eq. (2.4). In particular, Eq. (2.4)a states that the contribution of Q_s to temperature variability is given

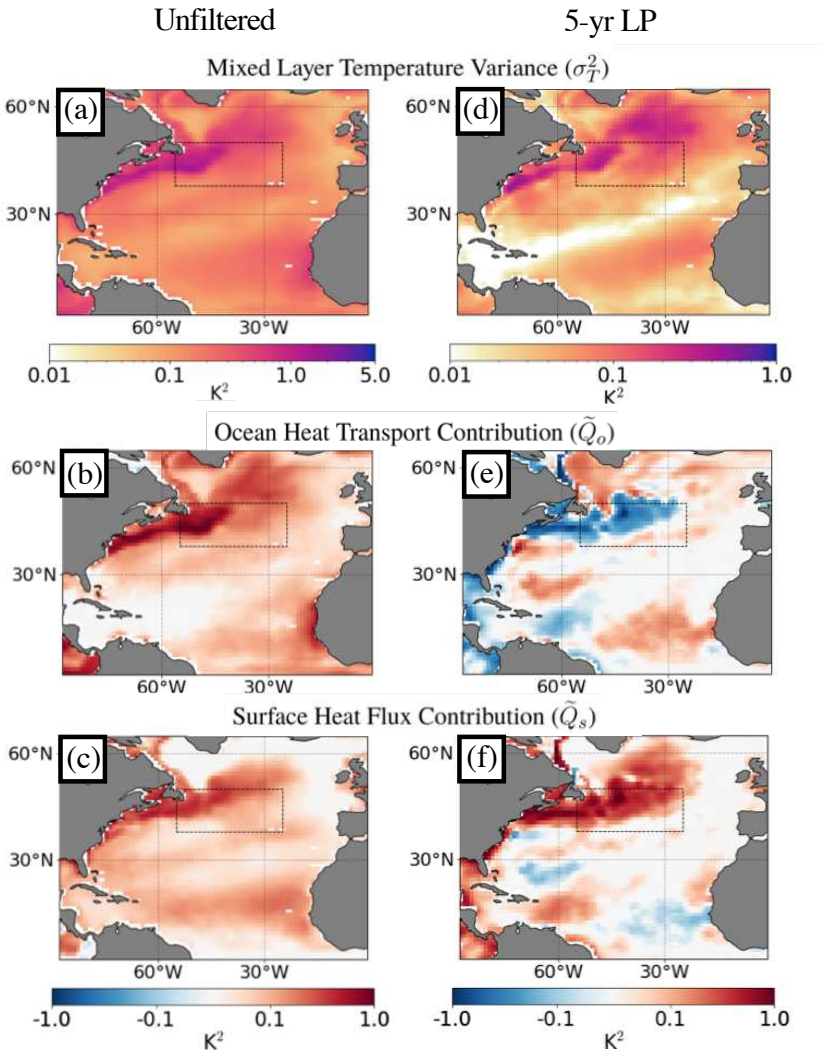

Figure 2.13: As in Fig. 2.4, left column, but focused on the North Atlantic sector: (a) Monthly mixed-layer temperature variance from OAFlux. (b) Ocean heat transport contribution to mixed-layer temperature variance derived from the indirect method using OAFlux. (c) Surface heat flux contribution to mixed-layer temperature variance for OAFlux. (d), (e) and (f): As in the left column of Fig. 2.8, but for 5-year low-pass filtered data

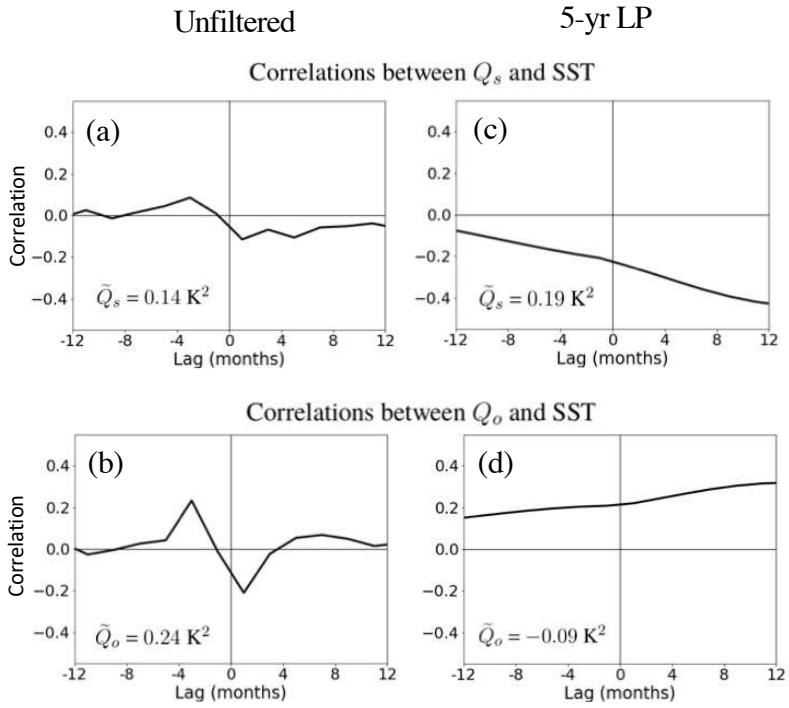

Figure 2.14: (a) Lag-correlations between the surface heat fluxes (Q_s) and SSTs for unfiltered monthly data averaged over the boxed midlatitude region (38°N to 50°N, 15°W to 55°W) shown in Fig. 2.13. (b) As in (a) but for lag correlations between the ocean heat transport (Q_o) and SSTs. (c, d) As in the left column, except for 5-year low-pass (LP) filtered data. Negative lags correspond to periods when the surface fluxes and ocean heat transport lead SSTs. The signs of Q_s and Q_o are such that positive values are into the local mixed layer. The contributions from the surface heat fluxes and ocean heat transport to the mixed-layer temperature variance (i.e. $\widetilde{Q}_s$ and $\widetilde{Q}_o$) averaged over the boxed midlatitude region are shown in the bottom left of each panel.

by the covariance between Q_s and the SST tendency, which relates to the *change* in the correlation across lag zero. This can be clearly seen by expanding the temperature tendency in the following:

$$\tilde{Q}_s = \overline{Q_s' \frac{\partial T'}{\partial t}} \approx \overline{Q_s'(t)\, T'(t+\Delta t)} - \overline{Q_s'(t)'\, T'(t-\Delta t)} \tag{2.6}$$

The first term on the RHS of Eq. (2.6) relates to the correlation at negative lags (i.e. Q_s *leads* SST), and the second term relates to the correlation at positive lags (i.e. Q_s *lags* SST). In the case of Fig. 2.14a, the correlation at negative lags exceeds the correlation at positive lags and hence $\tilde{Q}_s = \overline{Q_s' \frac{\partial T'}{\partial t}} > 0$. That is, Q_s contributes to SST variability because Q_s is positively correlated with the temperature tendencies $\frac{\partial T}{\partial t}$.

Importantly, the correlations between ocean heat transport and the SSTs are *also* positive when the transport leads SSTs (Fig. 2.14b), which suggests that ocean dynamics enhances temperature anomalies and hence drive SST variability in the unfiltered data. As is the case with the surface heat fluxes, the results inferred from lag-correlations are consistent with the results derived from Eq. (2.4), that is, $\widetilde{Q}_o$ is positive since the transport Q_o is positively correlated with the temperature tendencies (i.e. the change in the correlation across lag zero has the same sign as the case for Q_s). Importantly, the positive contributions of ocean dynamics to SST variance could not have been unequivocally inferred from the lag-correlations between surface heat fluxes and SSTs alone.

The results for low-pass filtered data (right column) are more nuanced. In this case, the correlations between Q_s and the SSTs are negative when the fluxes lead the SST field (Fig. 2.14c), that is, the surface heat fluxes are out of the ocean prior to the peak in the SST field. The sign of the correlations suggests that Q_s damps SST anomalies, and thus that ocean heat transport must play an essential role in driving the anomalies. The positive correlations between Q_o and the SSTs at negative lags appear to support this conclusion (Fig. 2.14d).

At first glance, the signs of the correlations at negative lags in Fig. 2.14c and Fig. 2.14d appear inconsistent with the results derived from Eq. (2.4). As noted above, previous research has interpreted the signs of the correlations to indicate that a) the surface heat fluxes damp the positive SST anomalies at negative lags while b) ocean heat transport enhances the SST anomalies. In contrast, the results suggest that on timescales longer than 5 years a) the surface heat fluxes *drive* SST variability and b) ocean heat transport *suppresses* SST variability. This apparent contradiction stems from the fact that the surface heat flux contribution to the SST variance ($\widetilde{Q}_s$) is a function not of the lag relationships between Q_s and the temperature, but of the covariance between Q_s and the temperature tendency, as shown by Eq. (2.6). Thus, as previously discussed, it is the change in the correlation between Q_s and SST across lag zero that determines the contribution of the surface heat fluxes to the temperature variance. In the case of Fig. 2.14c, the surface heat fluxes are negative (out of the ocean mixed layer) during periods preceding the SST anomaly, but they are *even more negative* after the peak in the SST anomaly. In this case, the sign of the change in the correlation across lag zero is the same as for the unfiltered case (Fig. 2.14a), and hence increases the low-frequency temperature variance.

Likewise, the ocean heat transport anomalies are positive (into the ocean mixed layer) during periods preceding the SST anomaly, but are *even more positive* after the peak in the SST anomaly. The change in the correlation across lag zero for Q_o is therefore opposite of that for Q_s (Fig. 2.14c) and hence Q_o reduces the low-frequency variance.

Why do ocean dynamics suppress SST variance on multiannual timescales? To answer this, Fig. 2.9 is revisited which shows the decomposition of ocean heat transport contribution into its diffusive (Fig. 2.9b) and advective (Fig. 2.9c) components. Importantly, Fig. 2.9 reveals that 1) advective ocean processes contribute to multiannual SST variance $\left(\overline{Q'_{o,adv}\frac{\partial T'}{\partial t}} > 0\right)$ but that 2) diffusive ocean processes suppress multiannual SST variance $\left(\overline{Q'_{o,dif}\frac{\partial T'}{\partial t}} < 0\right)$. Thus, as the timescale of the mixed layer variability increases, it appears that the negative contribution from diffusion becomes increasingly large and— over certain

regions of the ocean— overwhelms the positive contribution from advection. For example, in the boxed midlatitude region shown in Fig. 2.13, the contribution to 5-year low-pass filtered temperature variance from advection ($\widetilde{Q}_{o,adv}$) is $\sim$0.07 K^2, while the contribution from diffusion ($\widetilde{Q}_{o,dif}$) is ~ -0.18 K^2.

Overall, the interpretations provided here are consistent with those in Cane et al. (2017). Cane et al. (2017) use a series of idealized models to demonstrate that the signs of the lag-correlations between Q_s and SST do not unambiguously identify the relative importance of ocean dynamics. For example: It is possible for the atmosphere to dominate the forcing of SSTs, but for the correlations between Q_s and SST to be negative at low-frequencies, and hence suggest that the surface fluxes are damping low-frequency SST variability. This occurs in simple models as long as there is at least some amount of stochastic forcing from ocean dynamics, and is a consequence of quasi-equilibrium in the surface heat balance at low-frequency timescales.

Finally, note that a key advantage of the approach of this study is that it directly relates the variance in SSTs to the variances of the fluxes (Eq. 2.4c and Eq. 2.4d). As such, the increasingly small contributions of ocean dynamics to SST variance at lower-frequencies

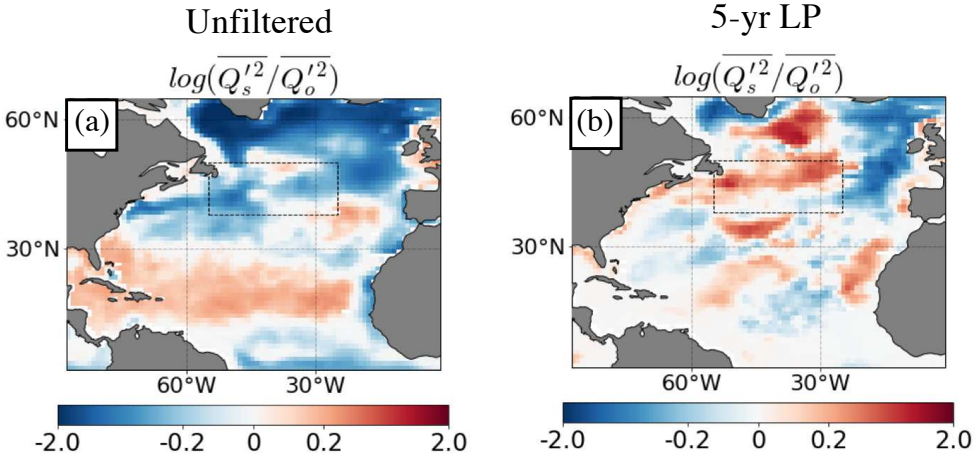

Figure 2.15: (a) Log-ratio of the variances of the surface heat fluxes (Q_s) to the variances of ocean heat transport (Q_o) in the North Atlantic for unfiltered monthly OAFlux data. (b) As in (a) except for 5-year low-pass filtered data.

indicates that—as the timescale increases—the variance of the ocean heat transport is decreasing more rapidly than the variance of the surface fluxes. This is depicted in Fig. 2.15, which shows the log-ratios of the variances in Q_s to the variances in Q_o for both unfiltered and 5-year low-pass filtered data. Clearly, the variability of the surface heat fluxes exceeds the variability of ocean heat transport in the boxed midlatitude region on longer timescales.

In summary, the diagnostic equation for temperature variance used here provides important insights into the relative roles of the surface heat fluxes and ocean dynamics in driving mixed layer temperature variance that cannot be readily deduced from the sign of the lag-correlation between Q_s and the SSTs. It has been shown that the sign of the correlations between Q_s and the SSTs when the fluxes lead the SSTs does not determine the role of ocean dynamics in mixed layer temperature variance (Fig. 2.14). In particular, we argue that it is the change in the lag-correlations about lag zero that indicates the contributions of different processes to the temperature variance, not the absolute sign of the correlations. This is most relevant on longer time scales, where the change in the correlation across lag zero is small and hence may be easily overlooked.

2.5 Conclusions

The results in this study add to an increasing body of literature that explores the role of ocean heat transport in driving SST variability. The primary novel aspects of the analyses are that a) we have provided a global survey of ocean heat transport using two distinct but complementary methodological approaches: one in which ocean heat transport is calculated directly from a state-of-the-art ocean state estimate (ECCO), and another in which it is calculated indirectly from observations; b) the resulting contributions of ocean heat transport to SST variability have been explored using a diagnostic rather than prognostic equation for the temperature variance, and 3) the role of ocean heat transport has been probed as a function of timescale across the globe in both the observations and the ECCO ocean state estimate.

The results provide novel quantitative estimates of the role of ocean dynamics in driving SST variance across the globe. Consistent with previous studies, they indicate that the largest contributions of ocean dynamics to mixed layer—and thus sea surface—temperature variability are found in the western boundary currents and their eastward extensions, the Antarctic circumpolar current, and the equatorial regions, most notably in the tropical Pacific (e.g., Bishop et al., 2017; Roberts et al., 2017; Small et al., 2019b). To leading order, the results based on the observations and the ECCO ocean state estimate yield similar spatial patterns throughout the global oceans. However, they also indicate important discrepancies in amplitude: In general, the contributions of ocean heat transport to temperature variance estimated indirectly from observations are twice as large as those estimated directly using the ocean state estimate. The reasons for the differences in amplitude may arise from the representation of mesoscale ocean processes in the 1° ECCO product but this remains to be explored in future work.

Importantly, the results presented here generally suggest that the ocean dynamical contribution to ocean-mixed layer temperature variability *decreases* with increasing timescale. The signature of decreasing fractional contributions from ocean dynamics to mixed layer temperature variance is most clear in the Northern Hemisphere oceans, and is reproducible in a number of atmospheric reanalyses spanning 1980-2017. The decreases in the ocean dynamical contributions to temperature variability on multiannual timescales are sufficiently large that they extend to the global average: In the case of the observations, ocean heat transport accounts for ∼65% of the globally integrated variance in mixed layer temperatures on timescales of a month and longer, but only ∼30% of the globally integrated variance on timescales longer than about four years. The results challenge the notion that ocean dynamics are increasingly important for SST variability at increasingly low frequencies (e.g., Bjerknes, 1964; Gulev et al., 2013; Buckley et al., 2014; O'Reilly et al., 2016) and they support the hypothesis that observed low-frequency variability in the North Atlantic is primarily forced by atmospheric processes (e.g. Clement et al., 2015; Cane et al., 2017). As

discussed in Section 2.4, the timescale dependent contributions of ocean heat transport to mixed layer temperature variability revealed here cannot be readily inferred from the sign of the lag-correlation between the surface heat fluxes and the SSTs.

Another key result is that over large regions of the Northern Hemisphere oceans, ocean dynamics act to reduce the variance of the SST field on timescales longer than a few years. Analyses of the ECCO product suggest that the suppression of SST variance arises from ocean diffusive processes: Advective ocean process contribute to SST variability across a range of timescales, but their contributions are overwhelmed by diffusion as the timescale of the SST variability increases.

The results shown here are derived from analyses of data extending back to 1980 (OAFlux) and 1992 (ECCO). We are hesitant to make inferences on the role of the ocean in climate variability over a longer period of record by applying a similar analysis procedure to sea surface temperatures and surface fluxes derived from, say, the 20CR product. The sea surface temperature and surface flux observations required to make such inferences are increasingly sparse and exhibit notable biases prior to $\sim$1970 (e.g. Kent et al., 2017; Davis et al., 2019). The findings revealed here thus highlight the critical importance of continued high-quality observations of the upper ocean for understanding the role of the ocean in multidecadal climate variability. It would be interesting to explore the dependence of the results shown here on the amplitude of the convective processes and parameterized isopycnal mixing that comprise the diffusive term, as well as the spatial resolution of the ocean model.

Overall, the results shown in Chapter 2 suggest that ocean dynamics generally play an increasingly *small* role in driving SST variability at increasingly low-frequencies, particularly in midlatitude regions. Further insights are provided into this result in Chapter 3. In particular, it is shown that the forcing and damping of midlatitude SST variability by ocean processes are in fact *both* important at low-frequencies, but that the effects of ocean damping outweigh the effects of ocean forcing at low-frequencies in many midlatitude regions.

Chapter 3

Understanding the Role of Ocean Dynamics in Midlatitude Sea-Surface Temperature Variability using a Simple Climate Model

3.1 Introduction

The results from Chapter 2 (Patrizio and Thompson, 2021a) suggest that ocean dynamical processes play an important role for SST variability in tropical regions, but also across broad midlatitude regions. As a brief review, recall that the role of ocean dynamics was quantified in two ways: 1) indirectly from observations of surface heat fluxes and SSTs, and 2) directly using output from the Estimating the Circulation and Climate of the Ocean (ECCO) project. A key result was that both methods showed that ocean dynamical processes contribute notably to midlatitude SST variability on monthly to interannual timescales, and act to damp lower-frequency SST variability throughout the Northern oceans.

The goal of this chapter is to provide further insights into the role of ocean dynamics in midlatitude SST variability using a simple climate model that includes representations of the forcing and damping of SST variability by ocean processes. This work is currently under review in Journal of Climate (Patrizio and Thompson, 2021b).

The so-called "Hasselmann" model of climate variability (Hasselmann, 1976; hereafter H76), provides the simplest possible model of midlatitude SST variability. This model was described in Chapter 2, but as a review the model is briefly discussed here as well. In its original formulation, fluctuations in SSTs are interpreted as the response of the ocean mixed-layer to stochastic atmospheric variability. As illustrated in Fig. 3.1, the SST anomalies, T', are forced by atmospheric variability through turbulent and radiative heat fluxes at the sea surface, F_a, and are linearly damped by $-\lambda_s T'$, which parametrizes the damping due to

the surface heat flux feedback. In the model, the high-frequency component of atmospheric variability is damped by the large heat capacity of the ocean mixed-layer, C_o, such that the resulting SST variability has a redder spectrum than the atmospheric forcing. Despite its simplicity, the H76 model has been shown to capture some key aspects of midlatitude SST variability, such as the shape of the power spectrum of midlatitude SSTs (e.g. Frankignoul and Hasselmann, 1977; Frankignoul, 1979) and the covariability between SSTs and the surface heat fluxes (e.g. Frankignoul et al., 1998).

As such, the H76 model can be viewed as a null hypothesis for SST variability, particularly in midlatitude regions where atmospheric weather drives large variations in the surface heat fluxes. The H76 model forms the basis for the widely held notion that midlatitude SST variability is driven primarily by atmospheric processes. However, such models are also known to be deficient in some regions. For example, previous studies have shown that the H76 model simulates closely the observed SST power spectra in the Northeast Pacific, but

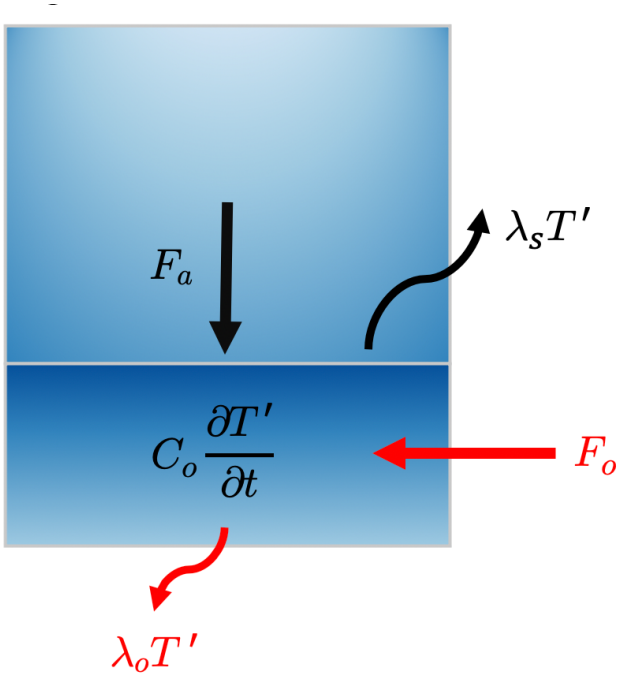

Figure 3.1: A schematic of the classical Hasselmann model (black terms) and the extension to the classical Hasselmann model (red terms). F_a is the atmospheric forcing, F_o is the ocean forcing, λ_s is the surface heat flux damping, λ_o is the ocean dynamical damping, C_o is the mixed-layer heat capacity and T' is the SST anomaly. Each term is described in more detail in the text.

does not closely reproduce the observed spectra in regions with more active ocean dynamics, such as in the western boundary currents or the North Atlantic subpolar gyre region (e.g. Reynolds, 1978; Hall and Manabe, 1997; Zhang, 2017). This is consistent with the results from Chapter 2, which highlight the important role of ocean processes for SST variability in midlatitude regions.

Thus, motivated by the results in Chapter 2, here the classical H76 model is extended to include both forcing (F_o) and damping (λ_o) of SST variability by ocean processes (see red terms in Fig. 3.1). Ocean processes have been included in previous simple models of midlatitude climate variability (e.g. Frankignoul and Reynolds, 1983; Frankignoul, 1985; Alexander and Penland, 1996; Hall and Manabe, 1997; Wu et al., 2006; Qiu et al., 2007; Bishop et al., 2017; Cane et al., 2017; Zhang, 2017). However, here a novel approach is used to estimate the ocean dynamical terms from observationally-based data and, in turn, draw novel conclusions about the role of ocean dynamics in midlatitude SST variability. The conclusions are tested in output from an atmospheric general circulation model coupled to a dynamically-active ocean model (hereafter referred to as the fully-coupled model) and a slab-ocean model using NCAR's Community Earth System Model (CESM1; Hurrell et al., 2013).

The key results are that 1) the classical H76 model driven solely by the observed surface heat fluxes yields midlatitude SST power spectra that are much redder than observed midlatitude SST power spectra, 2) the inclusion of both ocean forcing *and* ocean damping terms in the H76 model reduces the discrepancy with observations by decreasing the low-frequency SST variance and increasing the high-frequency SST variance, and 3) the resulting "whitening" of midlatitude SST variability by ocean dynamics is also apparent in the differences between SST variability in slab-ocean and fully-coupled configurations of CESM.

3.2 Data & Methods

This section is divided into four parts. Section 3.2.1 reviews the data sources used in the analyses. Section 3.2.2 describes the extended H76 model. Section 3.2.3 outlines the methods used for estimating the ocean forcing and damping terms in the extended H76 model. Section 3.2.4 provides a derivation of the SST power spectrum of the model.

3.2.1 Observational data sources and model output

As in Chapter 2, the primary observational data sources are objectively-analyzed surface turbulent heat fluxes (latent and sensible) and SSTs from OAFlux (Yu et al., 2008), and surface radiative heat fluxes and wind stress from the MERRA-2 reanalysis product (Gelaro et al., 2017). The OAFlux SSTs are from the NOAA Optimum Interpolation (OI) 0.25° SST analysis produced by (Reynolds et al., 2007) that has been averaged onto a 1° degree grid. In all cases, monthly-mean data are used over the period 1980-2017 and at 1° resolution. To calculate the monthly anomalies, both the linear trend and seasonal cycle have been removed from the SSTs and air-sea heat fluxes prior to all analyses.

Following the indirect method described in Chapter 2, the observations are used to estimate monthly anomalies in the ocean mixed-layer heat flux convergence, Q'_o, by calculating Q'_o as a residual in the mixed-layer energy budget as follows:

$$Q'_o = C_o \frac{\partial T'}{\partial t} - Q'_s \tag{3.1}$$

where T' is the monthly sea-surface temperature anomaly (assumed to be equal to the mixed-layer temperature anomaly) and Q'_s is the monthly surface heat flux anomaly. The ocean mixed-layer heat capacity is given by $C_o = \rho c_p \overline{h}$, where $\overline{h}$ is the annual mean mixed-layer depth. The annual mean mixed-layer depth is shown in Fig. 3.2b and is derived from the ECCO ocean state estimate, which, as discussed in Chapter 2, provides output from an ocean GCM (MITgcm) constrained to ocean observations between 1992-2015. Note that the

pattern and magnitude of the mean mixed-layer depths from ECCO agrees well with other ocean reanalyses and observational estimates (e.g. de Boyer Montégut et al., 2004; Carton and Giese, 2008; Forget et al., 2015; Holte et al., 2017). The seasonality of the mixed-layer depth plays an important role in the persistence of midlatitude SSTs (e.g. Deser et al., 2003). But the use of a time-invariant mixed-layer depth provides consistency with the formulation of the H76 model (discussed in the following subsection) and does not appear to influence the broad results. Note that indirect estimates of ocean heat flux convergence derived using (1) may be biased due biases in the SST and/or surface heat flux data (e.g. Hall and Bryden, 1982; Talley, 1984; Bryden and Imawaki, 2001). As such, estimates of the error in the SSTs and air-sea heat flux that are provided in the OAFlux product have been included in select figures throughout the paper.

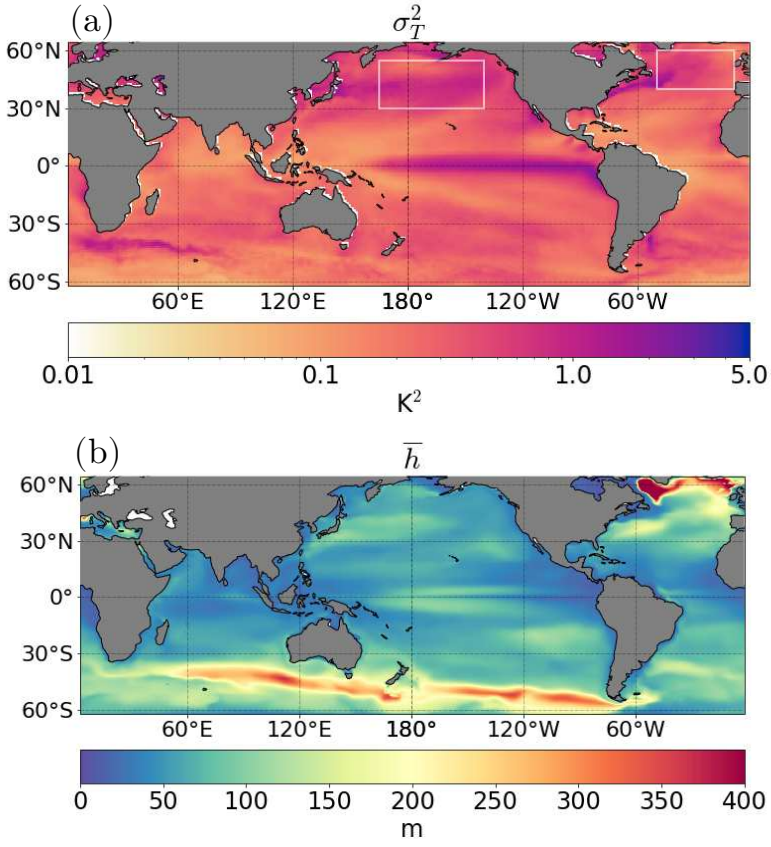

Figure 3.2: (a) Observed monthly SST variance (K^2) from OAFlux. The white boxes illustrate the averaging regions used for the analyses. (b) Annual-mean mixed-layer depth (m) from ECCO.

SSTs are also analyzed from slab-ocean model and fully-coupled configurations of CESM1 (Hurrell et al., 2013) under pre-industrial radiative forcing conditions at approximately 1° horizontal resolution. The model output was acquired from multi-century control runs provided in the CESM Large Ensemble Project (Kay et al., 2015). Only the last $\sim$ 500 years of output have been analyzed to avoid potential issues with model spin-up. Both the slab-ocean and fully-coupled runs use the Community Atmosphere Model, version 5 (CAM5), but only the fully-coupled run includes an ocean GCM (POP2). In the case of the slab-ocean model (SOM), the atmospheric model is coupled to a spatially-varying but annual-repeating mixed layer depth (i.e., the seasonal cycle of mixed-layer depths is prescribed). The SOM has no ocean heat transport and is thus forced with a climatological-mean "q-flux" in order to maintain a realistic climate. Note that variations in SSTs are driven entirely by the surface heat fluxes in the SOM, but by both the surface heat fluxes and ocean dynamical processes in the fully-coupled model.

3.2.2 The extended H76 model

Before reviewing the extension of the H76 model, first the *classical* H76 model is defined as illustrated by the black terms in Fig. 3.1. In this case, SST (and mixed-layer temperature) anomalies (T') are forced by atmospheric variability via the surface heat fluxes (F_a), and are damped via the surface heat flux feedback ($-\lambda_s T'$). The associated equation is as follows:

$$C_o \frac{\partial T'}{\partial t} = F_a - \lambda_s T' \tag{3.2}$$

Here, F_a is the forcing of SSTs by the surface heat fluxes associated with stochastic atmospheric dynamics, and $-\lambda_s T'$ is the damping of SSTs by the surface heat flux feedback. As previously discussed, an annual-mean mixed layer depth from ECCO (Fig. 3.2b) is used to calculate the mixed-layer heat capacity, C_o, which is consistent with previous formulations of the H76 model that use a time-invariant mixed layer depth.

The *extended* H76 model is defined as the classical H76 model with two additional terms: forcing and damping by ocean processes (red terms in Fig. 3.1). Ocean processes that act to force SST anomalies have been included in simple models of midlatitude SST variability as 'ocean weather' (e.g. Wu et al., 2006; Smirnov et al., 2014; Bishop et al., 2017; Cane et al., 2017) and geostrophic advection (e.g. Qiu et al., 2007). Ocean processes that act to damp temperature anomalies, such as vertical entrainment, have also been discussed in previous studies that apply variations of the H76 model (e.g. Frankignoul and Reynolds, 1983; Frankignoul, 1985; Alexander and Penland, 1996; Hall and Manabe, 1997). However, the H76 model has not been used to quantify the relative effects of ocean forcing and ocean damping processes on the frequency-dependent behavior of the observed SSTs.

The equation for the extended H76 model used here is as follows:

$$C_o \frac{\partial T'}{\partial t} = F_a + F_o - \lambda T' \tag{3.3}$$

where

$$\lambda = \lambda_s + \lambda_o \tag{3.4}$$

Here, F_o and $-\lambda_o T'$ represent the ocean forcing and damping terms, respectively, and hence $\lambda T'$ represents the total damping by both the surface heat fluxes and ocean processes. Equation (3.3) is equivalent to the classical Hasselmann model when the ocean forcing and ocean damping terms are set to zero, i.e., $F_o = 0$ and $\lambda_o = 0$.

The ocean forcing term, F_o, can be considered the oceanic counterpart to the atmospheric forcing term, F_a, i.e., the forcing of SSTs by ocean dynamics. In other words, F_o accounts for ocean dynamical processes that act to drive SST variability in the ocean mixed-layer, such as the transport of heat by ocean eddies. No *a priori* assumptions are made about either the ocean forcing term, F_o, or atmospheric forcing term, F_a, because both terms are estimated from observations as discussed in the following subsection.

The ocean damping term, $-\lambda_o T'$, accounts primarily for the damping of mixed-layer temperatures by vertical entrainment and diffusive processes (e.g. Frankignoul, 1985; Hall and Manabe, 1997; Frankignoul et al., 002b; Mignot and Frankignoul, 2003; Zhang, 2017) and mean advection in regions of strong ocean currents (Frankignoul and Reynolds, 1983; Mignot and Frankignoul, 2003). The role of ocean processes in damping SST variability has not been as widely explored as the role of ocean processes in forcing SST variability. Nevertheless, some studies have suggested that damping by ocean processes has comparable amplitude to damping by the surface heat fluxes (e.g. Frankignoul, 1985; Hall and Manabe, 1997; Mignot and Frankignoul, 2003; Zhang, 2017).

3.2.3 Estimating the forcing and damping terms

The forcing (F_a, F_o) and damping (λ_s, λ_o) terms are estimated from observations following the method of Frankignoul and Kestenare (2002a; hereafter FK02; see also Park et al., 2005; Hausmann et al., 2016; Myers and Mechoso, 2020). In this case the surface heat flux anomalies (Q'_s) are decomposed into a forcing term, Q^*_s, and a feedback term, $\lambda_s T'$, as follows:

$$Q'_s = Q^*_s - \lambda_s T' \tag{3.5}$$

where primes denote departures from the seasonal cycle. The surface heat flux damping coefficient, λ_s, is estimated using the following formula:

$$\lambda_s = -\frac{\overline{Q'_s T'_{-1}}}{\overline{T' T'_{-1}}} \tag{3.6}$$

Here, T'_{-1} denotes the SST anomalies leading the heat fluxes by one month. The surface heat flux damping is thus defined as the component of Q'_s that is linearly related to T' at a lag of one month (i.e., Q'_s lags T'), and the forcing term Q^*_s is defined as the residual. This definition assumes that the correlation between T' and the surface heat flux forcing Q^*_s approaches zero at a time lag of one month (this can be shown by multiplying both sides of

Eq. 3.5 by T'_{-1} and solving for λ_s). In other words, it assumes that the persistence of the atmospheric forcing is less than about one month. As discussed in FK02, if the atmospheric forcing persistence exceeds the time resolution of the lag used to compute λ_a, Q_s^* will be positively correlated with T' when Q_s^* lags T', and this will lead to a negative bias in the surface heat flux damping. In order to reduce this bias, the components of the fields that are linearly related to ENSO variability— which gives rise to persistence in the atmosphere on timescales longer than 2 months— are removed from the fields prior to computing the damping and forcing terms. Here ENSO variability is estimated from the Niño 3.4 index.

The FK02 method is likewise applied to the ocean heat flux convergence anomalies (Q'_o) to estimate the ocean forcing term, F_o, and the ocean damping coefficient, λ_o, as follows:

$$Q'_o = Q_o^* - \lambda_o T' \tag{3.7}$$

where

$$\lambda_o = -\frac{\overline{Q'_o T'_{-1}}}{\overline{T' T'_{-1}}} \tag{3.8}$$

As in the surface heat flux decomposition, Q_o^* is the ocean heat flux forcing, and λ_o is the ocean heat flux damping coefficient. Thus, in the formulation of the extended H76 model (Eq. 3.3), F_a is set to be equal to Q_s^* and the surface heat flux damping is set to λ_s, as calculated from (Eq 3.5) and Eq. 3.6), respectively. Likewise, F_o is set to be equal to Q_o^* and the ocean damping is set to λ_o, as calculated from (Eq. 3.7) and (Eq. 3.8), respectively.

To justify the similar treatment of Q'_s and Q'_o, Fig. 3.3 shows the lag-correlations between Q'_o and T' (blue), and Q'_s and T' (green), averaged over two midlatitude regions in the North Pacific and North Atlantic (depicted by the boxes in Fig. 3.2a). Consistent with previous studies, Q'_s is positively correlated with the SST field at negative lags, which indicates forcing of the SST anomalies, and negatively correlated with the SST field at positive lags, which indicates damping of the SST anomalies (e.g. Cayan, 1992a,b; Frankignoul et al., 1998;

von Storch, 2000; Frankignoul and Kestenare, 2002; Bishop et al., 2017). Notably, the lag-correlations between Q'_o and the SSTs have a very similar structure, suggesting that SST anomalies are driven and damped by Q'_o in a similar manner. The correlations approach zero a few months after the peak of the SST anomaly, suggesting that both the atmospheric and oceanic persistence is small in these regions on timescales longer than about one month. Hence, the key assumptions of the FK02 method appear to hold for both the surface heat fluxes and ocean heat flux convergence in both of these midlatitude regions.

The Northern midlatitude regions discussed previously are the focus of the analysis mainly because they feature prominent SST variance (Fig. 3.2a), but it is important to note that the FK02 method appears to be applicable to both Q'_s and Q'_o throughout the midlatitudes, including the Southern oceans. In particular, the structure of the lag-correlations between the heat fluxes and the SSTs in most midlatitude regions is similar to that shown in Fig. 3.3, albeit with weaker forcing from the surface heat fluxes in the western boundary current regions. On the other hand, the FK02 method does not appear suitable in tropical regions where the lag-correlation between the ocean heat flux convergence and SST anoma-

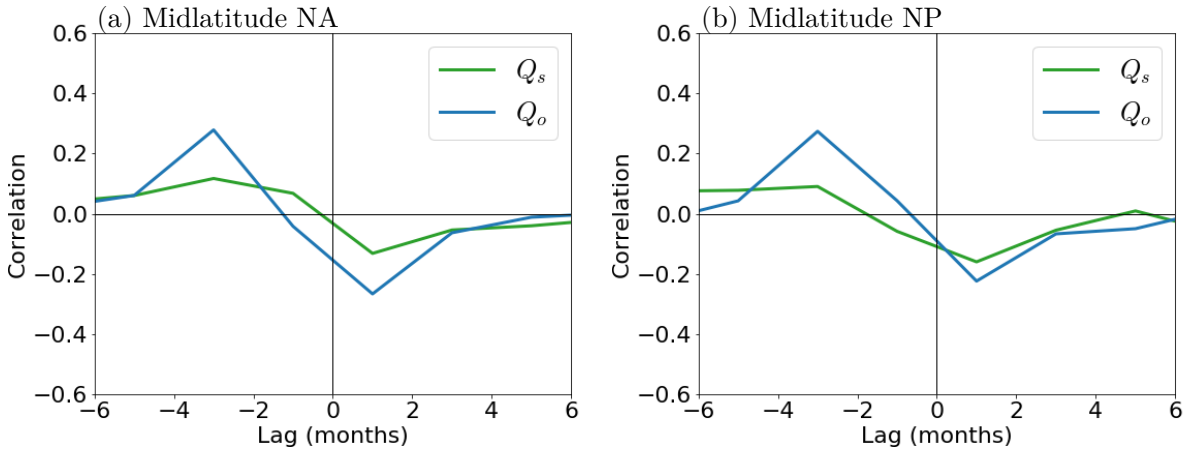

Figure 3.3: (a), (b) Lag-correlations between the observed surface heat flux anomalies (Q'_s) and SST anomalies (green), and the observed estimate of ocean heat flux convergence anomalies (Q'_o) and SST anomalies (blue), averaged over the midlatitude North Atlantic region and the midlatitude North Pacific depicted by the boxes in Fig. 3.2a. Negative lag corresponds to the heat fluxes leading the SST anomalies.

lies generally remains positive at positive lags, indicating greater oceanic persistence there. Hence, some analyses are extended to all midlatitude regions, but not to the tropics.

Note also that the ocean forcing term F_o reflects all ocean dynamical processes that drive SST variability, including ocean heat flux convergences due to the wind-driven currents and mesoscale eddies. Some previous studies interpret Ekman transport as an atmospheric forcing rather than oceanic forcing (e.g. Frankignoul and Reynolds, 1983; Deser et al., 2010) since this transport is driven directly by the surface winds. However, the wind-driven Ekman transport is retained in F_o in order to maintain physical consistency with other processes that transport heat in the ocean mixed-layer. Nevertheless, as shown in Section 3.3, F_o is generally dominated by non-Ekman transport throughout the midlatitudes, and hence the conclusions are not sensitive to whether the Ekman transport is included in F_o or F_a.

3.2.4 Power spectra

Analytic solutions to the power spectrum of the extended H76 model are found as follows. First, Eq. (3.3) is transformed to frequency-space as:

$$T' = |T'|e^{2\pi i\omega t} \tag{3.9}$$

where ω is the frequency and t is the time. Equation (3.9) is then inserted into Eq. (3.3), yielding:

$$(C_o 2\pi i\omega - \lambda)T' = F_a + F_o \tag{3.10}$$

Then, taking the squared-magnitude of both sides of Eq. (3.10) yields the SST power spectrum, i.e., $|T'^2|$:

$$|T'|^2 = \frac{|F_a|^2 + |F_o|^2}{\lambda^2 + 4\pi^2 C_o^2 \omega^2} \tag{3.11}$$

where we have assumed that the forcing terms are independent of each other, i.e., $|F_a F_o| = 0$. The assumption is predicated on the interpretation of F_a and F_o operating independently of each other. In principle, ocean dynamical processes are at least partially driven by atmospheric processes. But in practice, the covariance between F_a and F_o is negligible in the regions considered here.

3.3 Results

The results are presented in three subsections. In Section 3.3.1, the observed estimates of the atmospheric and oceanic forcing and damping terms are shown. In Section 3.3.2, the extended H76 model is used to explore the relative importance of both terms in driving midlatitude SST variability. The key conclusion is that the model only reproduces the observed SST variability when the combined effects of ocean forcing and damping act to reduce the low-frequency SST variance and increase the high-frequency SST variance. In Section 3.3.3, the reproducibility of the conclusions drawn from the simple model is tested in output from slab-ocean and fully-coupled configurations of CESM.

3.3.1 Observed forcing and damping terms

Figure 3.4a,b shows the variances of the atmospheric forcing (F_a) and oceanic forcing (F_o) terms, and Fig. 3.4c,d shows the surface heat flux damping (λ_s) and ocean damping (λ_o) coefficients. All fields are derived from observations using the methodology described in Section 3.2. Note that the forcing and damping terms are only shown at midlatitude regions for the reasons discussed in Section 3.2.3.

In general, the atmospheric forcing has the largest variance where the climatological-mean meridional SST gradients are strongest, such as in the vicinity of the Gulf Stream and Kuroshio currents. One plausible reason for this is because regions of larger mean surface temperature gradients are associated with enhanced variability in the advective heat transport by the atmospheric flow (i.e., $u' \cdot \nabla\overline{T_a}$ is enhanced because $\nabla\overline{T_a}$ is larger), and

thus in the forcing of SSTs via the surface heat fluxes. The variance of the ocean forcing term exhibits a similar pattern, but with even more pronounced variance in regions with high ocean-eddy activity, including, for example, the Antarctic circumpolar current, and other regions where ocean dynamics are considered more active such as the North Atlantic subpolar gyre. Notably, the variance of the ocean forcing term exceeds the variance of the atmospheric forcing term in many midlatitude regions. Note that the pattern and magnitude of the variances are similar when horizontal Ekman transport— as estimated using surface wind-stress from MERRA2 reanalysis— is included in F_a rather than F_o (compare Fig. 3.5b,c with Fig. 3.4a,b). This suggests that the ocean forcing term is dominated by ocean dynamical processes other than horizontal Ekman transport.

The pattern of the surface heat flux damping coefficient (λ_s; Fig. 3.4c) is consistent with previous studies (e.g Frankignoul and Kestenare, 2002; Park et al., 2005; Hausmann et al., 2016). In particular, the surface heat flux damping coefficient is generally largest

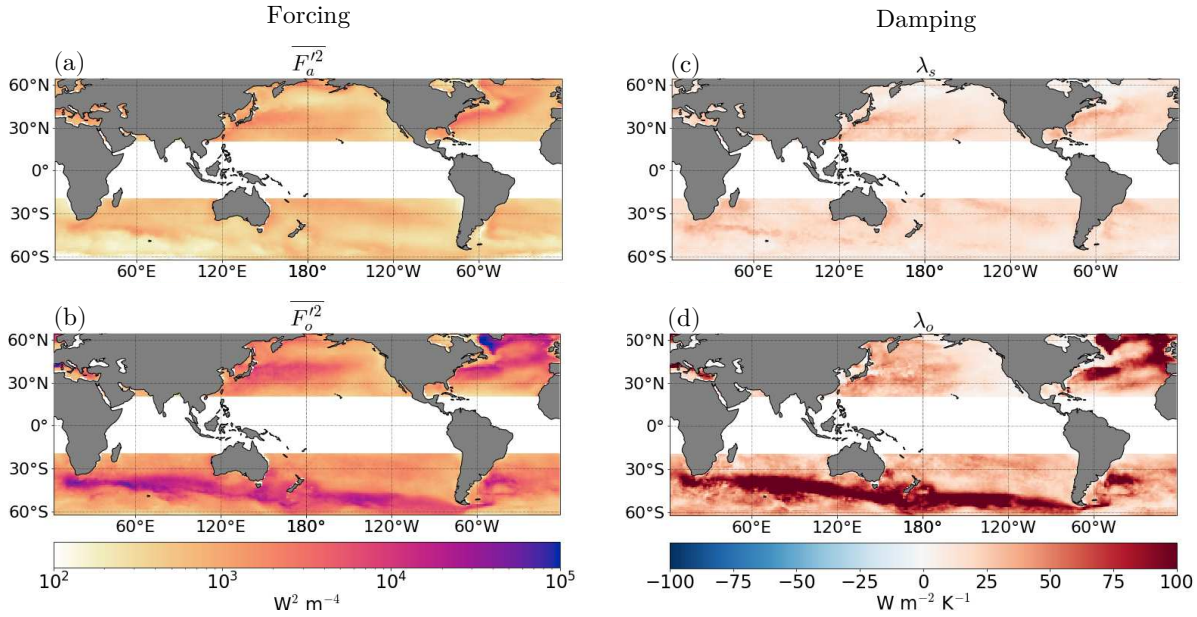

Figure 3.4: (a), (b) Variance of the atmospheric forcing and oceanic forcing terms (W^2 m^{-4}). (c), (d) Surface heat flux damping coefficient and ocean damping coefficient (W m^{-2} K^{-1}). As discussed in the text, tropical regions have been masked because our method of estimating the forcing and damping terms is not suitable there.

in the western parts of the Northern Hemisphere ocean basins, consistent with the large air-sea humidity and temperature gradients in these regions. The surface heat flux damping coefficient is quite weak in some Northern high latitude regions, which appears to be due to the effects of sea-ice. That is, since the OAFlux product only provides data for ice-free points, high latitude regions are effectively masked when sea-ice forms during the winter, and thus the surface heat flux damping term is dominated by the relatively weak damping that occurs during the warm season months (e.g Park et al., 2005).

The pattern of the ocean damping coefficient (λ_o; Fig. 3.4d) closely resembles the pattern of the mean mixed-layer depth (Fig. 3.2b). That is, regions with stronger vertical mixing, such as the along the Antarctic circumpolar current or in the North Atlantic, are generally

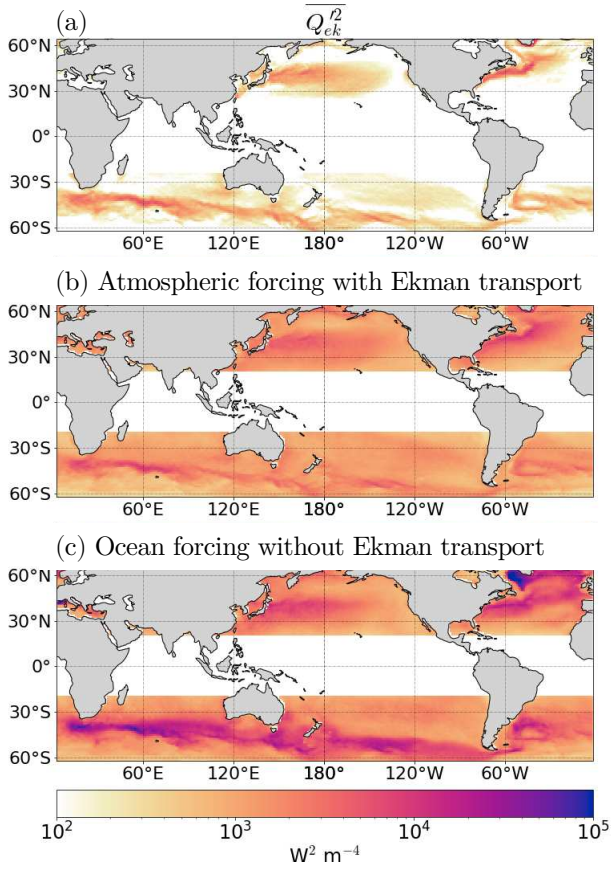

Figure 3.5: (a) Variance of ocean heat transport by horizontal Ekman currents (W^2 m^{-4}). (b) Variance of the atmospheric forcing including horizontal Ekman transport (W^2 m^{-4}). (c) Variance of the ocean forcing term excluding horizontal Ekman transport (W^2 m^{-4}).

associated with stronger ocean damping. An exception to this is in some regions along the Kuroshio current, where the mixed-layer is relatively deep, but the estimate of ocean damping is relatively small. It is unclear whether this discrepancy reflects a bias in the methodology (see discussion in Section 3.2.3). Regardless, the discrepancy in this region does not change the broad conclusions supported by Fig. 3.4c,d, namely that the damping by ocean processes exceeds the damping by surface heat fluxes over vast regions of the midlatitudes. Finally, note that the spatial patterns and magnitudes of the ocean forcing and ocean damping terms are generally similar when using a seasonally-varying mixed-layer depth from ECCO to estimate the ocean heat flux convergence, rather than an annual-mean mixed-layer depth as discussed in Section 3.2.1.

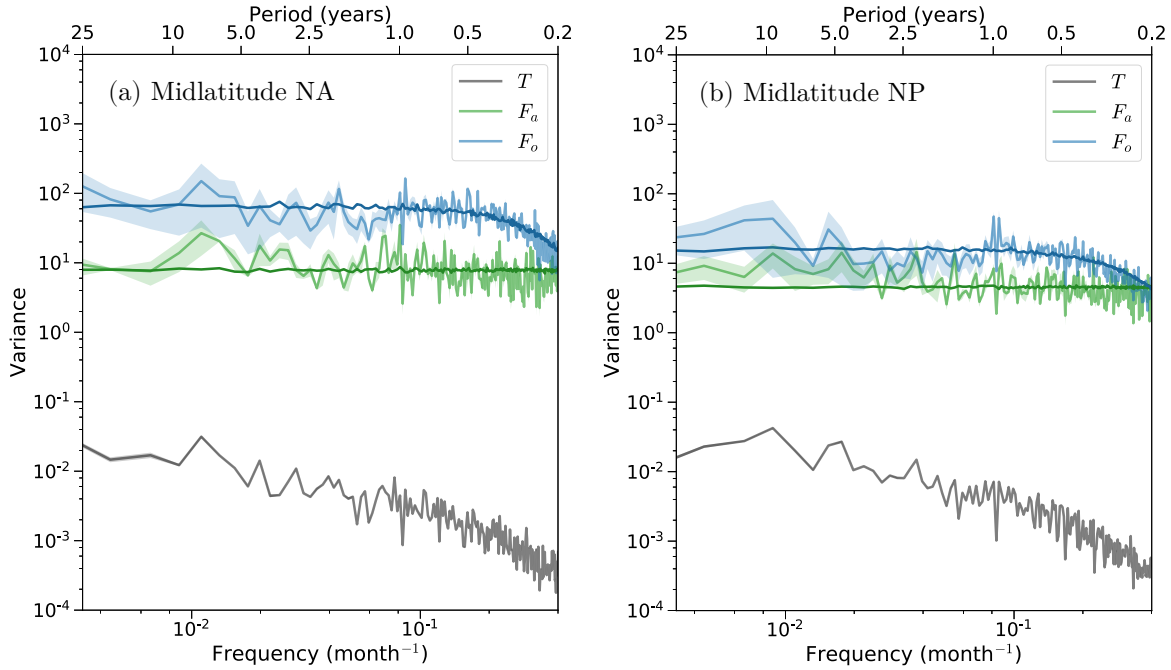

Figure 3.6: (a), (b) Power spectra of forcing terms and SST anomalies averaged over the midlatitude North Atlantic and the midlatitude North Pacific for the atmospheric forcing term (green; W^2 m^{-4}), oceanic forcing term (blue; W^2 m^{-4}), and SST anomalies (K^2; grey). Transparent shading indicates uncertainty in the forcing terms, which has been calculated from the error estimates provided by the OAFlux product. The darker green line indicates a white-noise fit to the atmospheric forcing, and the darker blue line indicates a red-noise fit to the oceanic forcing.

Figure 3.6 shows the spectral properties of F_a and F_o for the midlatitude North Atlantic (Fig. 3.6a) and midlatitude North Pacific (Fig. 3.6b) regions depicted by the boxes in Fig. 3.2a. The variance of the ocean forcing term (blue) exceeds that of the atmospheric forcing term (green) at almost all resolved timescales in both midlatitude regions. This is particularly true in the midlatitude North Atlantic region, where the ocean forcing variance is an order of magnitude greater than the atmospheric forcing variance. Note that the differences between the variances of the atmospheric and oceanic forcing exceed the range of uncertainty provided by the OAFlux product, which has been plotted as transparent shading. Figure 3.6 also indicates that the atmospheric forcing term can be roughly approximated by white-noise (darker green line), whereas the ocean forcing term is better approximated as red noise (darker blue line). The red-noise fit is computed by first producing a white-noise time series with total variance equal to the variance of $Q_o^*(t)$, and then reddening the resulting time series with lag-one autocorrelation given by $Q_o^*(t)$. This supports existing evidence that ocean dynamical processes are generally redder than their atmospheric counterparts (e.g Bjerknes, 1964; Gulev et al., 2013).

At first glance, the results shown in Fig. 3.6 appear to contradict the findings in Chapter 2, i.e., that ocean processes play a small role in driving low-frequency variability in midlatitude SSTs. However, as will become clear in the following subsection, the large effect of ocean forcing indicated in Fig. 3.6 is generally overwhelmed by the pronounced effect of ocean damping at low-frequencies.

3.3.2 Using the simple model to interpret the role of ocean forcing and damping in SST variability

In this section, the extended H76 model described in Section 3.2.2 is used to estimate the role of ocean forcing and damping in SST variability. To do so, the model is evaluated with and without the ocean dynamical terms described in the previous section. As shown in Table 3.1, the notation “H76" is used to refer to the classical Hasselmann model solution (i.e., with-

out ocean forcing F_o and damping λ_o) and "H76$_{\lambda_o,F_o}$" to refer to the extended Hasselmann model solution (i.e., with ocean processes). Figure 3.7 illustrates the SST power spectra for H76 (green), H76$_{\lambda_o,F_o}$ (black), and the observed SST power spectra (grey), averaged over the two midlatitude Northern ocean regions depicted by the boxes in Fig. 3.2a. Spectra are first calculated at individual grid points using Eq. (3.11) and then averaged over the domains. The forcing and damping values found in these regions are generally representative of most midlatitude regions. Later, it is shown how the results vary across all midlatitude oceans.

Importantly, Fig. 3.7 shows that the classical H76 model produces midlatitude SST power spectra that are too *red* relative to the observed power spectra (compare the green and grey lines). That is, the modeled spectra have too much power spectra at low frequencies, but too little power at high frequencies. The inclusion of ocean processes (i.e., both ocean forcing and damping) acts to increase the power of the SST power spectra at high frequencies, but decrease it at low frequencies, which leads to an overall whitening of the midlatitude SST spectra. As such, the agreement between H76$_{\lambda_o,F_o}$ and the observed power spectrum is very

Table 3.1: Configurations of the Hasselmann model. H76 corresponds to the Hasselmann model with atmospheric processes only ($F_o = 0$ and $\lambda = \lambda_s$), H76$_{\lambda_o}$ corresponds to the Hasselmann model with ocean damping ($F_o = 0$ and $\lambda = \lambda_s + \lambda_o$), and H76$_{\lambda_o,F_o}$ corresponds to the extended Hasselmann model with ocean forcing and ocean damping ($F_o = Q_o^*$ and $\lambda = \lambda_s + \lambda_o$).

Model	Forcing	Damping
H76	$F_a = Q_s^*$ $F_o = 0$	$\lambda = \lambda_s$
H76$_{\lambda_o}$	$F_a = Q_s^*$ $F_o = 0$	$\lambda = \lambda_s + \lambda_o$
H76$_{\lambda_o,\, F_o}$	$F_a = Q_s^*$ $F_o = Q_o^*$	$\lambda = \lambda_s + \lambda_o$

good, with the exception of frequencies higher than ~ 0.5 years. Also note that the differences between $\text{H76}_{\lambda_o,F_o}$ and H76 are significant as measured by the uncertainty estimates provided by the OAFlux product (transparent shading). The high level of agreement between the observed spectra and the $\text{H76}_{\lambda_o,F_o}$ model is in part due to the indirect method of estimating the ocean heat flux convergence in the ocean mixed layer. However, recall that the covariance between the forcing terms has been neglected in the derivation of the model SST power spectra (Section 3.2.4). The close correspondence between the black and grey spectra thus indicates that the covariance between forcing terms is small and is not essential for capturing the general shape of the midlatitude SST power spectra.

The results highlighted in Fig. 3.7 are generally consistent with the results in Chapter 2, which showed that ocean dynamics act to reduce the variance of SSTs at low-frequencies throughout the Northern oceans. The results here similarly indicate the critical importance

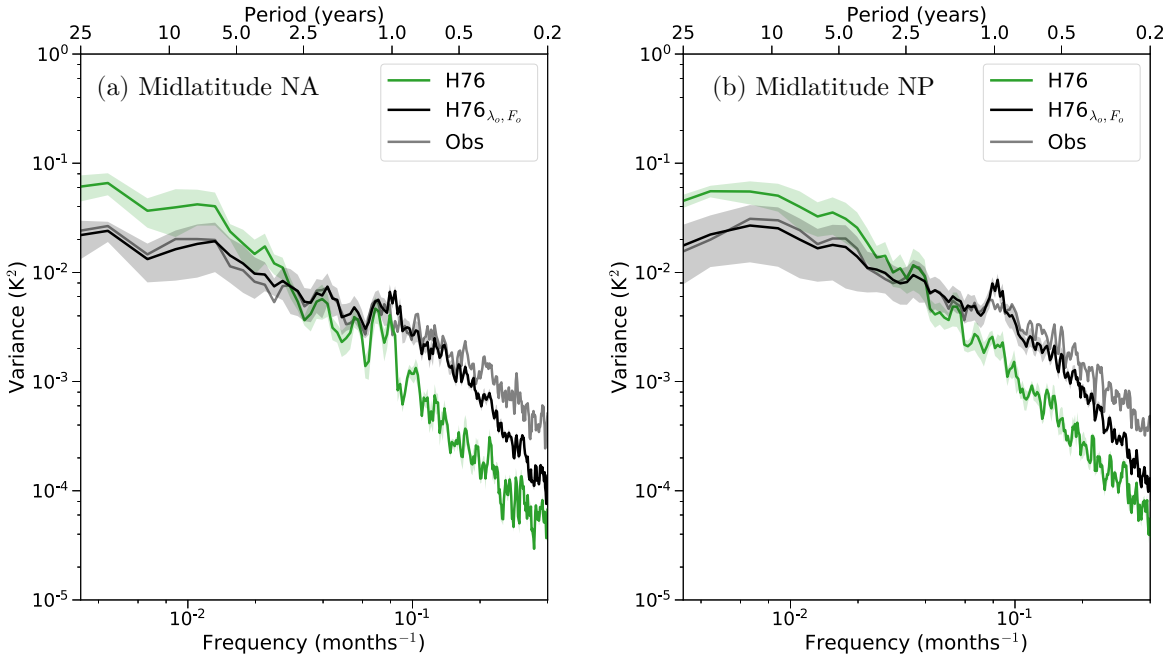

Figure 3.7: (a), (b) SST power spectra (K^2) averaged over the midlatitude North Atlantic and North Pacific for the classical Hasselmann model (H76; green), extended Hasselmann model ($\text{H76}_{\lambda_o,F_o}$; black) and observations (grey). Transparent shading indicates uncertainty in the power spectra, which have calculated from the error estimates provided by the OAFlux product. Note that a 3-point average has been applied to the power spectra.

of ocean damping processes for low-frequency SST variability in the Northern midlatitudes. In fact, as shown below, the results reveal that 1) the effects of ocean damping overwhelm the effects of ocean forcing at timescales longer than ~ 2 years in these regions, even though 2) ocean forcing is an important source of midlatitude SST variance across many timescales as shown in Fig Fig. 3.6.

Figure 3.8 quantifies the relative effects of the ocean forcing and ocean damping terms in the extended H76 model. Figure 3.8a,b, is reproduced from Fig. 3.7 but shows another solution of the model that *includes* ocean damping ($\lambda_o T'$) but *excludes* ocean forcing (F_o) (orange lines). The effect of ocean damping on the SST power spectra is thus given by the difference between the green line (H76) and orange line (H76_{λ_o}), and the effect of ocean *forcing* on the SST power spectra is given by the difference between the black line ($\text{H76}_{\lambda_o,F_o}$) and orange line ($\text{H76}_{\lambda_o}$). As evidenced in the figure, ocean damping acts to reduce the low-frequency SST variability (blue arrow in Fig. 3.8a,b), whereas ocean forcing increases the SST variability across many timescales (red arrows in Fig. 3.8a,b).

Figure 3.8c,d further quantifies the relative effects of ocean forcing and ocean damping on the modeled SST variability. Here the log-ratio of the power spectra is shown for different configurations of the simple model: the red lines show the log-ratio of the modeled SST spectra with both ocean damping and ocean forcing ($\text{H76}_{\lambda_o,F_o}$) to the modeled SST spectra with ocean damping only (H76_{λ_o}), and the blue lines show the log-ratio of the modeled SST spectra with ocean damping only (H76_{λ_o}) to the modeled SST spectra without any ocean processes (H76). Hence the red lines quantify the effects of ocean forcing as depicted by the red arrows in Fig. 3.8a,b, and the blue lines quantify the effect of ocean damping as depicted by the blue arrows in Fig. 3.8a,b. The *net* effect of both ocean forcing and ocean damping is thus given by the sum of the red and blue lines and is shown as the black line.

From Fig. 3.8c,d it is clear that ocean forcing (F_o) is an important source of variability in both regions across many timescales, increasing the modeled SST power by a factor of about $10^{0.5} \approx 3$ on timescales between 0.2 to 25 years. However, it is also clear that the

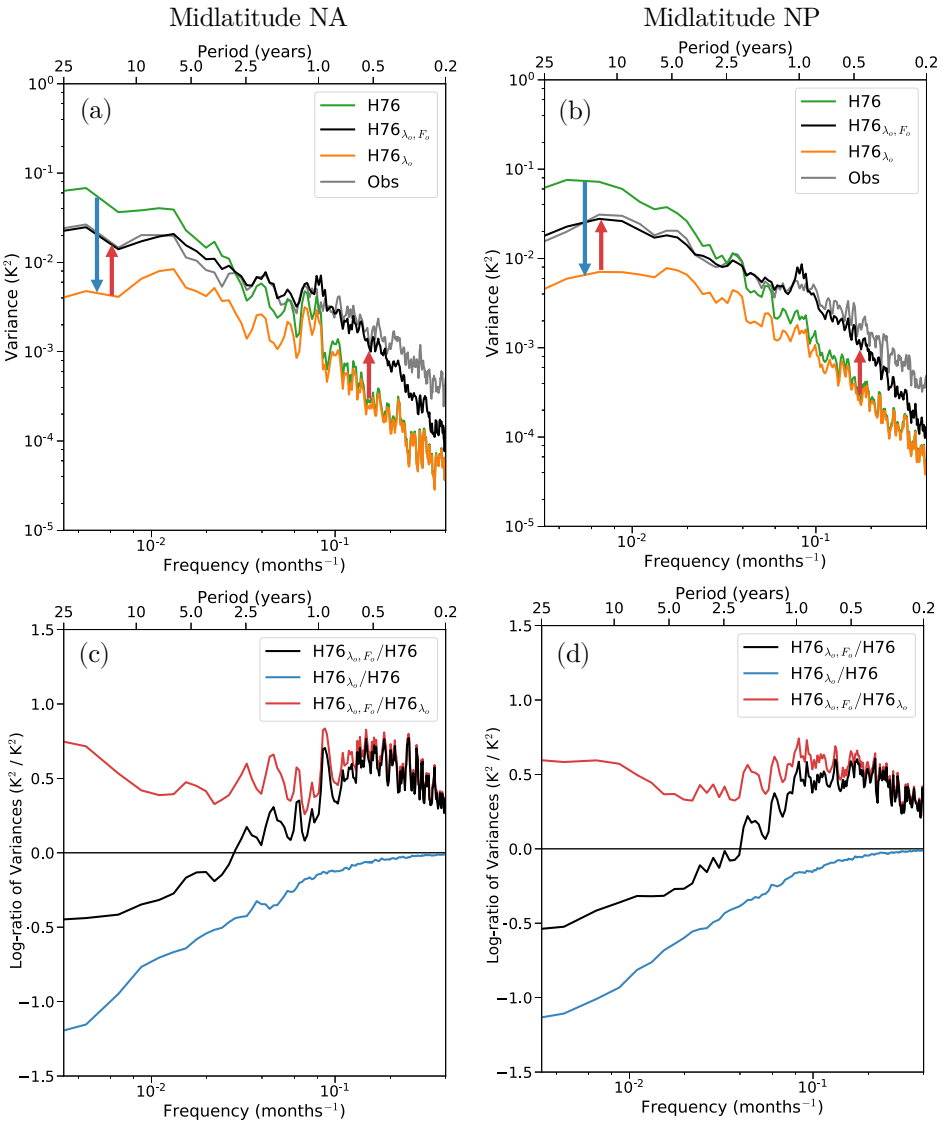

Figure 3.8: (a), (b) SST power spectra (K^2) averaged over the midlatitude North Atlantic and midlatitude North Pacific for the classical Hasselmann model (H76; green), classical Hasselmann model with ocean damping ($H76_{\lambda_o}$), extended Hasselmann model ($H76_{\lambda_o,F_o}$; black) and observations (grey). The blue arrow in (a) and (b) illustrates the effect of ocean damping, and the red arrows in (a) and (b) illustrate the effect of ocean forcing. (c), (d) Log-ratio of the power spectra for various configurations of the simple model for the midlatitude North Atlantic and North Pacific regions. The red line corresponds to $log\,(H76_{\lambda_o,F_o}/H76_{\lambda_o})$ and hence shows the effect of ocean forcing as illustrated by the red arrows in (a) and (b). The blue line corresponds to corresponds to $log\,(H76_{\lambda_o}/H76)$ and hence shows the effect of ocean damping as illustrated by the blue arrow in (a) and (b). The black line corresponds to $log\,(H76_{\lambda_o,F_o}/H76)$ and hence shows the net effect of ocean forcing and ocean damping (i.e., the sum of the red and blue lines).

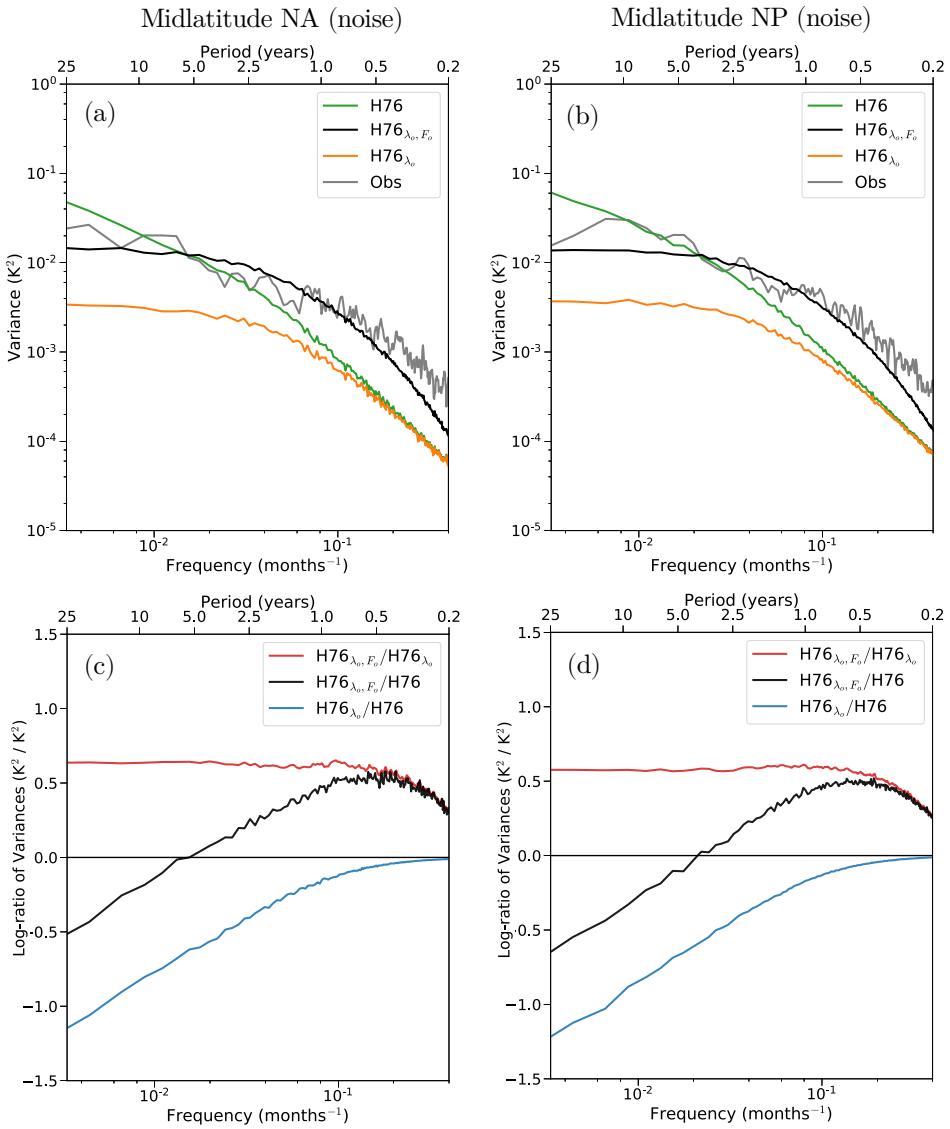

Figure 3.9: As in Fig Fig. 3.8, except the atmospheric and oceanic forcing terms have been approximated by the white and red-noise fits shown in Fig. 3.6.

effects of ocean damping processes ($\lambda_o T'$) outweigh the effects of ocean forcing on timescales longer than $\sim$ 2 years. Thus, the combined effects of ocean forcing and damping increase the variability of the SST field on timescales $<$ 2 years, but decrease it on timescales $>$ 2 years. Figure 3.8c,d also shows that the whitening effect of the combined ocean forcing and damping terms is substantial. As the maximum effect, together they act to enhance the high-frequency power by about a factor of 3, but decrease the low-frequency power by roughly the same amount. Finally, Fig. 3.9 shows that the effects of ocean forcing and damping illustrated in Fig. 3.8 are reproducible when the model is forced by the white and red-noise fits indicated in Fig. 3.6.

The above results indicate that at low-frequencies, ocean damping reduces midlatitude SST variance more than ocean forcing increases it. But the results are shown only for the two Northern midlatitude regions depicted by the boxes in Fig. 3.2a. Figure 3.10 considers the relative effects of ocean forcing and damping on the modeled low-frequency SST variance throughout the midlatitudes. Figure 3.10a shows the observed 5-year low-pass filtered SST variance and Fig. 3.10b,c,d show the corresponding modeled variances derived from the various configurations of the simple model. Figure 3.10,e-g shows maps of the log-ratio of the variances for the various configurations of the model.

In general, the classical H76 model yields low-frequency SST variances that are notably larger than the observations throughout much of the midlatitudes (compare Fig. 3.10a,b), particularly in Northern high latitude regions where the surface heat flux damping is weak (Fig. 3.4). The inclusion of ocean damping in the simple model ($\mathrm{H76}_{\lambda_o}$) acts to greatly reduce the SST variance across the midlatitudes (Fig. 3.10e). However, the resulting variances are much too low compared to the observations (Fig. 3.10c). The inclusion of both ocean damping *and* ocean forcing in the model ($\mathrm{H76}_{\lambda_o,F_o}$) acts to increase the SST variance relative to the ocean damping case (Fig. 3.10f) and the modeled SST variances are much closer to the observations (compare Fig. 3.10a,d). As quantified in Fig. 3.10h, the differences between

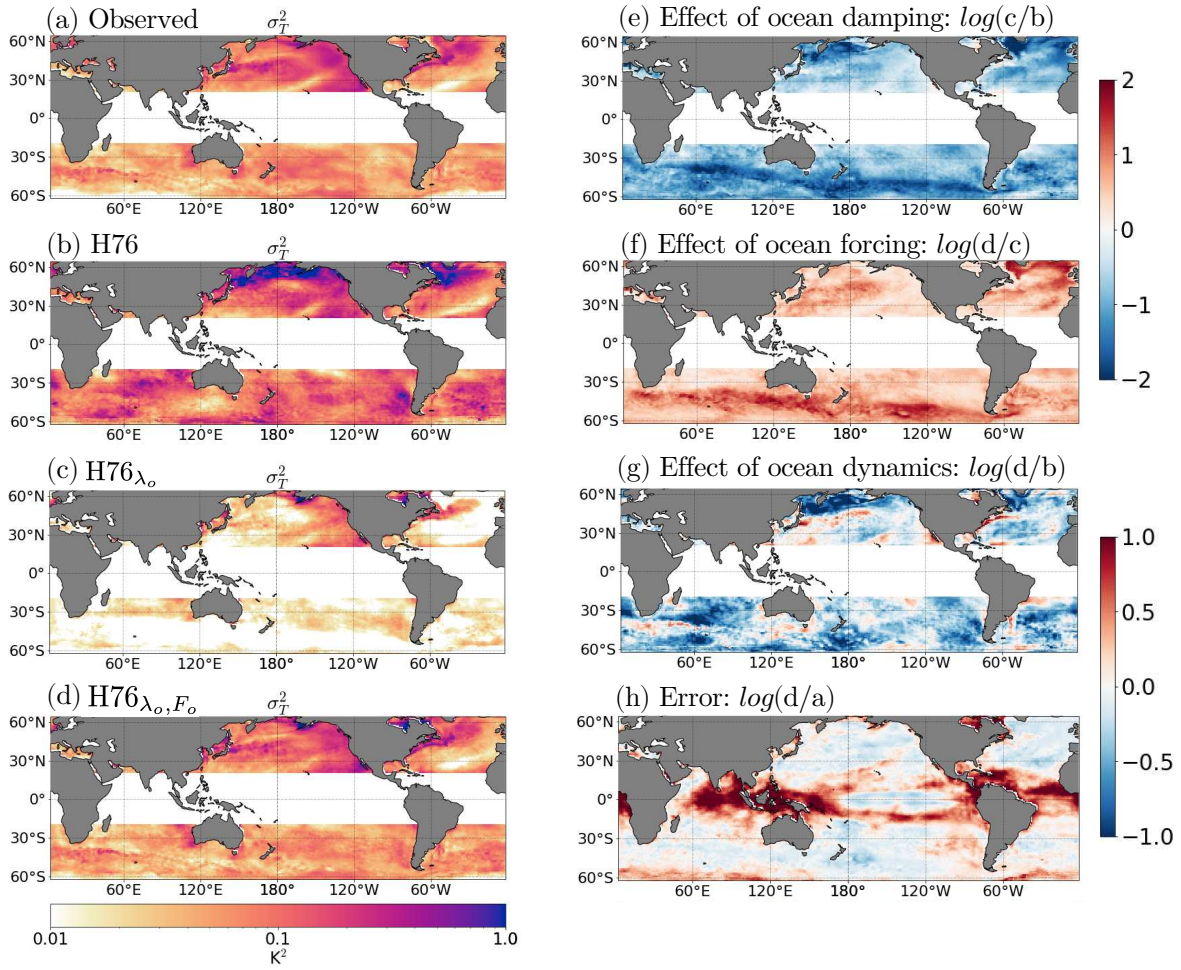

Figure 3.10: 5-year low-pass filtered SST variance (K^2) for (a) observations, (b) classical Hasselmann model (H76), (c) classical Hasselmann model with ocean damping (H76$_{\lambda_o}$), and (d) extended Hasselmann model (H76$_{\lambda_o,F_o}$). Log-ratio of the 5-year low-pass filtered SST variance for (e) H76$_{\lambda_o}$/ H76, i.e., the effects of ocean damping, (f) H76$_{\lambda_o,F_o}$/ H76$_{\lambda_o}$, i.e., the effects of ocean forcing (g) H76$_{\lambda_o,F_o}$/ H76, i.e., the net effects of ocean forcing and damping, and (h) H76$_{\lambda_o,F_o}$ to the observations, i.e., the error in the extended Hasselmann model. Note that the color bar range in (e) and (f) is different than in (g) and (h).

the observed and modeled variances are generally small throughout the midlatitudes when both ocean forcing and ocean damping are included in the model.

Note that the net effects of both ocean processes—as obtained by summing Fig. 3.10e and Fig. 3.10f—is to reduce the modeled low-frequency SST variance throughout most of the midlatitudes (Fig. 3.10g). Thus, in general, Fig. 3.10 shows that ocean forcing and damping *both* contribute substantially to midlatitude low-frequency SST variance, but the effects of ocean damping outweigh the effects of ocean forcing throughout the midlatitudes. Notable exceptions are found in western boundary current regions of the NH and the Agulhas current where the effects of ocean forcing outweigh the effects of ocean damping. This is consistent with previous studies that have found that ocean dynamical processes are important for driving SST variability in such regions (e.g. Kwon et al., 2010; Smirnov et al., 2014; Roberts et al., 2017; Small et al., 2019b; Patrizio and Thompson, 2021a).

3.3.3 Slab-ocean and fully-coupled simulations with CESM

In this section, the extended Hasselmann model is used to interpret the differences in SST variability between simulations run with an atmospheric model coupled to a slab-ocean model (hereafter referred to as the SOM) and a dynamically-active ocean model (hereafter referred to as the fully-coupled model).

As discussed in Section 3.2.1, 500 years of data have been analyzed from pre-industrial runs with CESM1 (Hurrell et al., 2013). Both are run with preindustrial radiative forcing. The classical H76 model is considered to be analogous to the slab-ocean configuration since neither include ocean dynamical processes, and likewise, the extended H76 model is considered to be analogous to the fully-coupled configuration since both *do* include ocean dynamical processes: the extended H76 model through the terms F_o and $-\lambda_o T'$, and the fully-coupled model through simulated ocean dynamical processes.

Figure 3.11 shows the 5-year low-pass filtered SST variance in the SOM (Fig. 3.11a) and the fully-coupled model (Fig. 3.11b), as well as the log-ratio of their variances (Fig. 3.11c).

In the tropics, the low-frequency SST variance is larger in the fully-coupled model, which is expected given that ocean dynamics are known to play a prominent role in driving SST variabilit y in these regions (e.g. Philander, 1983; Jin, 1997; McPhaden et al., 2006). However, in the extratropics, the low-frequency SST variance is generally *larger* in the SOM configuration. This seemingly surprising result is consistent with the results in the previous section, namely that ocean processes act to decrease the low-frequency variance of extratropical SSTs (e.g., Fig. 3.10g).

Figure 3.12 compares the SST power spectra averaged over the midlatitude North Atlantic and North Pacific regions computed from both the simple model (Fig. 3.12a,d) and the

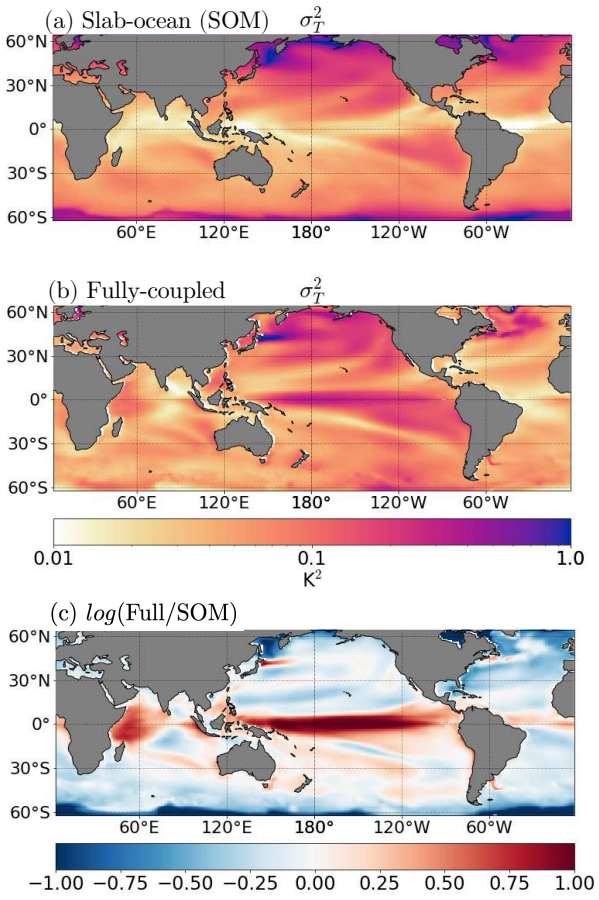

Figure 3.11: 5-year low-pass filtered SST variance (K^2) for (a) the slab-ocean model (SOM) configuration of CESM and (b) the fully-coupled configuration of CESM. (c) Log-ratio of the fully-coupled to the SOM 5-year low-pass filtered SST variance, *log* (Full/SOM).

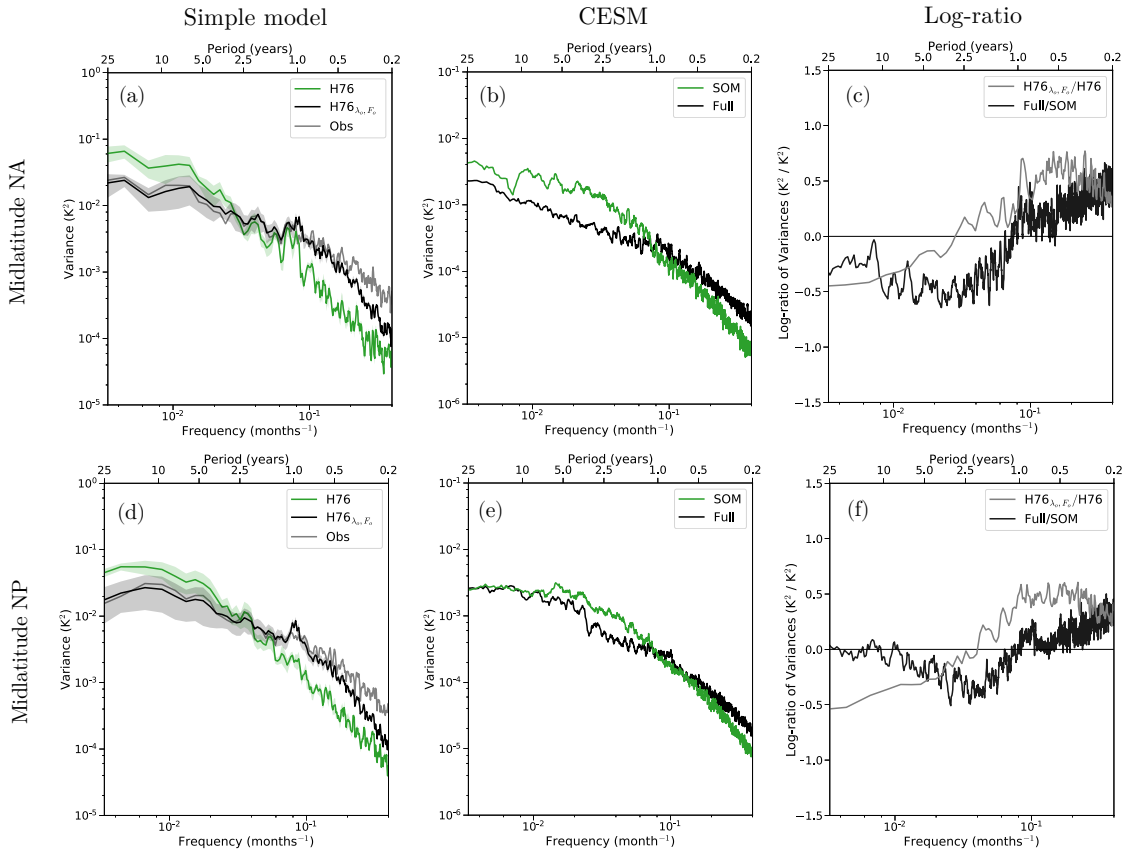

Figure 3.12: SST power spectra (K^2) averaged over the midlatitude North Atlantic for (a) the simple model and (b) CESM. Models with ocean dynamical processes are shown in black, and models without ocean dynamical processes are shown in green. (c) Log-ratio of the simulated power spectra with ocean processes to the simulated power spectra without ocean processes for CESM (black) and the simple model (grey). Positive values indicate that ocean dynamical processes increase the power. (d)–(f) As in (a)–(c) except for the midlatitude North Pacific region. Note that a 3-point average has been applied to the simple model power spectra, and a 12-point average has been applied to the CESM power spectra.

SOM and fully-coupled configurations of CESM (Fig. 3.12b,e). Note that all power spectra are first calculated at individual grid points and then averaged over the respective domains. Clearly, the models that include ocean processes (black lines in Fig. 3.12a,b,d,e) have relatively less low-frequency SST variance but relatively more high-frequency variance than the models that do not include ocean dynamical processes (green lines in Fig. 3.12a,b,d,e). The similarities between spectra are striking, particularly in the midlatitude North Atlantic. This is also reflected in Fig. 3.12c,f, which show the log-ratio of the modeled SST spectra with ocean processes to the modeled SST spectra without ocean processes for both the simple model (grey) and CESM (black). Here, it can be seen that the simple model captures the overall whitening effect of ocean dynamical processes in CESM (i.e., decrease in low-frequency variance but increase in high-frequency variance), particularly in the midlatitude North Atlantic (Fig. 3.12c). Note that the damping of low-frequency SST variability by ocean dynamics in CESM is equally robust when 1) spectra are calculated at the grid point level and then averaged over the North Atlantic and North Pacific domains as in Fig. 3.12, or 2) or calculated for area-averaged SSTs as in Fig. 3.13. In the latter case there is an even more pronounced reduction in the low-frequency SST variance in the fully-coupled model compared to the SOM, which is consistent with the small-scale effects of horizontal advection being averaged out over large spatial scales. Finally, note that qualitatively similar results to those shown in Fig. 3.12 are derived for midlatitude Southern ocean regions as well, particularly in the South Atlantic and South Indian oceans.

Figure 3.12 also indicates two interesting differences between the simple model and CESM. One, in the midlatitude North Pacific, CESM does not show any reduction in SST variance on timescales > 5 years in the fully-coupled model relative to the SOM (Fig. 3.12f). This could be due to the presence of atmosphere-ocean interactions that are unique to the fully-coupled model, which might act to enhance decadal SST variance in the North Pacific (e.g. Qiu et al., 2007; Kwon and Deser, 2007; Kwon et al., 2010; Wills et al., 2019a) and offset the effects of ocean damping. Zhang (2017) argued that such interactions give rise to a simi-

lar feature in the power spectra of North Atlantic subpolar gyre SSTs. However, our analysis suggests that this effect is relatively weak in the midlatitude North Atlantic compared to the overall whitening effect of ocean dynamics (Fig. 3.12c). The differences between Zhang (2017) and our analysis could derive from their use of a different GCM (GFDL's CM2.1), a different averaging region, and/or their use of normalized power spectra. Two, the crossover frequency at which the models with ocean processes have more variance than the models without ocean processes occurs at higher frequencies for CESM compared to the simple model (i.e., in Fig. 3.12c,f the curve for CESM is shifted to the right compared to the simple model). Our interpretation of this discrepancy is as follows: 1) ocean forcing is likely unrealistically weak in CESM due to its relatively coarse 1° horizontal resolution, and 2) the unrealistically

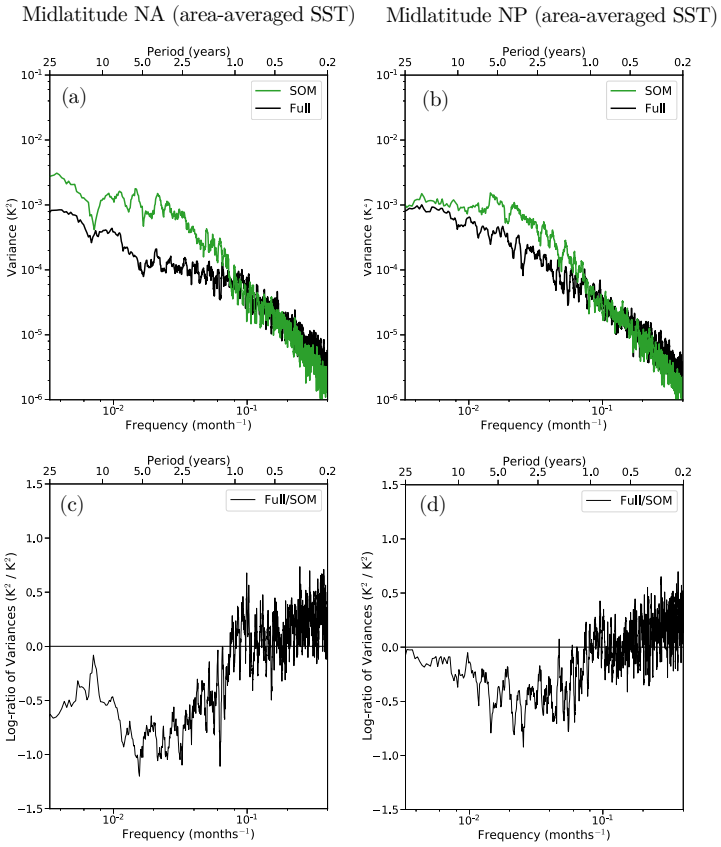

Figure 3.13: (a),(b) As in the CESM results shown in Fig. 3.12b,e, except power spectra have been calculated for area-averaged SSTs. (c), (d) Log-ratio of the power spectra shown in panels a,b (i.e. ratio of the power spectra in the fully-coupled model to the power spectra in the slab-ocean model).

weak ocean forcing means that the effects of ocean damping will likely overwhelm the effects of ocean forcing at higher-frequencies compared to the observationally-constrained simple model. According to our analyses, unrealistically weak ocean forcing would manifest most clearly as reduced high-frequency SST variance. Indeed, the 1-year high-pass filtered SST variance is lower in CESM than in the observations in most regions (Fig. 3.14), supporting the hypotheses above.

Despite these two discrepancies, the broad agreement between the low-frequency variances and SST spectra derived from the simple model and CESM (as shown in Fig. 3.10g, Fig. 3.11c and Fig. 3.12) support our primary hypothesis that the net impact of ocean dynamics is to decrease the low-frequency SST variance and increase the high-frequency SST variance throughout the midlatitudes.

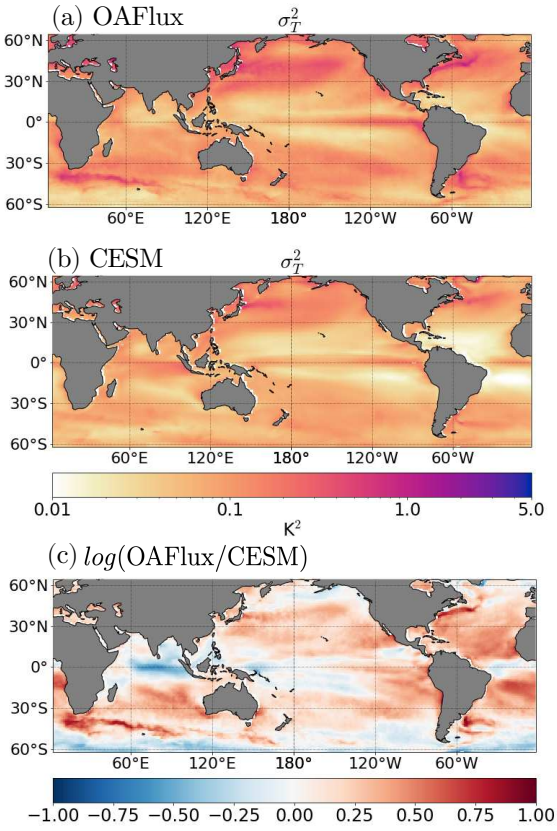

Figure 3.14: 1-year high-pass filtered SST variance for (a) OAFlux and (b) fully-coupled CESM, and (c) the log-ratio of the 1-yr high-pass filtered SST variance in OAFlux to CESM.

3.4 Discussion and Conclusions

The goal of this study is to provide novel insights into the role of ocean dynamics in midlatitude SST variability using a simple climate model. In particular, we have considered an extension of Hasselmann's model of climate variability (Hasselmann, 1976) that explicitly includes the forcing and damping of SSTs by ocean processes.

The key conclusion is that throughout most of the midlatitudes, the net effect of ocean processes is to increase the variance of SST anomalies at high-frequencies, but *decrease* the variance at low-frequencies. Specifically, it has been found that:

1. The classical H76 model driven by observed surface heat fluxes yields midlatitude SST power spectra that are much redder than observed midlatitude SST power spectra (Fig. 3.7).

2. Including observed estimates of both ocean forcing and ocean damping in the H76 model reduces the discrepancy with the observations by decreasing the SST variance on timescales > 2 years and increasing the SST variance on timescales < 2 years, leading to an overall "whitening" of the midlatitude SST variability (Fig. 3.7). The whitening effect arises because ocean forcing is an important source of SST variance across many timescales, but the effects of ocean damping exceed the effects of ocean forcing timescales $> \sim 2$ years (Fig. 3.8). Exceptions to this result were found to occur in regions of strong currents such as the Kuroshio, Gulf stream and Agulhas currents, where the effects of ocean forcing exceed the effects of ocean damping.

3. Model output from GCM simulations run on slab-ocean and dynamically-active ocean (i.e., fully-coupled) model configurations of CESM1 also shows that ocean dynamical processes reduce the low-frequency variance and increase the high-frequency variance of the SST field in many midlatitude regions (Fig. 3.11 and Fig. 3.12).

This study extends previous work that has also added ocean processes to simple models of midlatitude climate variability (i.e., models based on Hasselmann, 1976 or Barsugli and Battisti, 1998) in two key ways:

- The ocean forcing and ocean damping terms are estimated from observations. This is in contrast to studies that have assumed the form of the ocean forcing (e.g Wu et al., 2006; Cane et al., 2017; Bishop et al., 2017) or estimated the total damping from the autocorrelation of SSTs (e.g. Frankignoul and Hasselmann, 1977; Reynolds, 1978; Frankignoul, 1979; Hall and Manabe, 1997).

- The extended H76 model is used to quantify the relative roles of ocean forcing and ocean damping in observed SST variability. This is in contrast to studies that more generally comparing red-noise SST power spectra to observed SST power spectra (e.g Frankignoul and Hasselmann, 1977; Reynolds, 1978; Frankignoul, 1979; Hall and Manabe, 1997; Zhang, 2017).

The results shown here provide insight into the processes that give rise to low-frequency SST variability in models with and without ocean dynamics (e.g. Clement et al., 2015; Cane et al., 2017; Zhang, 2017; Murphy et al., 2020). For example, Cane et al. (2017) and Murphy et al. (2020) demonstrated that AMV is reduced in a fully-coupled configuration of CESM relative to a slab-ocean configuration (see Fig. 1 of Cane et al., 2017 and Fig. 4 of Murphy et al., 2020). As evidenced in Fig. 3.12a,b,c, the differences in North Atlantic SST variability between the fully-coupled and slab-ocean (SOM) configurations of CESM are remarkably well-captured by the simple model. Thus, the simple model can be used to interpret the effects of ocean dynamics on North Atlantic SST variability in CESM: ocean forcing increases the variance of SSTs across many timescales, but the effects of ocean damping outweigh the effects of ocean forcing at low-frequencies. It would be interesting to use the insights provided by the extended H76 model here to better understand the differences between other SOM and fully-coupled GCMs, including models with higher spatial resolution.

Clement et al. (2015) argued that ocean dynamics are not essential for generating AMV. Here, it has been also been shown that slab-ocean models can generate AMV, and in fact too much low-frequency variance throughout the midlatitudes in the case of CESM. However, our simple model also suggests that the processes that give rise to such SST variability in models with ocean dynamics are different. Importantly, without either ocean damping or ocean forcing in the simple model, the low-frequency SST variance is significantly different in terms of both spatial pattern and magnitude throughout the midlatitudes (Fig. 3.10). The broad agreement between the observationally-constrained simple model and CESM suggests that both of these effects are important in reality.

In Chapter 2, it was argued that midlatitude ocean dynamics play an increasingly small role in driving SST variability at increasingly low-frequencies. The results presented here provide key insights into this hypothesis. In agreement with results from Chapter 2, the simple model and CESM results shown in Chapter 3 suggest that the *net* effect of ocean dynamical processes is to decrease the SST variance at low-frequencies, and increase it at high-frequencies throughout the midlatitudes. The simple model provides insights into how this happens. That is, it reveals that ocean forcing in fact acts to redden the spectra of midlatitude SST anomalies (Fig. 3.6), but that this effect is generally overwhelmed by the effects of ocean damping away from western boundary currents (Fig. 3.10g). This result was not clearly revealed in Chapter 2 because there the primary focus was the diagnosis of the *net* effects of ocean dynamics, whereas here the *individual* effects of ocean dynamical forcing and damping have been quantified using the extended Hasselmann model.

Hence the results presented in Chapter 3 indicate that midlatitude ocean dynamics play an important role in driving low-frequency SST variability through the combined effects of both ocean forcing and ocean damping processes. The importance of ocean forcing supports previous studies that have linked low-frequency variations in SSTs to ocean dynamical processes (e.g. Kwon et al., 2010; Buckley et al., 2014; Kim et al., 2018; O'Reilly et al., 2016; Wills et al., 2019b,a; Zhang et al., 2019). However, the importance of ocean damping

also explains why previous studies have found that passive ocean models (e.g., slab-ocean models) can generate low-frequency SST variance that is comparable (or even exceeds) that in models with comprehensive ocean dynamics (e.g Clement et al., 2015; Cane et al., 2017; Murphy et al., 2020).

Overall, the conclusions discussed here have implications for our understanding of the role of the ocean in midlatitude SST variability, and hence for midlatitude climate variability. It has been found that the extended Hasselmann model can be used to interpret midlatitude SST variability, and the results suggest that forcing and damping from ocean dynamical process are critical mechanisms of midlatitude SST variability. In the final chapter, the extended Hasselmann model is used to explore the response of the atmospheric circulation to oceanic-forced SST variability in the midlatitudes.

Chapter 4

The Atmospheric Circulation Response to Midlatitude Ocean-Forced SST Variability

4.1 Introduction

In the first two chapters, a few important aspects of the role of ocean dynamical processes in midlatitude SST variability were revealed. In Chapter 2 and Chapter 3 it was shown that—in the *net*—ocean dynamical processes act to damp midlatitude SST variance at low-frequencies, but in Chapter 3 it was also shown that ocean dynamical processes are an important source of midlatitude SST variance across many timescales. Does such oceanic-forced SST variability impact the variability of the atmospheric circulation and other aspects of the climate? In this short chapter, this question is addressed using the simple model developed in Chapter 3. This work is currently in preparation for submission to Geophysical Research Letters (Patrizio and Thompson, 2021c).

Understanding the impacts of midlatitude oceanic dynamics on the atmosphere is key to understanding the role of the midlatitude ocean in the climate system. The long-term *mean* ocean heat transport along western boundary currents, such as the Kuroshio-Oyashio Extension (KOE) and the Gulf Stream, have been linked to important impacts on the overlying atmosphere. In particular, the strong mean SST gradients that exist in such regions has been to affect the position and strength of the midlatitude storm tracks as well as other aspects of the free-tropospheric flow (e.g. Nakamura et al., 2004, 2008; Brayshaw et al., 2008; Minobe et al., 2008, 2010; Small et al., 2014; Ma et al., 2017).

The atmospheric impacts of *variability* in midlatitude ocean heat transport are less well-understood. While there is increasing evidence that the midlatitude ocean plays an active role in driving SST variability, particularly in western boundary current regions (e.g., Bishop

et al., 2017; Roberts et al., 2017; Small et al., 2019b; Patrizio and Thompson, 2021a,b), the effects of such oceanic-forced SST variability on the large-scale atmospheric circulation are unclear. In this study, this outstanding issue is addressed using a novel observationally-based method to demonstrate a strong link between the large-scale atmospheric circulation and oceanic-forced SST anomalies in the KOE region.

The atmospheric response to midlatitude SST anomalies is both complex and subtle in theory, which makes its detection challenging in practice. Linear quasigeostrophic theory predicts that the surface heat flux anomalies associated with midlatitude SST anomalies are balanced by horizontal temperature advection by the lower-tropospheric flow (Hoskins and Karoly, 1981). For example, the heat fluxes associated with warm SST anomalies are balanced by meridional cold advection from a low-level cyclonic anomaly east of the SST anomalies. In this case, the formation of the low-level cyclonic (low-pressure) anomaly can be explained by the lower-tropospheric warming, which is associated with an expansion of the atmospheric column and hence mass divergence aloft. In any case, the predicted circulation anomalies are weak and hence can be easily obscured by the strong internal variability of the extratropical atmosphere. The response is further complicated by nonlinear feedbacks between the atmospheric mean flow and transient eddies (e.g., Peng et al., 1997; Peng and Whitaker, 1999; Kushnir et al., 2002). In this case, the response often resembles the pattern of atmospheric variability that forces the SST anomalies in the first place (e.g., Peng and Robinson, 2001). For example, the nonlinear response to warm midlatitude SST anomalies is typically associated with warm advection from a low-level anticyclonic anomaly downstream of the SST anomalies (e.g., Liu and Wu, 2004; Ferreira and Frankignoul, 2005; Deser et al., 2004, 2007).

Nonetheless, with advances in observations and modeling systems over the last few decades, there is increasing evidence that the atmospheric circulation responds to midlatitude SST anomalies, particularly in regions of strong oceanic currents such as along the KOE (e.g., Kwon and Deser, 2007; Kwon et al., 2010, 2011; Frankignoul et al., 2011; Taguchi et al.,

2012; Smirnov et al., 2015; O'Reilly and Czaja, 2015; Révelard et al., 2016, 2018; Wills and Thompson, 2018). For example, Wills and Thompson (2018) showed that the observed SST anomalies in the KOE region precede an atmospheric pattern that broadly resembles the linear response to midlatitude SST anomalies described by Hoskins and Karoly (1981). Yook et al. (2021) showed that a similar atmospheric pattern emerges in atmospheric general circulation model (AGCM) experiments wherein the Community Atmosphere Model 5 (CAM5 Hurrell et al., 2013) is forced with SST anomalies in the KOE region. Various atmospheric responses have also been linked to other metrics of Kuroshio current variability (e.g., Frankignoul et al., 2011; Smirnov et al., 2015; O'Reilly and Czaja, 2015; Révelard et al., 2016), such as its meridional displacements (e.g., Frankignoul et al., 2011; Smirnov et al., 2015).

The previously discussed studies suggest that the midlatitude ocean may have an active role in influencing the variability of the atmospheric circulation. However, direct links between atmospheric circulation anomalies and midlatitude SST variability forced by ocean heat flux convergence anomalies have not been clearly shown in the observations, particularly in the KOE region. Does the atmospheric circulation respond to KOE SST anomalies forced by ocean heat transport? Or does the atmospheric circulation primarily respond to KOE SST anomalies forced by atmospheric dynamics? The distinction is important because oceanic and atmospheric-forced SST anomalies may have different characteristics, such as their magnitude, spatial scale, and persistence, and hence may be associated with different atmospheric responses. It is also important to understand the forcing mechanisms of the atmospheric response in order to accurately account for such processes in climate models.

In this study, we explore the relative importance of oceanic and atmospheric-forced SST anomalies in the KOE region for the atmospheric circulation response. To do so, we apply the extension of Hasselmann's model of climate variability to isolate the oceanic and atmospheric-forced components of the observed SST variability in the KOE region. The model was used in Chapter 3 to quantify the relative roles ocean dynamical forcing and damping in driving SST

variability throughout the midlatitudes. Here, the model is applied to explore the impacts of midlatitude ocean dynamical forcing on the atmospheric circulation. The key result is that a large-scale atmospheric circulation response to SST variability in the KOE region, resembling that found in some previous studies (e.g., Kwon et al., 2011; Frankignoul et al., 2011; Wills and Thompson, 2018 Yook et al., 2021), is strongly linked to *oceanic-forced* SST variability, but *not* to atmospheric-forced SST variability. The findings thus provide novel evidence of the importance of midlatitude ocean dynamical processes for climate variability.

4.2 Methods

4.2.1 Observational data sources

The primary observational data sources are similar to those used in Chapter 3 (see section Section 3.2.1), with the addition of sea-level pressure, precipitation and 2m temperatures from the ERA5 reanalysis (Hersbach et al., 2020). In all cases, monthly-mean data are used over the period 1980-2017 and at 1° resolution. Monthly anomalies are calculated by removing the linear trend and seasonal cycle from the SSTs and air-sea heat fluxes prior to all analyses. The remote impact of ENSO on the midlatitude variability is minimized by removing the components of the fields that are linearly related to ENSO variability as estimated from the Niño 3.4 index.

4.2.2 Oceanic and atmospheric-forced SST indices

The oceanic-forced component of the observed SST anomalies is estimated by evaluating the extended Hasselmann model as in Chapter 3, except with *only* the observed estimate of oceanic forcing ($F_o = Q_o^*$ and $F_a = 0$). We define T_{ocn} as the oceanic-forced component of the SST anomalies, which is computed from the extended Hasselmann model with *oceanic forcing only* as follows:

$$C_o \frac{\partial T_{ocn}}{\partial t} = F_o - \lambda T_{ocn} \tag{4.1}$$

Likewise, we define T_{atm} as the atmospheric-forced component of the SST anomalies, which is computed from the extended Hasselmann model with *atmospheric forcing only* as follows:

$$C_o \frac{\partial T_{atm}}{\partial t} = F_a - \lambda T_{atm} \tag{4.2}$$

Equations (4.1) and (4.2) are then discretized at monthly resolution and integrated using a 1st order Runge-Kutta method (i.e. forward-difference) to obtain the time evolution of T_{ocn} and T_{atm} as follows:

$$T_{ocn}(t + \Delta t) = \left(1 - \frac{\lambda \Delta t}{C_o}\right) T_{ocn}(t) + \frac{\Delta t}{C_o} F_o(t) \tag{4.3}$$

and

$$T_{atm}(t + \Delta t) = \left(1 - \frac{\lambda \Delta t}{C_o}\right) T_{atm}(t) + \frac{\Delta t}{C_o} F_a(t) \tag{4.4}$$

where $\Delta t = 1$ month, and initial conditions are provided by the observed SSTs at the beginning of the observed record.

Figure 4.1a shows the log-ratio of the resulting variances in T_{ocn} to T_{atm} evaluated at each point in the North Pacific. Note that T_{ocn} and T_{atm} are evaluated using all months of the year, but Fig. 4.1a highlights variances for the winter months (DJF). Results are similar for other seasons. The variance of T_{ocn} exceeds the variance of T_{atm} in the KOE current region and its associated extension, but the opposite is generally true in the eastern basin where atmospheric forcing of SSTs is large (e.g., Smirnov et al., 2014).

Throughout the rest of the study, we focus on SSTs averaged over the KOE region (37°-44°N, 140°-171°E) indicated by the black box in Fig. 4.1a. This region has been the focus of many previous studies because it is a region with marked ocean dynamical activity, as evidenced in Fig. 4.1a. The observed SSTs (T) and the components linked to oceanic and atmospheric processes (T_{ocn} and T_{atm}) are averaged over the KOE region to provide

area-averaged indices of the oceanic- and atmospheric-forced SST anomalies in the KOE region. Monthly sea-level pressure (SLP) anomalies are then linearly regressed onto the area-averaged SST indices to understand the relationships between the atmospheric circulation and the different components of the observed SST variability in the KOE region. We focus primarily on winter months (DJF) when air-sea interactions are generally strongest.

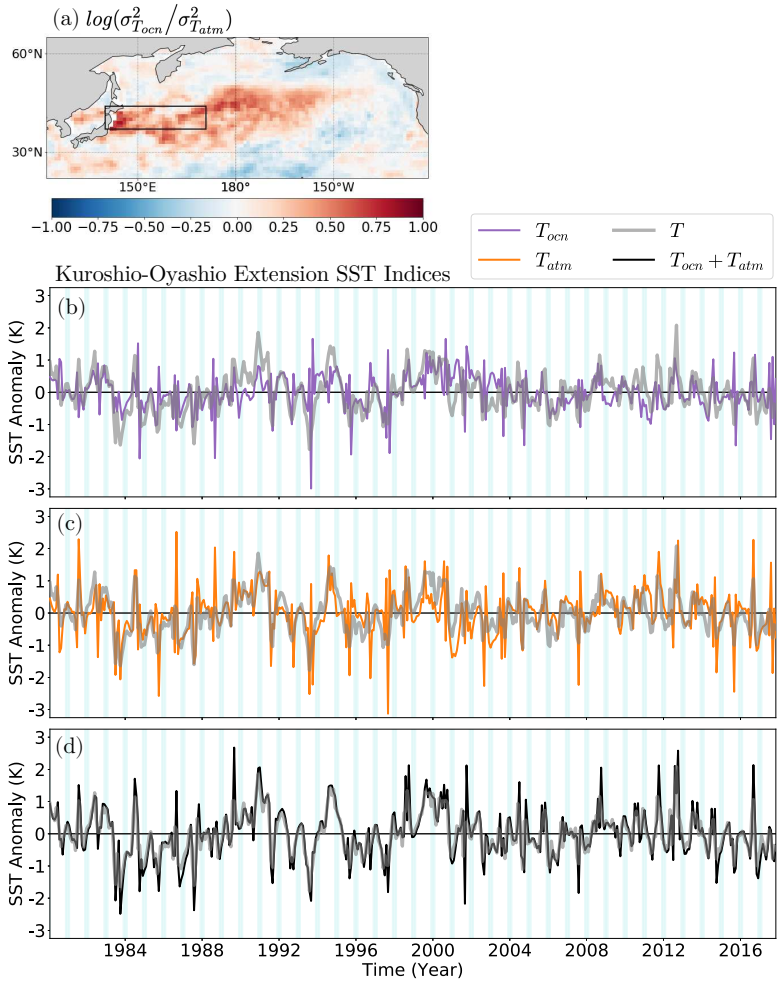

Figure 4.1: (a) Log-ratio of wintertime (DJF) variances for oceanic-forced SST variance (T_{ocn}) to atmospheric-forced SST variance to (T_{atm}) for the North Pacific basin. The time evolution of oceanic-forced and atmospheric-forced SST indices averaged over the KOE region (black box in panel a) is shown in purple in (b) and orange in (c). The time evolution of the sum of oceanic and atmospheric-forced SST indices ($T_{ocn} + T_{atm}$) averaged over the KOE region. The observed total SST index averaged over the KOE region is shown in grey. The teal stripes indicate winter months (DJF).

4.3 Results

4.3.1 Kuroshio-Oyashio Extension SST indices

Figure 4.1b-d shows the KOE-averaged observed SST anomalies (T; grey) superposed on the associated estimates of oceanic-forced SST anomalies (T_{ocn}; purple in Fig Fig. 4.1b) and atmospheric-forced SST anomalies (T_{atm}; orange in Fig. 4.1c). The sum of the atmospheric and oceanic components (black in Fig. 4.1d) agrees well with observed SST index (grey), which is expected because the ocean heat flux convergence anomalies have been estimated indirectly as a residual in the mixed-layer energy budget.

It is important to note that the observational uncertainty in the SST indices is small, as quantified by observational uncertainty in the SSTs and air-sea heat fluxes provided by the OAFlux product. The mean-squared observational uncertainty is ± 0.002 K^2 for the T index, ± 0.02 K^2 for the T_{ocn} index, and ± 0.006 K^2 for the T_{atm} index. Other sources of observational uncertainty related to, for example, the monthly mean mixed-layer depths, are not accounted for here and could also contribute to uncertainty in our estimates of T_{atm} and T_{ocn}.

Figure 4.1b-d indicates that both T_{ocn} and T_{atm} contribute to variability in the observed SSTs averaged over the KOE region. Interestingly, the wintertime variance of the T_{atm} index exceeds that of the T_{ocn} index, indicating that $\sim$40% of the KOE-averaged SST variance is forced by the ocean (0.17 K^2 for T_{ocn} versus 0.28 K^2 for T_{atm}). This suggests that a substantial fraction of oceanic-forced SST variance shown in Fig. 4.1a derives from small-scale eddy-driven heat transport which effectively cancels out when averaged over KOE region. It is also important to note that the T_{ocn} and T_{atm} indices are both strongly correlated with the observed SST index ($r \sim 0.6$ and $r \sim 0.7$, respectively). Interestingly, however, the T_{ocn} and T_{atm} indices have little to no correlation with each other at lags ranging from -12 to +12 months. This suggests that the oceanic-forced SST variability in the KOE region arises primarily from intrinsic ocean processes that are not well-explained by wind forcing, such

as the interaction between the mean large-scale oceanic currents and the mesoscale eddies in this region (e.g., Taguchi et al., 2007). It is possible that delayed interactions between atmospheric and oceanic dynamics are important for driving decadal SST variability in this region (e.g., Kwon and Deser, 2007; Qiu et al., 2007; Wills et al., 2019b). For example, in GCM simulations it has been shown that decadal SST variability in the KOE region is linked to geostrophic adjustment of the North Pacific subpolar gyre to changes in wind forcing several years earlier (e.g. Kwon and Deser, 2007; Wills et al., 2019b). However, such lagged-interactions are not readily apparent in the monthly SST indices used here.

4.3.2 Atmospheric circulation and SST patterns associated with oceanic and atmospheric-forced SST variability in the KOE region

Figure 4.2 shows the SLP and SST regression patterns associated with each of the KOE SST indices (T, T_{ocn} and T_{atm}). Note that the indices are standardized before performing the linear regression. Results at negative lags indicate the SLP and SST fields leading the KOE indices, and positive lags indicate vice versa. Figure 4.3 shows the associated significance of the SLP anomalies, as measured by the Student's two-tailed t-test.

The SLP and SST regression patterns associated with the full KOE SST index (Fig. 4.2a-c) generally support previous findings. In particular, the SST pattern shows pronounced warm SST anomalies along the KOE region, with weaker cold SST anomalies in the eastern North Pacific. The SLP pattern that *leads* the observed SST index (Fig. 4.2a) is associated with significant high-pressure anomalies in the North Pacific, warm advection over the KOE region and hence forcing of SST anomalies there (e.g., Deser and Timlin, 1997; Kushnir et al., 2002). As such, this pattern been interpreted as the "atmospheric forcing" pattern by previous studies (e.g., Wills and Thompson, 2018).

The SLP pattern that *lags* the full KOE index SST index (Fig. 4.2c) exhibits low-pressure anomalies in the North Pacific with remote anomalies in the Arctic and North Atlantic. The

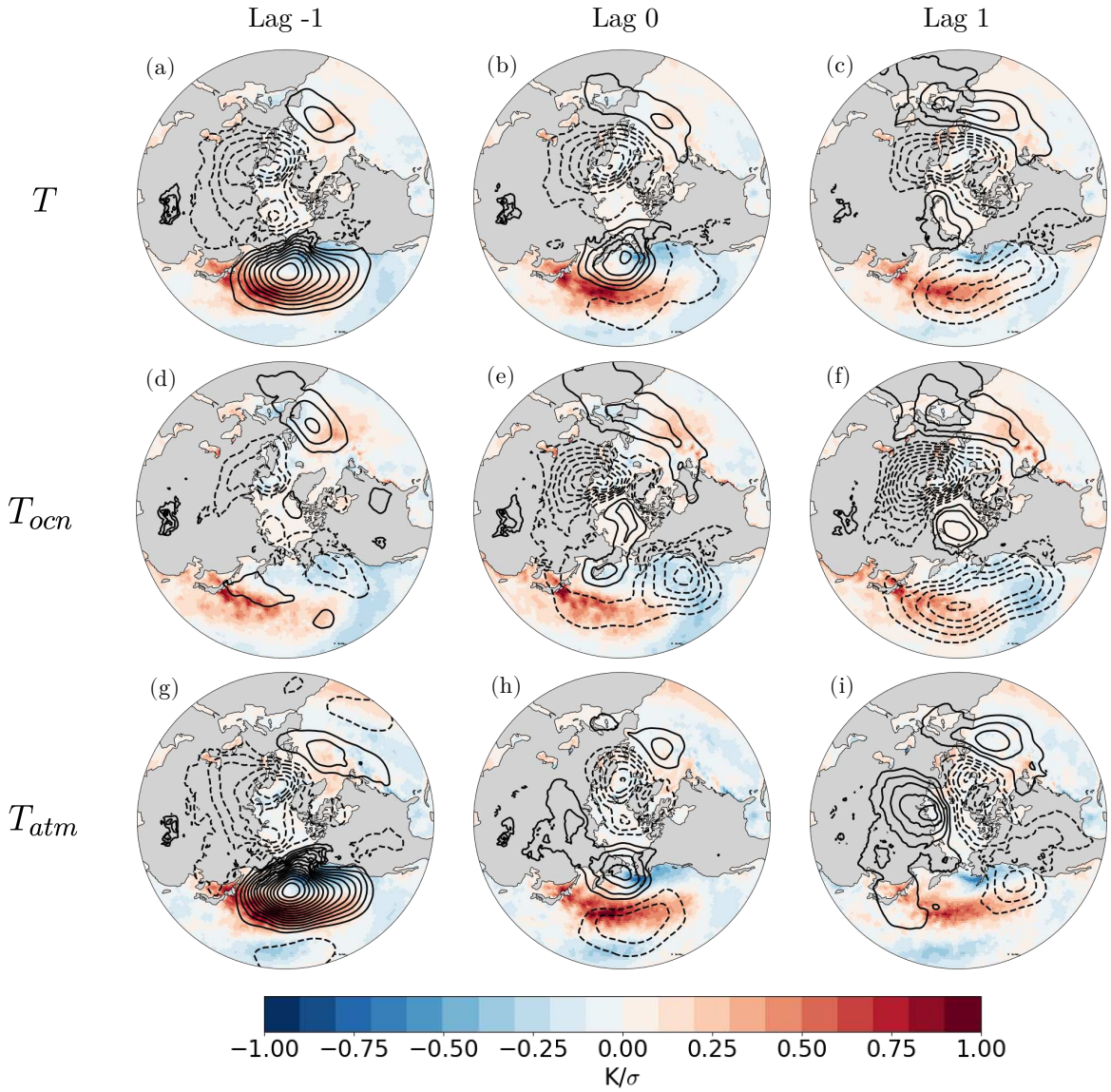

Figure 4.2: (a)-(c) Wintertime (DJF) lagged-regression of SLP (lines; hPa) and SST (shading; K) anomalies onto the observed KOE SST index for the extratropical Northern hemisphere (25°-90°N). The SST index has been standardized before performing the regression. Negative lag means the SLP and SST fields lead the SST index, and positive lag indicates vice versa. SLP contour levels are drawn every 0.4 hPa and dashed lines indicate negative SLP anomalies. (d)-(f) As in (a)-(c), except for the oceanic-forced SST index. (g)-(i) As in (a)-(c), except for the atmospheric-forced SST index.

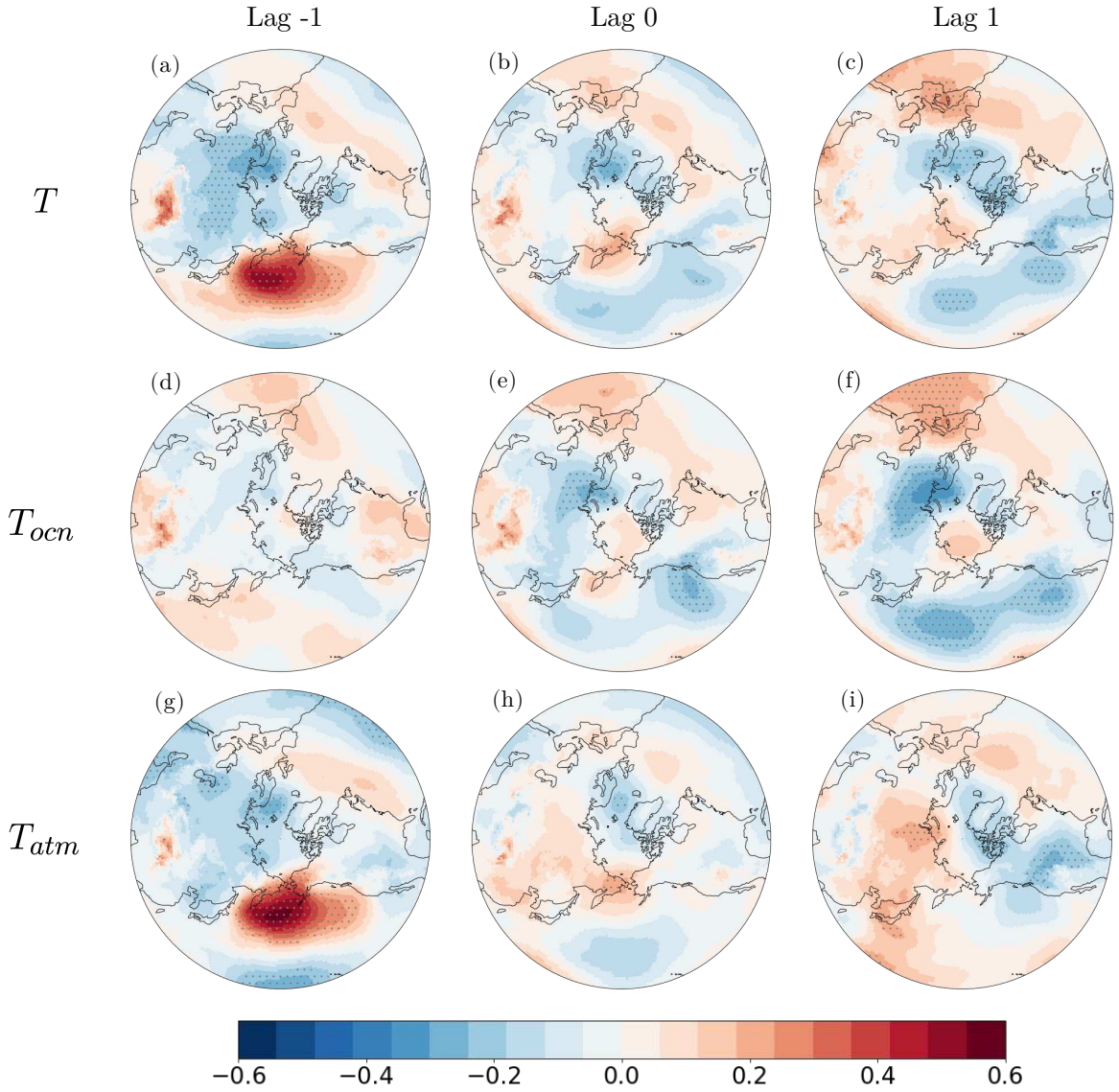

Figure 4.3: As in Fig. 4.2, except for the correlation between SLP anomalies and the KOE SST indices. Grey stippling indicates the points that are statistically significant at the 95% level as measured by the Student's two-sided t-test.

low-pressure anomaly is consistent with the linear atmospheric response to midlatitude SST anomalies Hoskins and Karoly (1981) and hence has been interpreted as the "atmospheric response" pattern (e.g., Wills and Thompson, 2018). The remote SLP anomalies lagging the KOE SST index resemble the remote SLP anomalies associated with the atmospheric forcing pattern, but are generally more significant, particularly the high-pressure anomalies in the North Atlantic, Southern Europe and North Africa (Fig. 4.3c). It is unclear what causes the remote SLP anomalies at a lag of one month. On the one hand, such anomalies may reflect a nonlinear atmospheric response to KOE SST anomalies, which can project onto hemispheric-scale circulation anomalies resembling the leading pattern of extratropical atmospheric variability (e.g., Ferreira and Frankignoul, 2005; Deser et al., 2004, 2007). On the other hand, it is possible that such remote anomalies may arise from sources other than KOE SST variability, such as the persistence in the atmospheric pattern of variability that forces the KOE SST variability to begin with (Fig. 4.2a). This result thus merits further investigation in future work.

The results shown in the middle and bottom rows of Fig. 4.2 provide further insights into the origins of the atmospheric circulation and SST anomalies associated with the KOE SST variability. To first order, the SST patterns associated with the T, T_{ocn} and T_{atm} indices bear strong resemblance to each other. However, there are some differences. Notably, the SST pattern associated with T_{ocn} (Fig. 4.2d-f) generally has the largest amplitude in a narrow region in the immediate vicinity of the KOE region, consistent with local oceanic forcing, whereas the SST pattern associated with T_{atm} (Fig. 4.2g-i) has largest amplitude over a much broader region, consistent with relatively large-scale atmospheric forcing.

In contrast, the SLP patterns associated with the T_{ocn} and T_{atm} exhibit very different structures from each other. The large region of high pressure that leads the KOE SST variability in the full SST index is only apparent in the regressions based on T_{atm}. The results are thus consistent with the notion that the high-pressure anomaly is forcing SST anomalies and hence should be interpreted as the atmospheric forcing pattern. Since T_{ocn}

is not clearly associated with any distinct pattern of atmospheric circulation anomalies, the results also support the notion that the SST pattern associated with T_{ocn} is primarily driven by intrinsic ocean dynamics as previously discussed.

Importantly, the low-pressure anomaly that lags the observed SST index is only apparent in the regressions based on T_{ocn}. In fact, the SLP anomalies that lag T_{ocn} are even more significant than those that lag the full SST index (compare Fig. 4.3c and Fig. 4.3f). The results thus provide evidence that only oceanic-forced SST variability in the KOE region is linked to the basin-wide low-pressure anomaly. The T_{ocn} index is also associated with remote SLP anomalies at a lag of one month that resemble, but are more pronounced, than remote SLP anomalies found in the full regression (e.g. the high-pressure anomalies in Southern Europe and North Africa). This result suggests that oceanic-forced SST variability in the North Pacific may project onto climate variability across the hemisphere. However, as previously discussed, it remains to be determined whether the remote circulation anomalies are part of the atmospheric response to oceanic-forced SST variability in the KOE region.

It is important to emphasize that the circulation anomalies associated with the atmospheric response shown in Fig. 4.2—including the far-field circulation anomalies— are highly significant. They are significant at the 95% confidence level (Fig. 4.3) and are reproducible in analyses repeated for the first and second halves of the data record (not shown).

Why is only oceanic-forced SST variability in the KOE region strongly linked to a large-scale atmospheric circulation response at a lag of one month? This is a particularly interesting result because, as previously discussed, i) the variance of the T_{atm} index exceeds the variance of the T_{ocn} index and both indices are associated with similar SST patterns and yet ii) the variability in T_{ocn} is required to explain the observed SLP anomalies at positive lag. To help explain this result, Fig. 4.4 shows maps of the surface heat flux anomalies regressed onto the three KOE SST indices. Importantly, the T_{ocn} index is associated with stronger and more persistent heat loss by the ocean, whereas the T_{atm} index is associated with heat gain prior to the peak of the SST anomaly, and weak heat loss during and after the peak of

the SST anomaly. When averaged over the KOE region and the winter months (DJF), the surface heat flux anomaly associated with T_{ocn} variability is -12.1 W/m^2 (heat lost by the ocean and *gained* by the atmosphere), and the surface heat flux anomaly associated with T_{atm} variability is 1.4 W/m^2 (heat gained by the ocean and *lost* by the atmosphere).

The results shown in Fig. 4.4 thus suggest that the oceanic-forced SST variability is more persistent than the atmospheric-forced SST variability. Indeed, the lag-autocorrelation of the T_{ocn} index exceeds that of the T_{atm} index: the wintertime lag-autocorrelation averaged over lags of 1-3 months is 0.53 for T_{ocn} and 0.32 for T_{atm}. This is consistent with results from Chapter 3, which showed that the power spectra of the observed estimate of the oceanic forcing is generally redder than that of the atmospheric forcing throughout the midlatitude oceans. It also supports existing evidence that ocean dynamical processes are generally redder than their atmospheric counterparts (e.g., Bjerknes, 1964; Gulev et al., 2013). Thus, both the persistence and magnitude of the surface heat flux anomalies associated with ocean-driven SST anomalies appear to be key to driving an atmospheric response during the winter months.

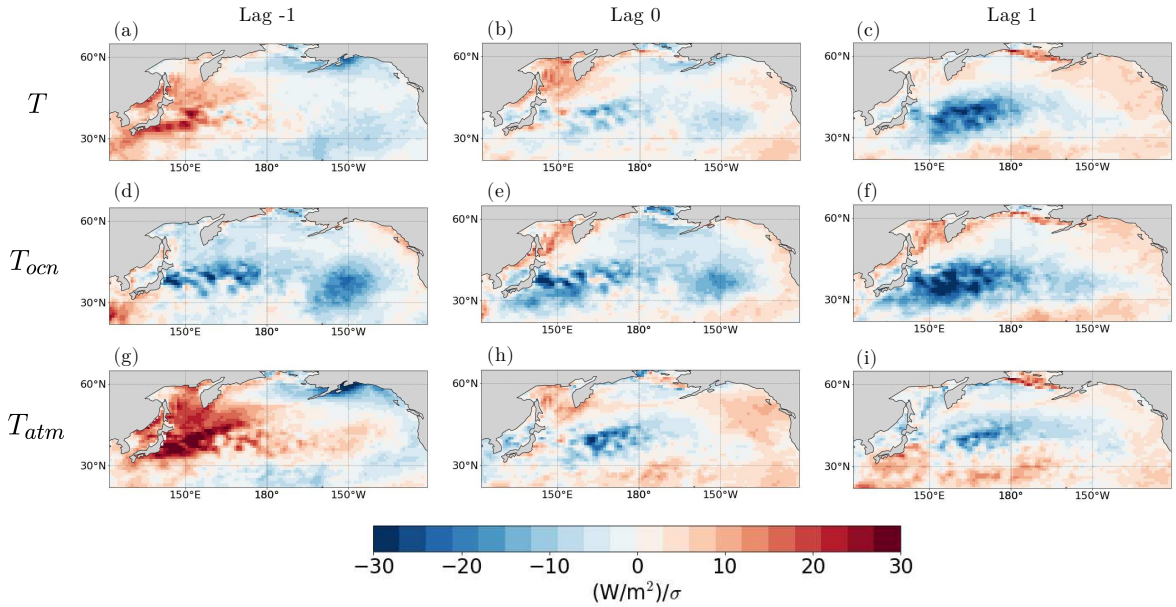

Figure 4.4: As in Fig. 4.2, except for surface heat flux anomalies (W/m^2) for the North Pacific basin. Cool colors indicate surface heat loss and warm colors indicate surface heat gain.

4.4 Discussion and Conclusions

There is increasing evidence that the atmosphere responds to midlatitude SST variability in regions of strong oceanic currents, such as the Kuroshio-Oyashio Extension (KOE) region (e.g. Kwon et al., 2010; Frankignoul et al., 2011; Smirnov et al., 2015; O'Reilly and Czaja, 2015; Révelard et al., 2016; Wills and Thompson, 2018). However, it is unclear whether such atmospheric responses arise primarily from SST variability driven by ocean heat transport or by atmospheric dynamics. Distinguishing between the forcing mechanisms behind the atmospheric response is essential to understanding and accurately modeling climate variability, particularly in the extratropics.

In this study, a novel method is used to diagnose the atmospheric circulation anomalies associated with oceanic and atmospheric-forced SST anomalies in the KOE region. The extension of Hasselmann's climate model discussed in Chapter 3 is used to isolate the oceanic and atmospheric-forced components of the observed monthly SST variability averaged over the KOE region, and then the associated atmospheric circulation anomalies are diagnosed by lagged-regression of monthly sea-level pressure (SLP) onto the oceanic and atmospheric components of the KOE-averaged SST anomalies.

An atmospheric circulation pattern lagging the KOE-averaged SST anomalies by one month is found to be strongly linked to oceanic-forced SST variability, but *not* atmospheric-forced SST variability (Fig. 4.2f and Fig. 4.2i). The atmospheric circulation pattern lagging the oceanic-forced SST anomalies by one month is associated with a significant low-pressure anomaly spanning the North Pacific. The low-pressure anomaly is generally consistent with the theoretical response from linear theory Hoskins and Karoly (1981), and hence is interpreted as an atmospheric response to the KOE SST anomalies as in several recent studies (e.g., Frankignoul et al., 2011; Wills and Thompson, 2018 Yook et al., 2021).

Far-field SLP anomalies are also found to be associated with the oceanic-forced SST anomalies at a lag of one month, for example, in the North Atlantic, Europe, and Northern

Africa. These circulation anomalies resemble the far-field anomalies associated with the atmospheric pattern that forces the KOE SST anomalies, but are even more pronounced. It is unclear if such circulation anomalies reflect the nonlinear response to midlatitude SST anomalies (e.g., Ferreira and Frankignoul, 2005; Deser et al., 2004, 2007) or if they arise from sources other than KOE SST variability. In future work, it would be interesting to explore statistical methods apart from linear regression to better infer causal links between observed KOE SST anomalies and the atmospheric circulation (e.g., McGraw and Barnes, 2018).

The strong link between oceanic-forced SST anomalies in the KOE region and a large-scale atmospheric response in the North Pacific is nontrivial because we also found that i) atmospheric-forced SST variance is larger than oceanic-forced SST variance when averaged over the KOE region, and ii) oceanic and atmospheric-driven KOE SST anomalies are associated with similar SST patterns. To help explain the strong link, we found that oceanic-forced SST anomalies in the KOE region are associated larger and more persistent surface heat loss to the atmosphere compared to atmospheric-forced SST anomalies.

Overall, our results suggest that SST anomalies forced by ocean dynamical processes in the KOE region play an important role in influencing the month-to-month variability of the large-scale atmospheric circulation in the observations. Other potential climate impacts should be investigated in future work. As a preliminary analysis, Fig. 4.5 shows that precipitation and surface air temperature anomalies along the west coast of North America lag the KOE T_{ocn} index by one month, which suggests that ocean-driven SST variability in the KOE region may impact the climate variability in remote continental regions. However, modeling experiments performed by Yook et al. (2021) wherein an AGCM was forced by observed KOE SST variability, resulted in considerably weaker precipitation anomalies in these regions at a lag of one month, suggesting that the observed lagging anomalies may not be directly driven by KOE SST variability.

It also remains to be determined whether the oceanic-forced SST variability in the KOE region provides a source of climate predictability. The predictability of the observed KOE

SST variability and the associated atmospheric circulation anomalies could be tested with an ensemble of GCM simulations that have been periodically initialized with ocean observations over the course of the observed record (i.e. so-called "hindcast" simulations). Recently, this method been used to reveal predictable aspects of the atmospheric variability in the North Atlantic, such as multidecadal variability in the extratropical jet stream and blocking (e.g. Simpson et al., 2019; Athanasiadis et al., 2020).

Finally, note that we have focussed on the KOE region in this chapter, but the methods used here could in principle be applied to other regions. Preliminary results based on a similar analysis of oceanic-forced SST variability along the Gulf stream current reveal qualitatively similar results as for the KOE region, but the atmospheric circulation anomalies lagging the T_{ocn} anomalies are weaker. The reasons for this are currently being investigated, however it is possible that the strong internal atmospheric variability associated with the North Atlantic Oscillation (NAO) obscures the atmospheric response. Another reason could

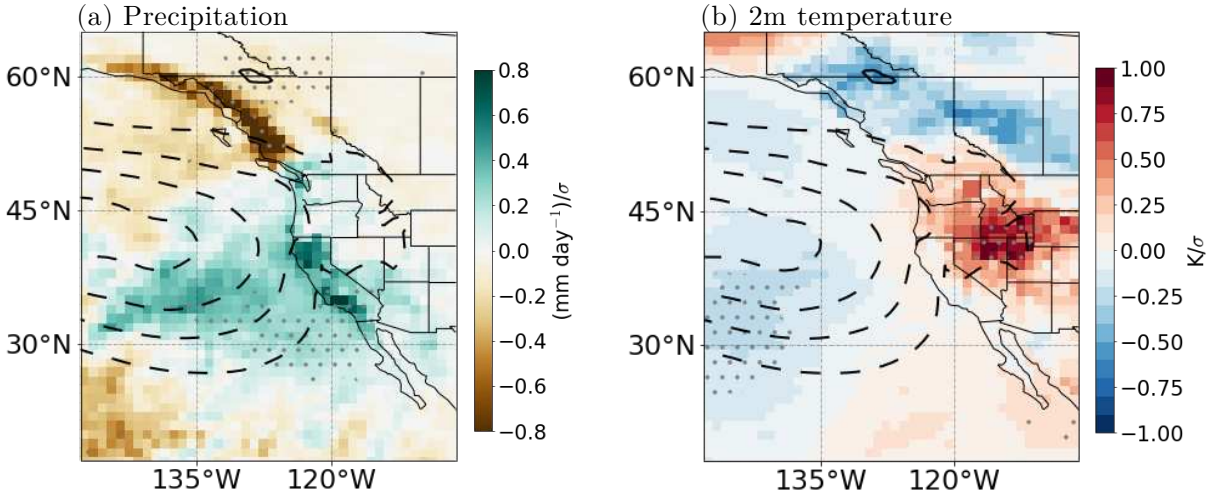

Figure 4.5: (a) Wintertime (DJF) regression of precipitation (green and brown shading; mm/day) and SLP (lines; hPa) anomalies onto the standardized oceanic-forced KOE SST index (T_{ocn}) at a lag of +1 month (precipitation and SLP anomalies lagging the SST index), shown for the west coast of North America. Grey stippling indicates precipitation anomalies that are significant at the 95% significance level, as measured by the Students two-tailed t-test. (b) As in (a), except for 2m air temperature (red and blue shading; K). Precipitation and 2m air temperature data are from the ERA5 reanalysis.

be the smaller footprint of the SST pattern associated with Gulf stream SST variability compared to that of the KOE SST variability. The latter hypothesis could be tested in GCM experiments, for example, by varying the size of the SST anomaly prescribed in atmospheric GCM experiments.

Chapter 5

Conclusions of Dissertation & Future Directions

Conclusions

The ocean plays a key role in regulating Earth's mean climate, both because of its massive heat capacity, but also its heat transport via its slow-moving overturning circulations and other dynamics. In principle, fluctuations in such ocean heat transport can influence the climate variability, by influencing the sea-surface temperature (SST) variability and in turn the atmospheric variability through surface heat exchange, however this remains incompletely understood, particularly in the extratropics. Understanding the role of the ocean in climate variability is an essential step toward predicting variability in the climate and hence toward societal benefit.

As discussed in the introduction of this dissertation, the ocean's role in climate variability can be conceptualized in two ways: 1) the passive ocean, wherein the ocean simply acts to suppress the relatively fast fluctuations in the atmosphere, yielding relatively slow fluctuations in SSTs, and 2) the dynamic ocean, wherein the heat transport by the ocean circulations and other dynamical processes are important mechanisms of climate variability. In general, it is well-understood that ocean dynamics play a key role in one of the most prominent modes of climate variability known as the El-Nino–Southern Oscillation (ENSO), however apart from ENSO it is unclear whether the ocean primarily behaves passively, or if ocean dynamics play an important role in driving climate variations observed in nature.

The goal of this dissertation is to provide a more complete understanding of the role of ocean dynamics in climate variability across the global oceans and across multiple timescales. To this end, two general questions have been addressed:

1. What is the role of ocean dynamics in SST variability? (Chapter 2 and Chapter 3)

2. What is the impact of midlatitude ocean-driven SST variability on the atmosphere? (Chapter 4)

In general, the results point to the important role of ocean dynamical processes in climate variability apart from ENSO. In particular, it has been found that midlatitude ocean processes both force and damp SST variability, and that the large-scale atmospheric circulation can respond to midlatitude oceanic-forced SST variability. Hence the results suggest that the ocean has an important dynamical role outside of the Tropical Pacific.

In Chapter 2 (Patrizio and Thompson, 2021a), the contribution of ocean dynamics to ocean-mixed layer temperature variance was quantified in two ways: i) indirectly from observations of surface heat fluxes and SSTs, and ii) directly using output from the Estimating the Circulation and Climate of the Ocean (ECCO) project. Both methods showed that ocean dynamical processes contribute notably to SST variability in western boundary current regions, their eastward extensions, and equatorial regions on monthly to interannual timescales, but act to damp lower-frequency SST variability over broad midlatitude regions.

In Chapter 3 (Patrizio and Thompson, 2021b), the role of ocean dynamics in midlatitude SST variability was explored further using an extension of Hasselmann's model of climate variability, which included observational estimates of the forcing and damping of midlatitude SSTs by ocean dynamical processes. The broad results found in Chapter 3 were consistent with the results in Chapter 2, namely that the net effect of ocean processes is to reduce the midlatitude SST variance at low-frequencies and increase it at high-frequencies, which leads to a "whitening" of the midlatitude SST variability. Two novel results were highlighted in Chapter 3: i) ocean dynamical processes force substantial midlatitude SST variance across all timescales, a result that was not clearly revealed in the diagnosis performed in Chapter 2 due to the overwhelming effects of ocean damping at low-frequencies, and ii) the simple model captured many aspects of the differences in midlatitude SST variability between fully-coupled and slab-ocean model configurations of a more complex GCM (CESM). This suggests that

the extended Hasselmann model can be used to interpret the drivers of midlatitude SST variability, and hence supports the hypothesis that the midlatitude atmosphere and ocean generally operate independently of each other in nature.

In Chapter 4 (Patrizio and Thompson, 2021c), the atmospheric circulation response to midlatitude ocean-forced SST anomalies was explored using the simple model developed in Chapter 3. In particular, the extended Hasselmann model was used to isolate the oceanic and atmospheric-forced components of the observed SST variability in the Kuroshio-Oyashio Extension (KOE) region. The associated atmospheric circulation anomalies were diagnosed by lagged-regression of the monthly sea-level pressure (SLP) anomalies onto the monthly KOE SST anomalies, and their oceanic and atmospheric-forced components. Consistent with previous studies, a large-scale SLP pattern was found to lag the KOE SST anomalies by one month. In this study, it was shown that this pattern is strongly linked to oceanic-forced SST variability, but *not* atmospheric-forced SST variability. The results therefore suggest that the midlatitude North Pacific ocean actively influences the variability of the large-scale atmospheric circulation.

Future Directions

Overall, the results of this dissertation contribute to a deeper understanding of the role of the ocean in climate variability. However, this work also elicits a number of questions, particularly regarding the role of the midlatitude ocean in climate variability, that could be explored in more detail in future research:

1. Is midlatitude ocean-forced SST variability associated with robust large-scale impacts on the climate?

   The findings from Chapter 4 provide evidence that wintertime oceanic-forced SST variability in the KOE region impacts the atmospheric circulation variability across the North Pacific basin, with weaker evidence that such impacts extend to remote continental regions and other variables like precipitation and surface air temperature

along the west coast of North America. Thus, in future work it would be interesting to explore:

- the structure of the atmospheric response in more detail, including the remote continental responses, but also in the vertical dimension. For example, previous studies have linked SST variability in the KOE region to responses extending the depth of the troposphere, including changes in eddy transports of heat and momentum (e.g. Taguchi et al., 2012; Kwon and Joyce, 2013; Smirnov et al., 2014), and it would be interesting to determine whether such responses can be linked more directly to oceanic-forced SST variability in the KOE region.
- the atmospheric responses to other sources of midlatitude ocean-forced SST variability, such as along the Gulf stream, Agulhas and Antarctic Circumpolar currents. In general, methods apart from the lagged-regression analysis could be used to better infer causality between observed oceanic-forced SST anomalies and atmospheric anomalies (e.g., McGraw and Barnes, 2018).

2. What are the key mechanisms of the atmospheric response to midlatitude ocean-forced SST variability?

   The findings from Chapter 4 highlighted that oceanic-forced SST anomalies are associated with stronger and more persistent heat loss during the winter months. Thus, it would be interesting to understand:

   - the relative importance of the persistence and strength of low-level heating in the atmospheric response, for example, using a series of idealized GCM experiments with prescribed heating anomalies.
   - the physical mechanisms of the atmospheric response itself more completely. Linear theory accounts for the low-pressure anomaly in the North Pacific, but the mechanisms behind the far-field atmospheric circulation anomalies are less clear.

Previous studies have shown by use of model experiments that nonlinear feedbacks between the extratropical jet stream and the transient eddies can transform the linear response to a hemispheric-wide response (e.g., Ferreira and Frankignoul, 2005; Deser et al., 2004, 2007), however, it remains to be determined if such mechanisms are active in reality.

3. To what extent are dynamical interactions between midlatitude ocean and atmosphere important for climate variability?

   The findings from Chapters 3 and 4 suggest that the midlatitude ocean and atmosphere operate relatively independently of each other nature. However, some previous studies have argued that two-way interactions between ocean and atmosphere are important for extratropical climate variability on decadal timescales (e.g., Kwon and Deser, 2007; Qiu et al., 2007; Wills et al., 2019b). It is possible that such two-way interactions (i.e. coupling) are only readily apparent at low-frequencies, which are not well resolved by the observational record. Thus, in future work it would be interesting to investigate:

   - the impacts of atmosphere-ocean coupling on extratropical climate variability using a modeling approach. For example, the extratropical modes of climate variability could be compared across a series of GCM experiments with increasing degrees of coupling between midlatitude ocean and atmosphere, from no coupling (with prescribed SST anomalies, e.g., Yook et al., 2021), to thermodynamical coupling only (with ocean heat-flux convergence anomalies prescribed in a slab-ocean model, e.g., Kwon et al., 2011), to fully-coupled.

4. How does the role of ocean dynamics vary across many GCMs?

   In Chapter 3 it was found that the extended Hasselmann model can be used to interpret the role of ocean dynamics in midlatitude SST variability and that the net impact of ocean dynamical processes is to whiten the midlatitude SST variability both in the observations and in CESM. In future work, it would be interesting to explore:

- how the role of midlatitude ocean dynamics varies across many GCMs, as inferred by slab-ocean and fully-coupled configurations of each GCM. Interestingly, Clement et al. (2015) found a wide range of differences in the power spectra of North Atlantic-averaged SSTs between slab-ocean and and fully-coupled configurations of a variety of GCMs (e.g. see their Fig. 3), but no systematic difference across all models (e.g. see their Fig 2). Since the CESM results highlighted in Chapter 3 agree well with the observationally-constrained extended Hasselmann model results, this suggests that GCMs that do not show a pronounced whitening effect may be deficient in their simulation of midlatitude ocean dynamics.
- formulations of the extended Hasselmann model that have been constrained by the GCM simulations instead of observations. The GCM-constrained Hasselmann model could be used as in Chapters 3 and 4 to diagnose the drivers of midlatitude climate variability in the GCM simulation and to identify possible discrepancies with the observations. It might also be useful to first apply the methods from Chapter 2 to more generally diagnosis the drivers of SST variance across the global oceans in a given GCM simulation.

5. What are the implications for climate predictability?

   Overall the results of this dissertation provide insights into the role of the ocean in climate *variability*, particularly the active influence of the midlatitude ocean on both SST variability, and the variability of the atmospheric circulation in the North Pacific basin. However, the extent to which the midlatitude ocean provides a source of atmospheric *predictability* remains uncertain. If models can predict, for example, oceanic-forced SST anomalies in the KOE region, and in turn the associated circulation anomalies, this may have important implications for the predictability of climate anomalies in remote regions. A possible approach to investigate this in future work could be:

- to use an ensemble of GCM simulations that have been periodically initialized with ocean observations over the course of the observed record (hindcast experiments). For example, subseasonal to seasonal (S2S) hindcast systems could be used to test the predictability of month-to-month SST variability in western boundary current regions, as well as the associated circulation anomalies. Recently, it has been shown that the correction of SST biases along the Gulf Stream in ECMWF's (European Centre for Medium-Range Weather Forecasts) S2S prediction system leads to improved subseasonal predictions of atmospheric circulation anomalies (e.g. Roberts et al., 2021), and that enhanced ocean resolution in S2S systems leads to changes in the variability and predictability of North Atlantic atmospheric circulation anomalies (e.g. Haarsma et al., 2019). To my knowledge, possible links between subseasonal predictability of the atmospheric circulation and ocean processes in the North Pacific have not yet been explored in this manner. While evidence is emerging that midlatitude ocean dynamical processes can provide a source of atmospheric predictability, there are still many open questions to address (e.g. Saravanan and Chang, 2019; Mariotti et al., 2020).

Bibliography

Alexander, M. et al. (2010). Extratropical air–sea interaction, sea surface temperature variability, and the Pacific decadal oscillation. *Climate Dynamics: Why Does Climate Vary?, Geophys. Monogr*, 189:123–148.

Alexander, M. A., Bladé, I., Newman, M., Lanzante, J. R., Lau, N.-C., and Scott, J. D. (2002). The atmospheric bridge: The influence of ENSO teleconnections on air–sea interaction over the global oceans. *Journal of climate*, 15(16):2205–2231.

Alexander, M. A. and Deser, C. (1995). A mechanism for the recurrence of wintertime midlatitude SST anomalies. *Journal of physical oceanography*, 25(1):122–137.

Alexander, M. A. and Penland, C. (1996). Variability in a mixed layer ocean model driven by stochastic atmospheric forcing. *Journal of Climate*, 9(10):2424–2442.

Amaya, D. J., DeFlorio, M. J., Miller, A. J., and Xie, S.-P. (2017). WES feedback and the Atlantic Meridional Mode: observations and CMIP5 comparisons. *Climate Dynamics*, 49(5-6):1665–1679.

Argo (2000). Argo float data and metadata from global data assembly centre (argo GDAC). *SEANOE*.

Athanasiadis, P. J., Yeager, S., Kwon, Y.-O., Bellucci, A., Smith, D. W., and Tibaldi, S. (2020). Decadal predictability of north atlantic blocking and the nao. *npj Climate and Atmospheric Science*, 3(1):1–10.

Barsugli, J. J. and Battisti, D. S. (1998). The basic effects of atmosphere–ocean thermal coupling on midlatitude variability. *Journal of the Atmospheric Sciences*, 55(4):477–493.

Bellomo, K., Murphy, L. N., Cane, M. A., Clement, A. C., and Polvani, L. M. (2018). Historical forcings as main drivers of the Atlantic multidecadal variability in the CESM large ensemble. *Climate Dynamics*, 50(9-10):3687–3698.

Bellucci, A., Athanasiadis, P., Scoccimarro, E., Ruggieri, P., Gualdi, S., Fedele, G., Haarsma, R., Garcia-Serrano, J., Castrillo, M., Putrahasan, D., et al. (2020). Air-sea interaction over the gulf stream in an ensemble of HighResMIP present climate simulations. *Climate Dynamics*, pages 1–19.

Bishop, S. P., Small, R. J., Bryan, F. O., and Tomas, R. A. (2017). Scale dependence of midlatitude air–sea interaction. *Journal of Climate*, 30(20):8207–8221.

Bjerknes, J. (1964). Atlantic air-sea interaction. In *Advances in geophysics*, volume 10, pages 1–82. Elsevier.

Booth, B. B., Dunstone, N. J., Halloran, P. R., Andrews, T., and Bellouin, N. (2012). Aerosols implicated as a prime driver of twentieth-century North Atlantic climate variability. *Nature*, 484(7393):228–232.

Boyer, T. P., Antonov, J. I., Baranova, O. K., Garcia, H. E., Johnson, D. R., Mishonov, A. V., O'Brien, T. D., Seidov, D., Smolyar, I., Zweng, M. M., et al. (2009). World ocean database 2009.

Brayshaw, D. J., Hoskins, B., and Blackburn, M. (2008). The storm-track response to idealized SST perturbations in an aquaplanet GCM. *Journal of the Atmospheric Sciences*, 65(9):2842–2860.

Bryden, H. L. and Imawaki, S. (2001). Ocean heat transport. In *International Geophysics*, volume 77, pages 455–474. Elsevier.

Buckley, M. W. and Marshall, J. (2016). Observations, inferences, and mechanisms of the Atlantic Meridional Overturning Circulation: A review. *Reviews of Geophysics*, 54(1):5–63.

Buckley, M. W., Ponte, R. M., Forget, G., and Heimbach, P. (2014). Low-frequency SST and upper-ocean heat content variability in the North Atlantic. *Journal of Climate*, 27(13):4996–5018.

Buckley, M. W., Ponte, R. M., Forget, G., and Heimbach, P. (2015). Determining the origins of advective heat transport convergence variability in the North Atlantic. *Journal of Climate*, 28(10):3943–3956.

Cane, M. A., Clement, A. C., Murphy, L. N., and Bellomo, K. (2017). Low-pass filtering, heat flux, and Atlantic multidecadal variability. *Journal of Climate*, 30(18):7529–7553.

Carton, J. A. and Giese, B. S. (2008). A reanalysis of ocean climate using Simple Ocean Data Assimilation (SODA). *Monthly weather review*, 136(8):2999–3017.

Cayan, D. R. (1992a). Latent and sensible heat flux anomalies over the northern oceans: Driving the sea surface temperature. *Journal of Physical Oceanography*, 22(8):859–881.

Cayan, D. R. (1992b). Latent and sensible heat flux anomalies over the northern oceans: The connection to monthly atmospheric circulation. *Journal of climate*, 5(4):354–369.

Chiang, J. C. and Vimont, D. J. (2004). Analogous Pacific and Atlantic meridional modes of tropical atmosphere–ocean variability. *Journal of Climate*, 17(21):4143–4158.

Clement, A., Bellomo, K., Murphy, L. N., Cane, M. A., Mauritsen, T., Rädel, G., and Stevens, B. (2015). The Atlantic Multidecadal Oscillation without a role for ocean circulation. *Science*, 350(6258):320–324.

Davis, L. L., Thompson, D. W., Kennedy, J. J., and Kent, E. C. (2019). The Importance of Unresolved Biases in Twentieth-Century Sea Surface Temperature Observations. *Bulletin of the American Meteorological Society*, 100(4):621–629.

de Boyer Montégut, C., Madec, G., Fischer, A. S., Lazar, A., and Iudicone, D. (2004). Mixed layer depth over the global ocean: An examination of profile data and a profile-based climatology. *Journal of Geophysical Research: Oceans*, 109(C12).

De Coëtlogon, G. and Frankignoul, C. (2003). The persistence of winter sea surface temperature in the North Atlantic. *Journal of climate*, 16(9):1364–1377.

Delworth, T. L., Zeng, F., Zhang, L., Zhang, R., Vecchi, G. A., and Yang, X. (2017). The central role of ocean dynamics in connecting the North Atlantic Oscillation to the extratropical component of the Atlantic Multidecadal Oscillation. *Journal of Climate*, 30(10):3789–3805.

Deser, C., Alexander, M. A., and Timlin, M. S. (2003). Understanding the persistence of sea surface temperature anomalies in midlatitudes. *Journal of Climate*, 16(1):57–72.

Deser, C., Alexander, M. A., Xie, S.-P., and Phillips, A. S. (2010). Sea surface temperature variability: Patterns and mechanisms. *Annual review of marine science*, 2:115–143.

Deser, C., Phillips, A. S., and Hurrell, J. W. (2004). Pacific interdecadal climate variability: Linkages between the tropics and the North Pacific during boreal winter since 1900. *Journal of Climate*, 17(16):3109–3124.

Deser, C. and Timlin, M. S. (1997). Atmosphere–ocean interaction on weekly timescales in the North Atlantic and Pacific. *Journal of climate*, 10(3):393–408.

Deser, C., Tomas, R. A., and Peng, S. (2007). The transient atmospheric circulation response to North Atlantic SST and sea ice anomalies. *Journal of Climate*, 20(18):4751–4767.

Dijkstra, H. (2006). The ENSO phenomenon: theory and mechanisms. *Advances in Geosciences*, 6:3–15.

Dijkstra, H. A. (2008). *Dynamical Oceanography*. Springer Science & Business Media.

Ferreira, D. and Frankignoul, C. (2005). The transient atmospheric response to midlatitude SST anomalies. *Journal of climate*, 18(7):1049–1067.

Folland, C. K., Palmer, T. N., and Parker, D. E. (1986). Sahel rainfall and worldwide sea temperatures, 1901–85. *Nature*, 320(6063):602–607.

Forget, G., Campin, J.-M., Heimbach, P., Hill, C. N., Ponte, R. M., and Wunsch, C. (2015). ECCO version 4: An integrated framework for non-linear inverse modeling and global ocean state estimation.

Frankignoul, C. (1979). Stochastic forcing models of climate variability. *Dynamics of Atmospheres and Oceans*, 3(2-4):465–479.

Frankignoul, C. (1985). Sea surface temperature anomalies, planetary waves, and air-sea feedback in the middle latitudes. *Reviews of geophysics*, 23(4):357–390.

Frankignoul, C., Czaja, A., and L?Heveder, B. (1998). Air–sea feedback in the North Atlantic and surface boundary conditions for ocean models. *Journal of climate*, 11(9):2310–2324.

Frankignoul, C. and Hasselmann, K. (1977). Stochastic climate models, Part ii: Application to sea-surface temperature anomalies and thermocline variability. *Tellus*, 29(4):289–305.

Frankignoul, C. and Kestenare, E. (2002). The surface heat flux feedback. Part i: Estimates from observations in the Atlantic and the North Pacific. *Climate dynamics*, 19(8):633–647.

Frankignoul, C., Kestenare, E., and Mignot, J. (2002b). The surface heat flux feedback. Part II: direct and indirect estimates in the ECHAM4/OPA8 coupled GCM. *Climate dynamics*, 19(8):649–655.

Frankignoul, C. and Reynolds, R. W. (1983). Testing a dynamical model for mid-latitude sea surface temperature anomalies. *Journal of physical oceanography*, 13(7):1131–1145.

Frankignoul, C., Sennéchael, N., Kwon, Y.-O., and Alexander, M. A. (2011). Influence of the meridional shifts of the Kuroshio and the Oyashio Extensions on the atmospheric circulation. *Journal of Climate*, 24(3):762–777.

Frenger, I., Gruber, N., Knutti, R., and Münnich, M. (2013). Imprint of Southern Ocean eddies on winds, clouds and rainfall. *Nature geoscience*, 6(8):608–612.

Fukumori, I., Wang, O., Fenty, I., Forget, G., Heimbach, P., and Ponte, R. M. (2017). ECCO version 4 release 3. Technical report.

Gaspar, P., Grégoris, Y., and Lefevre, J.-M. (1990). A simple eddy kinetic energy model for simulations of the oceanic vertical mixing: Tests at station Papa and Long-Term Upper Ocean Study site. *Journal of Geophysical Research: Oceans*, 95(C9):16179–16193.

Gelaro, R., McCarty, W., Suárez, M. J., Todling, R., Molod, A., Takacs, L., Randles, C. A., Darmenov, A., Bosilovich, M. G., Reichle, R., et al. (2017). The modern-era retrospective analysis for research and applications, version 2 (MERRA-2). *Journal of Climate*, 30(14):5419–5454.

Gent, P. R. and McWilliams, J. C. (1990). Isopycnal mixing in ocean circulation models. *Journal of Physical Oceanography*, 20(1):150–155.

Good, S. A., Martin, M. J., and Rayner, N. A. (2013). EN4: Quality controlled ocean temperature and salinity profiles and monthly objective analyses with uncertainty estimates. *Journal of Geophysical Research: Oceans*, 118(12):6704–6716.

Griffies, S. M., Winton, M., Anderson, W. G., Benson, R., Delworth, T. L., Dufour, C. O., Dunne, J. P., Goddard, P., Morrison, A. K., Rosati, A., et al. (2015). Impacts on ocean heat from transient mesoscale eddies in a hierarchy of climate models. *Journal of Climate*, 28(3):952–977.

Gulev, S. K., Latif, M., Keenlyside, N., Park, W., and Koltermann, K. P. (2013). North Atlantic Ocean control on surface heat flux on multidecadal timescales. *Nature*, 499(7459):464–467.

Haarsma, R. J., García-Serrano, J., Prodhomme, C., Bellprat, O., Davini, P., and Drijfhout, S. (2019). Sensitivity of winter North Atlantic-European climate to resolved atmosphere and ocean dynamics. *Scientific reports*, 9(1):1–8.

Hall, A. and Manabe, S. (1997). Can local linear stochastic theory explain sea surface temperature and salinity variability? *Climate Dynamics*, 13(3):167–180.

Hall, M. M. and Bryden, H. L. (1982). Direct estimates and mechanisms of ocean heat transport. *Deep Sea Research Part A. Oceanographic Research Papers*, 29(3):339–359.

Hartmann, D. L. (2015). *Global Physical Climatology*, volume 103. Newnes.

Hasselmann, K. (1976). Stochastic climate models part I. Theory. *tellus*, 28(6):473–485.

Hausmann, U., Czaja, A., and Marshall, J. (2016). Estimates of air–sea feedbacks on sea surface temperature anomalies in the southern ocean. *Journal of Climate*, 29(2):439–454.

Hersbach, H., Bell, B., Berrisford, P., Hirahara, S., Horányi, A., Muñoz-Sabater, J., Nicolas, J., Peubey, C., Radu, R., Schepers, D., et al. (2020). The ERA5 global reanalysis. *Quarterly Journal of the Royal Meteorological Society*, 146(730):1999–2049.

Hersbach, H. and Dee, D. (2016). ERA5 reanalysis is in production. *ECMWF newsletter*, 147(7):5–6.

Holte, J., Talley, L. D., Gilson, J., and Roemmich, D. (2017). An Argo mixed layer climatology and database. *Geophysical Research Letters*, 44(11):5618–5626.

Hoskins, B. J. and Karoly, D. J. (1981). The steady linear response of a spherical atmosphere to thermal and orographic forcing. *Journal of Atmospheric Sciences*, 38(6):1179–1196.

Hurrell, J. W., Holland, M. M., Gent, P. R., Ghan, S., Kay, J. E., Kushner, P. J., Lamarque, J.-F., Large, W. G., Lawrence, D., Lindsay, K., et al. (2013). The community earth system model: a framework for collaborative research. *Bulletin of the American Meteorological Society*, 94(9):1339–1360.

Jin, F.-F. (1997). An equatorial ocean recharge paradigm for ENSO. Part i: Conceptual model. *Journal of the atmospheric sciences*, 54(7):811–829.

Kay, J. E., Deser, C., Phillips, A., Mai, A., Hannay, C., Strand, G., Arblaster, J. M., Bates, S., Danabasoglu, G., Edwards, J., et al. (2015). The community earth system model (CESM) large ensemble project: A community resource for studying climate change in the presence of internal climate variability. *Bulletin of the American Meteorological Society*, 96(8):1333–1349.

Kent, E. C., Kennedy, J. J., Smith, T. M., Hirahara, S., Huang, B., Kaplan, A., Parker, D. E., Atkinson, C. P., Berry, D. I., Carella, G., et al. (2017). A call for new approaches to quantifying biases in observations of sea surface temperature. *Bulletin of the American Meteorological Society*, 98(8):1601–1616.

Kim, W. M., Yeager, S. G., and Danabasoglu, G. (2018). Key role of internal ocean dynamics in atlantic multidecadal variability during the last half century. *Geophysical Research Letters*, 45(24):13–449.

Kirtman, B. P., Bitz, C., Bryan, F., Collins, W., Dennis, J., Hearn, N., Kinter, J. L., Loft, R., Rousset, C., Siqueira, L., et al. (2012). Impact of ocean model resolution on CCSM climate simulations. *Climate dynamics*, 39(6):1303–1328.

Kushnir, Y., Robinson, W., Bladé, I., Hall, N., Peng, S., and Sutton, R. (2002). Atmospheric GCM response to extratropical SST anomalies: Synthesis and evaluation. *Journal of Climate*, 15(16):2233–2256.

Kwon, Y.-O., Alexander, M. A., Bond, N. A., Frankignoul, C., Nakamura, H., Qiu, B., and Thompson, L. A. (2010). Role of the Gulf Stream and Kuroshio–Oyashio systems in large-scale atmosphere–ocean interaction: A review. *Journal of Climate*, 23(12):3249–3281.

Kwon, Y.-O. and Deser, C. (2007). North Pacific decadal variability in the community climate system model version 2. *Journal of climate*, 20(11):2416–2433.

Kwon, Y.-O., Deser, C., and Cassou, C. (2011). Coupled atmosphere–mixed layer ocean response to ocean heat flux convergence along the Kuroshio Current Extension. *Climate dynamics*, 36(11-12):2295–2312.

Kwon, Y.-O. and Joyce, T. M. (2013). Northern hemisphere winter atmospheric transient eddy heat fluxes and the Gulf Stream and Kuroshio–Oyashio Extension variability. *Journal of Climate*, 26(24):9839–9859.

Latif, M. and Barnett, T. P. (1994). Causes of decadal climate variability over the North Pacific and North America. *Science*, 266(5185):634–637.

Liu, Z. and Wu, L. (2004). Atmospheric Response to North Pacific SST: The Role of Ocean–Atmosphere Coupling. *Journal of climate*, 17(9):1859–1882.

Ma, X., Chang, P., Saravanan, R., Montuoro, R., Hsieh, J.-S., Wu, D., Lin, X., Wu, L., and Jing, Z. (2015). Distant influence of Kuroshio eddies on North Pacific weather patterns? *Scientific reports*, 5:17785.

Ma, X., Chang, P., Saravanan, R., Montuoro, R., Nakamura, H., Wu, D., Lin, X., and Wu, L. (2017). Importance of resolving Kuroshio front and eddy influence in simulating the North Pacific storm track. *Journal of Climate*, 30(5):1861–1880.

Ma, X., Jing, Z., Chang, P., Liu, X., Montuoro, R., Small, R. J., Bryan, F. O., Greatbatch, R. J., Brandt, P., Wu, D., et al. (2016). Western boundary currents regulated by interaction between ocean eddies and the atmosphere. *Nature*, 535(7613):533–537.

Mantua, N. J., Hare, S. R., Zhang, Y., Wallace, J. M., and Francis, R. C. (1997). A Pacific interdecadal climate oscillation with impacts on salmon production. *Bulletin of the american Meteorological Society*, 78(6):1069–1080.

Mariotti, A., Baggett, C., Barnes, E. A., Becker, E., Butler, A., Collins, D. C., Dirmeyer, P. A., Ferranti, L., Johnson, N. C., Jones, J., et al. (2020). Windows of opportunity for

skillful forecasts subseasonal to seasonal and beyond. *Bulletin of the American Meteorological Society*, 101(5):E608–E625.

McGraw, M. C. and Barnes, E. A. (2018). Memory matters: A case for Granger causality in climate variability studies. *Journal of climate*, 31(8):3289–3300.

McPhaden, M. J., Zebiak, S. E., and Glantz, M. H. (2006). ENSO as an integrating concept in earth science. *science*, 314(5806):1740–1745.

Mignot, J. and Frankignoul, C. (2003). On the interannual variability of surface salinity in the atlantic. *Climate dynamics*, 20(6):555–565.

Minobe, S., Kuwano-Yoshida, A., Komori, N., Xie, S.-P., and Small, R. J. (2008). Influence of the Gulf Stream on the troposphere. *Nature*, 452(7184):206–209.

Minobe, S., Miyashita, M., Kuwano-Yoshida, A., Tokinaga, H., and Xie, S.-P. (2010). Atmospheric response to the Gulf Stream: Seasonal variations. *Journal of Climate*, 23(13):3699–3719.

Murphy, L. N., Bellomo, K., Cane, M. A., and Clement, A. C. (2017). The role of historical forcings in simulating the observed Atlantic multidecadal oscillation. *Geophysical Research Letters*, 44(5):2472–2480.

Murphy, L. N., Klavans, J. M., Clement, A. C., and Cane, M. A. (2020). Investigating the Roles of External Forcing and Ocean Circulation on the Atlantic Multidecadal Variability in a Large Ensemble Climate Model Hierarchy. *Journal Of Climate*.

Myers, T. A. and Mechoso, C. R. (2020). Relative contributions of atmospheric, oceanic, and coupled processes to north pacific and north atlantic variability. *Geophysical Research Letters*, 47(5):e2019GL086321.

Nakamura, H., Sampe, T., Goto, A., Ohfuchi, W., and Xie, S.-P. (2008). On the importance of midlatitude oceanic frontal zones for the mean state and dominant variability in the tropospheric circulation. *Geophysical Research Letters*, 35(15).

Nakamura, H., Sampe, T., Tanimoto, Y., and Shimpo, A. (2004). Observed associations among storm tracks, jet streams and midlatitude oceanic fronts. *Earth?s Climate: The Ocean–Atmosphere Interaction, Geophys. Monogr*, 147:329–345.

Newman, M., Alexander, M. A., Ault, T. R., Cobb, K. M., Deser, C., Di Lorenzo, E., Mantua, N. J., Miller, A. J., Minobe, S., Nakamura, H., et al. (2016). The Pacific decadal oscillation, revisited. *Journal of Climate*, 29(12):4399–4427.

Newman, M., Compo, G. P., and Alexander, M. A. (2003). ENSO-forced variability of the Pacific decadal oscillation. *Journal of Climate*, 16(23):3853–3857.

O'Reilly, C. H. and Czaja, A. (2015). The response of the pacific storm track and atmospheric circulation to Kuroshio Extension variability. *Quarterly Journal of the Royal Meteorological Society*, 141(686):52–66.

O'Reilly, C. H., Huber, M., Woollings, T., and Zanna, L. (2016). The signature of low-frequency oceanic forcing in the Atlantic Multidecadal Oscillation. *Geophysical Research Letters*, 43(6):2810–2818.

O'Reilly, C. H. and Zanna, L. (2018). The signature of oceanic processes in decadal extratropical SST anomalies. *Geophysical Research Letters*, 45(15):7719–7730.

Park, S., Deser, C., and Alexander, M. A. (2005). Estimation of the surface heat flux response to sea surface temperature anomalies over the global oceans. *Journal of climate*, 18(21):4582–4599.

Patrizio, C. R. and Thompson, D. W. (2021a). Quantifying the Role of Ocean Dynamics in Ocean Mixed-Layer Temperature Variability. *Journal of Climate*, pages 2567–2589. American Meteorological Society. Used with permission.

Patrizio, C. R. and Thompson, D. W. (2021b). Understanding the Role of Ocean Dynamics in Midlatitude Sea Surface Temperature Variability using a Simple Climate Model. *Journal of Climate*. in press.

Patrizio, C. R. and Thompson, D. W. (2021c). Atmospheric Circulation Response to Wintertime Oceanic-Forced Sea-Surface Temperature Variability in the Kuroshio-Oyashio Extension Region. *Geophysical Research Letters*. in prep.

Pedlosky, J. (2013). *Ocean Circulation Theory*. Springer Science & Business Media.

Peng, S. and Robinson, W. A. (2001). Relationships between atmospheric internal variability and the responses to an extratropical SST anomaly. *Journal of climate*, 14(13):2943–2959.

Peng, S., Robinson, W. A., and Hoerling, M. P. (1997). The modeled atmospheric response to midlatitude SST anomalies and its dependence on background circulation states. *Journal of Climate*, 10(5):971–987.

Peng, S. and Whitaker, J. S. (1999). Mechanisms determining the atmospheric response to midlatitude SST anomalies. *Journal of climate*, 12(5):1393–1408.

Philander, S. G. H. (1983). El-niño southern oscillation phenomena. *Nature*, 302(5906):295–301.

Putrasahan, D., Kamenkovich, I., Le Hénaff, M., and Kirtman, B. (2017). Importance of ocean mesoscale variability for air-sea interactions in the Gulf of Mexico. *Geophysical Research Letters*, 44(12):6352–6362.

Qiu, B., Schneider, N., and Chen, S. (2007). Coupled decadal variability in the North Pacific: An observationally constrained idealized model. *Journal of Climate*, 20(14):3602–3620.

Redi, M. H. (1982). Oceanic isopycnal mixing by coordinate rotation. *Journal of Physical Oceanography*, 12(10):1154–1158.

Révelard, A., Frankignoul, C., and Kwon, Y.-O. (2018). A multivariate estimate of the cold season atmospheric response to North Pacific SST variability. *Journal of Climate*, 31(7):2771–2796.

Révelard, A., Frankignoul, C., Sennéchael, N., Kwon, Y.-O., and Qiu, B. (2016). Influence of the decadal variability of the kuroshio extension on the atmospheric circulation in the cold season. *Journal of Climate*, 29(6):2123–2144.

Reynolds, R. W. (1978). Sea surface temperature anomalies in the North Pacific Ocean. *Tellus*, 30(2):97–103.

Reynolds, R. W., Smith, T. M., Liu, C., Chelton, D. B., Casey, K. S., and Schlax, M. G. (2007). Daily high-resolution-blended analyses for sea surface temperature. *Journal of Climate*, 20(22):5473–5496.

Roberts, C., Vitart, F., and Balmaseda, M. (2021). Hemispheric impact of North Atlantic SSTs in sub-seasonal forecasts. *Geophysical Research Letters*, page e2020GL091446.

Roberts, C. D., Palmer, M. D., Allan, R. P., Desbruyeres, D. G., Hyder, P., Liu, C., and Smith, D. (2017). Surface flux and ocean heat transport convergence contributions to seasonal and interannual variations of ocean heat content. *Journal of Geophysical Research: Oceans*, 122(1):726–744.

Saravanan, R. and Chang, P. (2019). Midlatitude mesoscale ocean-atmosphere interaction and its relevance to S2S prediction. In *Sub-Seasonal to Seasonal Prediction*, pages 183–200. Elsevier.

Schlesinger, M. E. and Ramankutty, N. (1994). An oscillation in the global climate system of period 65–70 years. *Nature*, 367(6465):723–726.

Schneider, N., Miller, A. J., and Pierce, D. W. (2002). Anatomy of North Pacific decadal variability. *Journal of climate*, 15(6):586–605.

Simpson, I. R., Yeager, S. G., McKinnon, K. A., and Deser, C. (2019). Decadal predictability of late winter precipitation in western europe through an ocean–jet stream connection. *Nature Geoscience*, 12(8):613–619.

Siqueira, L. and Kirtman, B. P. (2016). Atlantic near-term climate variability and the role of a resolved gulf stream. *Geophysical Research Letters*, 43(8):3964–3972.

Slivinski, L. C., Compo, G. P., Whitaker, J. S., Sardeshmukh, P. D., Giese, B. S., McColl, C., Allan, R., Yin, X., Vose, R., Titchner, H., et al. (2019). Towards a more reliable historical reanalysis: Improvements for version 3 of the Twentieth Century Reanalysis system. *Quarterly Journal of the Royal Meteorological Society*, 145(724):2876–2908.

Small, R., deSzoeke, S. P., Xie, S., O'neill, L., Seo, H., Song, Q., Cornillon, P., Spall, M., and Minobe, S. (2008). Air–sea interaction over ocean fronts and eddies. *Dynamics of Atmospheres and Oceans*, 45(3-4):274–319.

Small, R. J., Bryan, F. O., Bishop, S. P., Larson, S., and Tomas, R. A. (2019a). What Drives Upper-Ocean Temperature Variability in Coupled Climate Models and Observations? *Journal of Climate*, 33(2):577–596.

Small, R. J., Bryan, F. O., Bishop, S. P., and Tomas, R. A. (2019b). Air–Sea Turbulent Heat Fluxes in Climate Models and Observational Analyses: What Drives Their Variability? *Journal of Climate*, 32(8):2397–2421.

Small, R. J., Tomas, R. A., and Bryan, F. O. (2014). Storm track response to ocean fronts in a global high-resolution climate model. *Climate dynamics*, 43(3-4):805–828.

Smirnov, D., Newman, M., and Alexander, M. A. (2014). Investigating the role of ocean–atmosphere coupling in the North Pacific Ocean. *Journal of climate*, 27(2):592–606.

Smirnov, D., Newman, M., Alexander, M. A., Kwon, Y.-O., and Frankignoul, C. (2015). Investigating the local atmospheric response to a realistic shift in the Oyashio sea surface temperature front. *Journal of Climate*, 28(3):1126–1147.

Taguchi, B., Nakamura, H., Nonaka, M., Komori, N., Kuwano-Yoshida, A., Takaya, K., and Goto, A. (2012). Seasonal evolutions of atmospheric response to decadal SST anomalies in the North Pacific subarctic frontal zone: Observations and a coupled model simulation. *Journal of Climate*, 25(1):111–139.

Taguchi, B., Xie, S.-P., Schneider, N., Nonaka, M., Sasaki, H., and Sasai, Y. (2007). Decadal variability of the Kuroshio Extension: Observations and an eddy-resolving model hindcast. *Journal of Climate*, 20(11):2357–2377.

Talley, L. (1984). Meridional heat transport in the Pacific Ocean. *Journal of Physical Oceanography*, 14(2):231–241.

Trenberth, K. E. and Caron, J. M. (2001). Estimates of meridional atmosphere and ocean heat transports. *Journal of Climate*, 14(16):3433–3443.

von Storch, J.-S. (2000). Signatures of air–sea interactions in a coupled atmosphere–ocean GCM. *Journal of Climate*, 13(19):3361–3379.

Wang, C. and Picaut, J. (2004). Understanding ENSO physics: A review. *Earth?s Climate: The Ocean–Atmosphere Interaction, Geophys. Monogr*, 147:21–48.

Wills, R. C., Armour, K. C., Battisti, D. S., and Hartmann, D. L. (2019a). Ocean–atmosphere dynamical coupling fundamental to the Atlantic multidecadal oscillation. *Journal of Climate*, 32(1):251–272.

Wills, R. C., Battisti, D. S., Proistosescu, C., Thompson, L., Hartmann, D. L., and Armour, K. C. (2019b). Ocean circulation signatures of North Pacific decadal variability. *Geophysical Research Letters*, 46(3):1690–1701.

Wills, S. M. and Thompson, D. W. (2018). On the observed relationships between wintertime variability in Kuroshio–Oyashio Extension sea surface temperatures and the atmospheric circulation over the North Pacific. *Journal of Climate*, 31(12):4669–4681.

Wu, R., Kirtman, B. P., and Pegion, K. (2006). Local air–sea relationship in observations and model simulations. *Journal of climate*, 19(19):4914–4932.

Xie, S.-P. and Carton, J. A. (2004). Tropical Atlantic variability: Patterns, mechanisms, and impacts. *Earth Climate: The Ocean-Atmosphere Interaction, Geophys. Monogr*, 147:121–142.

Yan, X., Zhang, R., and Knutson, T. R. (2018). Underestimated AMOC variability and implications for AMV and predictability in CMIP models. *Geophysical Research Letters*, 45(9):4319–4328.

Yook, S., Thompson, D. W., Sun, L., and Patrizio, C. (2021). Interpretation of North Pacific atmosphere-ocean interactions. *Journal of Climate*. in press.

Yu, B. and Boer, G. (2006). The variance of sea surface temperature and projected changes with global warming. *Climate dynamics*, 26(7-8):801–821.

Yu, L., Jin, X., and Weller, R. A. (2008). Multidecade global flux datasets from the objectively analyzed air-sea fluxes (OAFlux) project: Latent and sensible heat fluxes, ocean evaporation, and related surface meteorological variables. *OAFlux Project Tech. Rep. OA-2008-01.*, 74.

Zhang, L. and Wang, C. (2013). Multidecadal North Atlantic sea surface temperature and atlantic meridional overturning circulation variability in CMIP5 historical simulations. *Journal of Geophysical Research: Oceans*, 118(10):5772–5791.

Zhang, R. (2017). On the persistence and coherence of subpolar sea surface temperature and salinity anomalies associated with the Atlantic multidecadal variability. *Geophysical Research Letters*, 44(15):7865–7875.

Zhang, R., Sutton, R., Danabasoglu, G., Delworth, T. L., Kim, W. M., Robson, J., and Yeager, S. G. (2016). Comment on "The Atlantic Multidecadal Oscillation without a role for ocean circulation". *Science*, 352(6293):1527–1527.

Zhang, R., Sutton, R., Danabasoglu, G., Kwon, Y.-O., Marsh, R., Yeager, S. G., Amrhein, D. E., and Little, C. M. (2019). A review of the role of the Atlantic Meridional Overturning Circulation in Atlantic multidecadal variability and associated climate impacts. *Reviews of Geophysics*, 57(2):316–375.

Appendix A

Derivation of the Diagnostic for Mixed Layer Temperature Variance and Uncertainty Contributions

A.1 Derivation of the diagnostic equation for mixed-layer temperature variance

To derive the diagnostic equation for monthly mixed layer temperature variance, i.e., Eq. (2.4), we start with the monthly mixed layer energy budget:

$$C_o \frac{\partial T}{\partial t} = Q_s + Q_o \tag{A.1}$$

Here, C_o is the heat capacity of the ocean mixed layer (i.e. $C_o = c_p \rho h$, where h is the ocean mixed layer depth), T is the monthly mean mixed layer temperature, Q_s is the net surface heat flux (sum of latent, sensible and radiative heat fluxes), Q_o is the heat convergence due to ocean dynamics, including wind-driven Ekman currents and vertical mixing. Since the focus is on understanding the processes that drive temperature anomalies, C_o, T, Q_s and Q_o are each expanded into the sum of a climatological mean (denoted by overbar), and and the departure from the mean (denoted by prime). As discussed in Section 2.2.1, both the linear trend and seasonal cycle are removed from the anomalies in C_o, T, Q_s and Q_o. Inserting the above yields the following equation for the temperature anomalies:

$$\overline{C}_o \frac{\partial T'}{\partial t} = Q'_s + Q'_o \tag{A.2}$$

To form an equation involving the mixed layer temperature variance, i.e., $\overline{T'(t)^2}$, a finite centered difference of the temperature tendency term in Eq. (A.2) is taken, and both sides are squared and averaged over time, yielding:

$$\frac{\overline{C}_o^2}{2\Delta t^2}\left(\overline{T'(t)^2} - \overline{T'(t+\Delta t)\,T'(t-\Delta t)}\right) \approx \overline{(Q'_s + Q'_o)^2} \tag{A.3}$$

Note that Δt is the sampling period of one month. Denoting $\overline{T'(t)^2}$ as σ_T^2 and using $\overline{T'(t+\Delta t)\,T'(t-\Delta t)} = \overline{T'(t)\,T'(t-2\Delta t)} = r_2\overline{T'(t)^2}$, where r_2 is the lag-2 autocorrelation for mixed layer temperature, Eq. (A.3) can be rewritten as:

$$\sigma_T^2 \approx \frac{2\Delta t^2}{\overline{C}_o^2\,(1-r_2)}\overline{(Q'_s + Q'_o)\,(Q'_s + Q'_o)} \tag{A.4}$$

Eq. (2.4) that is derived in the main text is formed by using the mixed layer energy budget, Eq. (A.2), to substitute for one of the $Q'_s + Q'_o$ in Eq. (A.4), and defining $\alpha = \frac{2\Delta t^2}{\left[\overline{C}_o(1-r_2)\right]}$:

$$\sigma_T^2 \approx \alpha\left(\overline{\frac{\partial T'}{\partial t}Q'_s} + \overline{\frac{\partial T'}{\partial t}Q'_o}\right) \tag{A.5}$$

Note that Eq. (A.5) is analogous to the 'fraction of variance (FOV)' metric used by Buckley et al. (2014) and Roberts et al. (2017) to understand the drivers of upper-ocean heat content variability, $H = \rho c_p \overline{h} T$. Buckley et al. (2014) express the fraction of variance $\frac{\partial H}{\partial t}$ that is explained by Q_o, which is denoted as $FOV\left(\frac{\partial H}{\partial t}, Q_o\right)$, as the following:

$$FOV\left(\frac{\partial H}{\partial t}, Q_o\right) = \frac{\overline{Q'_o}^2 + \overline{2Q'_oQ'_s}}{\overline{\left(\frac{\partial H'}{\partial t}\right)^2}} \tag{A.6}$$

Here the ocean dynamical contribution to the temperature variance is defined as:

$$\widetilde{Q}_o = \alpha\overline{\frac{\partial T'}{\partial t}Q'_o} = \frac{\alpha}{\overline{C}_o}\left(\overline{Q'^2_o} + \overline{Q'_sQ'_o}\right) \tag{A.7}$$

Thus, both Eqs. (A.6) and (A.7) relate to the sum of the variance of Q_o and the covariance between Q_o and Q_s. The main justification for using a single covariance term in the definition of the Q_o contribution (i.e. $\overline{Q'_s Q'_o}$ instead of $\overline{2Q'_s Q'_o}$) is to enable the contributions to sum to the total temperature variance, i.e., $\sigma_T^2 = \widetilde{Q}_o + \widetilde{Q}_s$. However, note that the covariance terms contribute equally to the surface heat flux and ocean dynamical contributions, and thus are not essential to understanding the relative contributions of Q_s and Q_o to temperature variance.

A.2 Derivation of the contributions of observational uncertainty to mixed-layer temperature variance

To quantify the contributions of observational uncertainty to the mixed layer temperature variance (as shown in Fig. 2.10 and Fig. 2.11), we start with:

$$\widetilde{Q}_s = \alpha \overline{\frac{\partial T'}{\partial t} Q'_s} = \alpha \overline{\left(\frac{\partial T'}{\partial t} \pm \varepsilon_{\frac{\partial T}{\partial t}} \right) \left(Q'_s \pm \varepsilon_{Q_s} \right)} \tag{A.8}$$

where $\varepsilon_{\frac{\partial T}{\partial t}}$ and ε_{Q_s} are the observational estimates of uncertainty in the temperature tendency and surface heat fluxes, respectively. Using $\varepsilon_{\frac{\partial T}{\partial t}} \approx \frac{\varepsilon_T}{\Delta t}$, where ε_T is the uncertainty in the mixed layer temperature, and expanding the RHS of Eq. (A.8) yields:

$$\widetilde{Q}_s = \alpha \overline{\frac{\partial T'}{\partial t} Q'_s} \pm \overline{\frac{\partial T'}{\partial t} \varepsilon_{Q_s}} \pm \overline{Q'_s \frac{\varepsilon_T}{\Delta t}} \pm \overline{\varepsilon_{Q_s} \frac{\varepsilon_T}{\Delta t}} \tag{A.9}$$

The uncertainty in the surface heat flux contribution is then defined as:

$$\varepsilon_{\widetilde{Q}_s} = \overline{\frac{\partial T'}{\partial t} \varepsilon_{Q_s}} + \overline{Q'_s \frac{\varepsilon_T}{\Delta t}} + \overline{\varepsilon_{Q_s} \frac{\varepsilon_T}{\Delta t}} \tag{A.10}$$

The uncertainty in the ocean heat transport contribution is estimated from the error in the temperature variance and the error in the surface heat flux contribution using the

following relation:

$$\varepsilon_{\widetilde{Q}_o} = \varepsilon_{\widetilde{Q}_s} + \varepsilon_{\sigma_T^2} \tag{A.11}$$

Thus, the uncertainty in the ocean heat transport contribution ($\varepsilon_{\widetilde{Q}_o}$) is defined to equal the sum of the uncertainty in the surface heat flux contribution ($\varepsilon_{\widetilde{Q}_s}$) and the uncertainty in the temperature variance ($\varepsilon_{\sigma_T^2}$). This is consistent with the fact that the indirect estimate of Q_o is calculated from the observed SSTs and surface heat fluxes as a residual in the mixed layer energy budget. Note that the uncertainty in the mixed layer temperature variance ($\varepsilon_{\sigma_T^2}$) is found from:

$$\sigma_T^2 = \overline{(T' \pm \varepsilon_T)^2} = \overline{T'^2} \pm 2\overline{T'\varepsilon_T} + \overline{\epsilon_T^2} \tag{A.12}$$

so that:

$$\varepsilon_{\sigma_T^2} = 2\overline{T'\varepsilon_T} + \overline{\epsilon_T^2} \tag{A.13}$$

Appendix B

Timescale dependency of the contributions to mixed-layer temperature variance in the North Pacific and North Atlantic

Figures B1 and B2 show the spatially-averaged contributions from the surface heat fluxes and the ocean heat transport as a function of low-pass filter length as in Fig. 2.10 and Fig. 2.11, except for the North Atlantic and North Pacific basins. Figure B1 shows results for the North Pacific and Fig. B2 shows results for the North Atlantic.

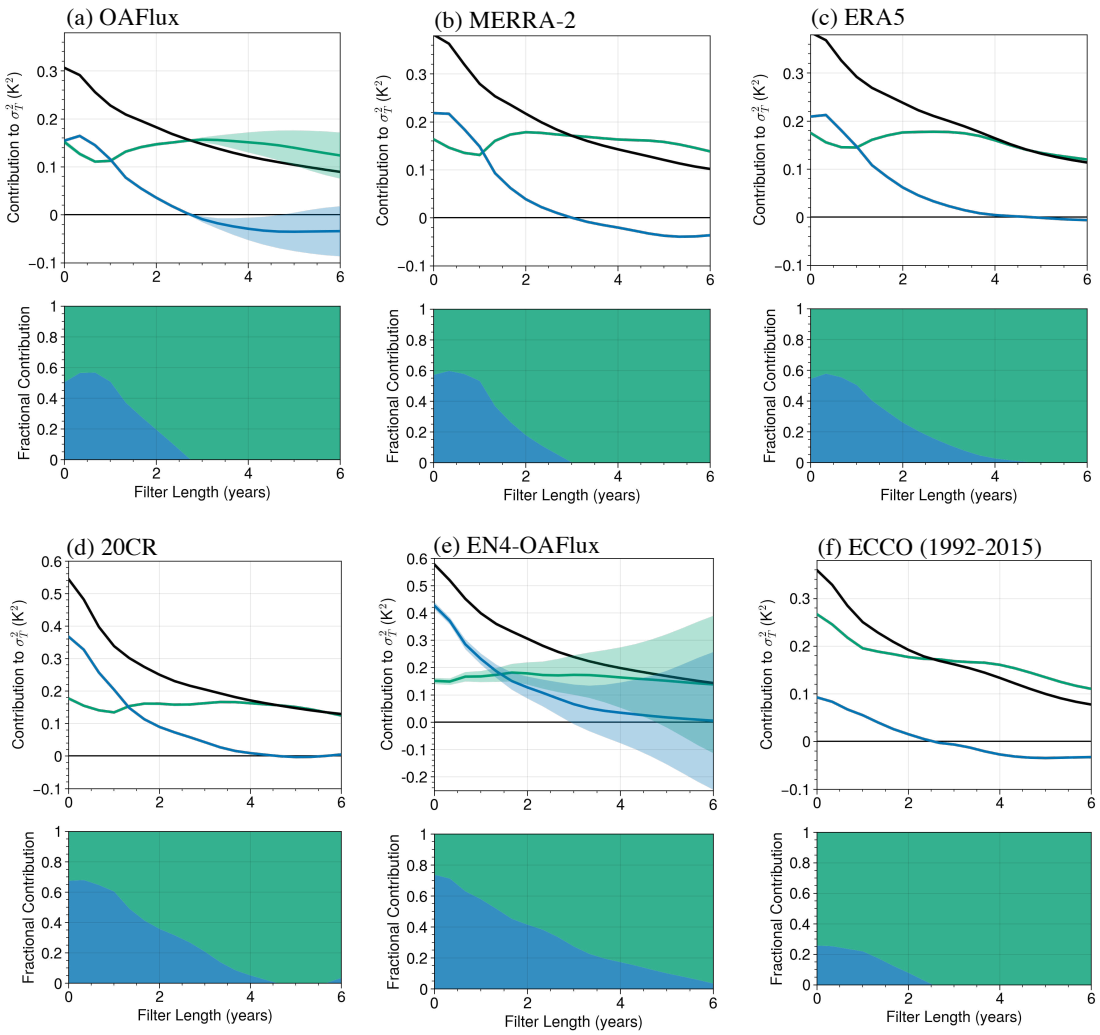

Figure B1: As in Fig. 2.10b,f and Fig. 2.11a-d, but for results averaged over the North Pacific sector (defined as 20°N-60°N and 120°E-270°E). Results in panels a-e are based on the period of record 1980-2017. Results in panel f are based on the ECCO period of record 1992-2015.

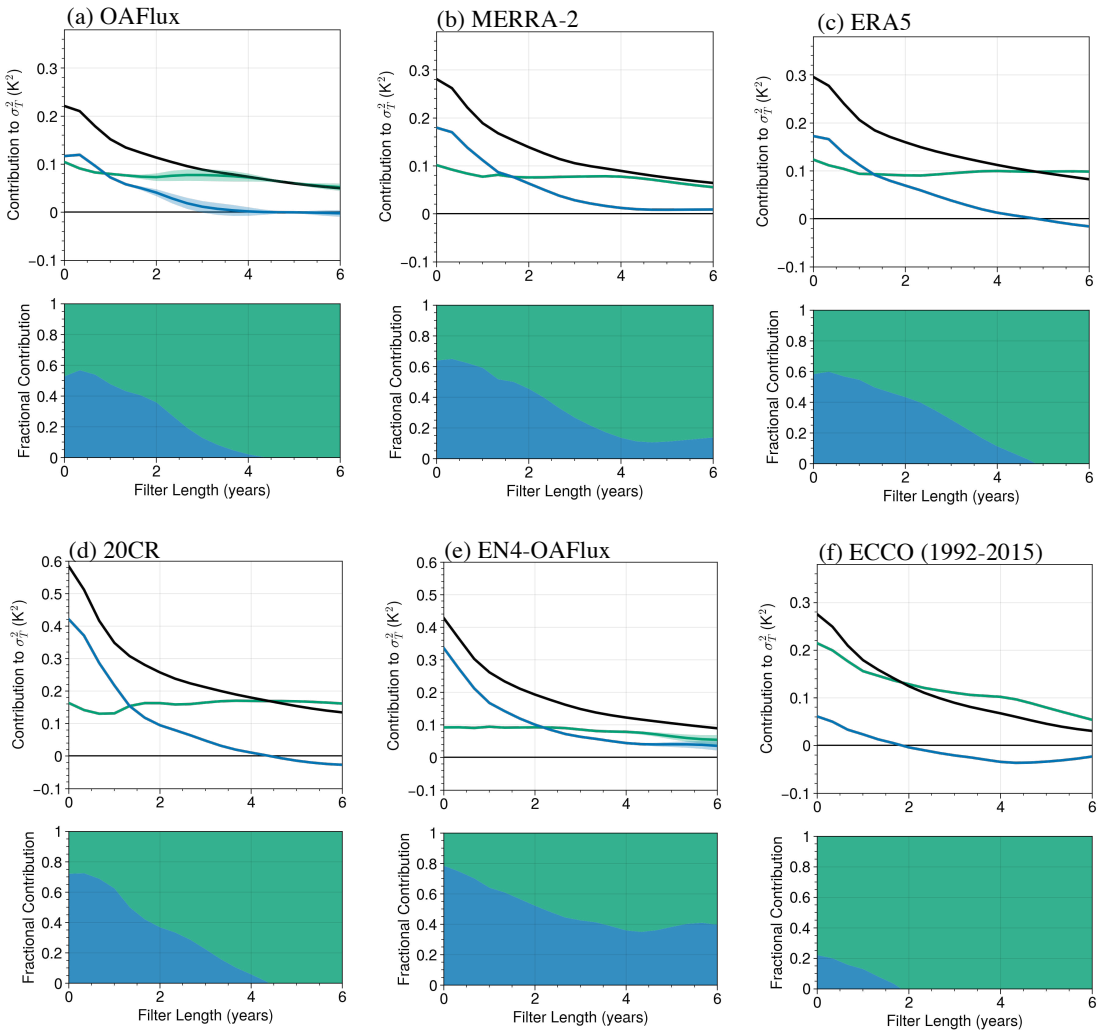

Figure B2: As in Fig. 2.10b,f and Fig. 2.11a-d, but for results averaged over the North Atlantic sector (defined as 20°N-60°N and 0-90°W). Results in panels a-e are based on the period of record 1980-2017. Results in panel f are based on the ECCO period of record 1992-2015.